A Mariner 9 Atlas of the Moons of Mars

JOSEPH VEVERKA, MICHAEL NOLAND, AND CARL SAGAN

Laboratory for Planetary Studies, Cornell University, Ithaca, New York 14850

JAMES POLLACK

NASA Ames Research Center, Moffet Field, California 94035

LYNN QUAM, ROBERT TUCKER, AND BOTAND EROSS

Artificial Intelligence Laboratory, Stanford University, Stanford, California 94305

AND

THOMAS DUXBURY AND WILLIAM GREEN

Jet Propulsion Laboratory, California Institute of Technology, Pasadena, California 91103

Received January 30, 1974; revised February 23, 1974

This paper contains a complete set of the best enhancements of Mariner 9 high resolution television pictures of Phobos and Deimos, consisting of 27 different views of Phobos, and 9 of Deimos. Pertinent data about the pictures are arranged in convenient tabular and graphical form.

1. Introduction

Following the discovery of Phobos and Deimos in 1877 by Asaph Hall, early earthbased observations concentrated on accurate ephemerides rather than on the satellites' physical characteristics. The first attempt at photometry was made between 1877 and 1882 by Oliver C. Wendell and E. C. Pickering, who found Phobos brighter than Deimos and both satellites apparently variable in brightness. But accurate photometry was difficult due to the intense scattered light from Mars, and it was impossible to decide whether these variations were real. The first good photometry of Phobos and Deimos was achieved by G. P. Kuiper during the 1956 opposition using the 82" reflector at McDonald Observatory (Harris, 1961). To minimize the effects of scattered light the satellites were only measured near elongation. No orbital brightness fluctuations were noted, or at least reported. The results indicated a mean opposition magnitude in the visual of $+11.6 (\pm 0.1)$ for

Phobos and $+12.8~(\pm 0.1)$ for Deimos. Assuming the satellites to be as reflective as the average lunar area this implied radii of about 6 and 3km respectively. Somewhat brighter values for the mean opposition magnitudes were found photographically by Pascu (1973) during the 1967 opposition. His results indicate that both satellites may be 0.4 mag brighter than found by Kuiper. Kuiper also measured the apparent (B-V) color of the satellites. The value of +0.6 indicates that the satellites are grey like many asteroids, and differ considerably from the red color of Mars $(B-V) \approx +1.3$.

The orbits of the satellites are nearly circular and lie close to the equatorial plane of Mars. Both satellites are relatively close to their primary: the distance of Deimos from the center of Mars is 23 500km (6.9 Rs), which is only 10% of the relative distance of our moon from the Earth; the inner satellite, Phobos, is at 9400km (2.7 Rs). Earth-based determinations of the satellites' orbits are summarized in a recent review article (Burns,

1972). The long-standing question of the secular acceleration of Phobos (Sinclair, 1972) is one important problem which Mariner data can help resolve.

The only pre-Mariner 9 spacecraft data on either satellite was obtained by Mariner 7 in 1969. Several exposures of Phobos against the disc of Mars occurred in the course of the far encounter picture sequence. The best of these, 7F91, was analyzed by Smith (1971). Even though the image of Phobos was only a few picture elements across it was clear that Phobos was irregular (about 18 by 23km) and probably dark.

The first photographs to show the surface of Phobos and Deimos were provided by Mariner 9. The main results obtained from the analysis of these television pictures are given by Masursky et al. (1972) and Pollack et al. (1972, 1973). To a first approximation both satellites are triaxial ellipsoids. Current estimates of the principal axes are given in Table I. Both satellites are also in synchronous rotation, and in each case the longest axis points toward Mars, while the shortest lies perpendicular to the orbital plane. This is the lowest energy configuration expected at the end of tidal evolution of the satellite spins.

Phobos and Deimos are heavily cratered, having crater populations close to the saturation limit. A comparison of this crater density with that of the Apollo 11 site on our moon, whose surface age is known, implies that the Martian moons are at least several billion years old, and probably date back to the early history of the solar system. Besides producing cra-

ters, the largest meteoroid impacts are thought to have caused extensive fracturing and spallation of the surfaces. An example of the latter process is the long linear feature that appears in the photograph of Phobos obtained on revolution 129 (Figs. P14 and P15). This feature appears to originate near the rim of the largest crater on Phobos, a crater 8km in diameter (1/3 the size of Phobos!).

When the size estimates of the satellites obtained from the Mariner 9 photographs are combined with Kuiper's earth-based visual magnitude estimates, their geometric albedos are found to be very low, about 0.05. This result is consistent with Smith's estimate from the Mariner 7 photograph of Phobos. Such a low reflectivity suggests that the satellites may consist of either carbonaceous chondritic or dark basaltic material. Comparison of the Mariner 9 brightness data for the two satellites indicates that they have the same albedo within an accuracy of 10%. Using Pascu's determinations of the mean opposition magnitudes, slightly higher geometric albedos (~ 0.07) result.

A study of the brightness variation of Phobos and Deimos with phase angle suggests that both satellites probably have a regolith (Pollack et al., 1973). The conclusion is strengthened by a set of temperature measurements made by the Mariner 9 Infrared Radiometer during and after an eclipse of Phobos (Gatley et al., 1974). The regolith is thought to have originated through meteoritic fragmentation of the surface material.

The presence of the long linear feature

TABLE I
PRINCIPAL AXES OF PHOBOS AND DEIMOS

Satellite	Largest	Intermediate	Smallest	Volume,	Mass, ^c
	axis, km	axis, km	axis, km	km³	10 ¹⁸ g
Phobos Deimos	$13.5 \pm 1 \\ 7.5^{+3}_{-1}$	10.7 ± 1 6.0 ± 1	9.6 ± 1 5.5 ± 1	5810 1040	17.4 3.1

^a From Pollack et al., 1973.

^b The axes are radii, not diameters.

^c A density of 3g/cm³ has been assumed.

mentioned above implies that most of the interior of Phobos (and probably Deimos) has the structural strength of rock, not the strength of a loose agglomerate of material held together gravitationally. This inference is supported by a study of the satellites' meteoroid impact history, which implies that if they were collections of sand grains, bound gravitationally, they would have been disintegrated by past collisions. Since the satellites' gravitational fields are too weak to produce well-consolidated material, it is suggested that they were once part of a much larger object (or objects). However, several alternative explanations of the satellites' rocky interiors are possible, such as heating (and hence melting) by a very strong primordial solar wind or by short-lived radioactive elements.

2. Mariner 9 Data

During its active lifetime Mariner 9 obtained 32 high-resolution pictures of Phobos, and 9 of Deimos. The spacecraft orbit (the parameters of which are given in Table IIA) was adequate for about 80% complete coverage of Phobos, but, since the spacecraft was entirely within the orbit of Deimos, the coverage of the outer satellite was restricted to the Mars-facing side.

Mariner 9 had a 3-axis spin-stabilized scan platform on which the science instrument package was mounted. These instruments, including two television cameras, could be pointed in almost any direction within the hemisphere away from the Sun. Some of the characteristics of the medium resolution A-camera and of the high resolution B-camera are summarized in Table IIB. The effective wavelength of the B-camera was near $0.56\,\mu\mathrm{m}$. A detailed description of the Mariner 9 television

TABLE IIA

MARINER 9 ORBITAL PARAMETERS

Period	~	12 hours
Inclination	=	$64^{\circ}.4$
Periapsis	=	$1650 \mathrm{km}$
Apapsis	=	$12650\mathrm{km}$

TABLE IIB

CAMERA CHARACTERISTICS

	Wide- angle	Narrow- angle
Characteristic	camera (A-camera)	camera (B-camera)
Focal length, millimeters	s 50	500
Focal ratio	f/4.0	f/2.35
Shutter speed range, milliseconds	3 to 6144	3 to 6144
Automatic shutter speeds, milliseconds	48, 96, 192	6, 12, 24
Angular field of view, degrees	11 × 14	1.1×1.4
Active vidicon target raster, millimeters	9.6×12.5	9.6 imes 12.5
Scan lines per frame	700	700
Picture elements per line	832	832
Bits/picture element	9	9

system is given by Snyder (1971), while accounts of the inflight photometric performance of the cameras may be found in Thorpe (1972, 1973).

The catalog of the present paper contains several computer-enhanced versions of each useful high-resolution satellite photograph obtained by Mariner 9, together with a coordinate grid showing latitude and longitude, subsolar and subspacecraft points, and the terminator. Throughout this paper we use the word photograph to describe television picture data.

Chronological lists of all high-resolution (B-camera) television frames of Phobos and Deimos are given in Tables III and IV. At closest approach (~5000km) Phobos was approximately 150 picture elements (pixels) across, while Deimos subtended about 75 pixels.

The available pictures are listed in order of increasing range in Tables V and VI, while the satellite coverage in terms of increasing solar phase angle is given in Tables VII and VIII. Maximum visibility of surface detail is achieved at minimum range and maximum phase angle. Figures 1 and 2 provide summaries of the Phobos and Deimos coverage on range/phase angle plots.

TABLE III
PHOBOS B FRAMES

		Sub-spacec	raft point		Approximate apparent			
Revolution DAS time			- Phase	diameter (Pixels)	Range (km)	Comments		
31	02711170	341°	-27°	76°	59	14530		
34ª	02816240	157	-69	58	150	5720	Top 1/8 out of picture	
34	02816310	160	-71	59	150	5710	20P 2/0 0mt 01 P100m1	
41ª	03067265	109	-41	34	116	7400	3/4 out of picture	
41	03067335	108	-43	34	118	7270	-,	
43	03136565	152	-19	66	116	7380		
43ª	03137335	176	-28	73	133	6450	1/2 out of picture	
48	03320875	55	-62	49	120	7160	1/2 sat s1 presars	
48	03320945	52	-62	50	120	7180		
53	03501965	24	-32	26	72	11880		
57	03642245	130	-61	52	144	5980		
73	04215685	135	-42	5 7	133	6460		
77	04365205	344	-31	80	106	8130		
80ª	04470485	356	-67	81	123	7000	3/4 out of picture	
80	04470625	356	-64	83	120	7170	of I out of picture	
87	04720805	75	-58	42	121	7120	Contains residual of 04720735	
89	04790455	172	-48	80	149	5760	01.20.00	
117	05773388	85	-28	55	84	10170		
129	06209278	17	-30	18	69	12500	*	
129	06209628	13	-27	19	68	12660		
131	06278438	65	-35	45	76	10410		
133	06350468	79	-82	73	128	6110		
145	06781038	52	-20	70	52	15260		
150	06968708	344	24	64	55	14510		
161	07360358	20	-39	45	79	10000		
171	07725968	333	43	71	58	13590		
207	09013274	45	-66	63	114	6950		
221	09518254	23	-41	41	90	9800		
430	11801371	341	62	77	74	10710		
444	12159217	249	79	65	60	13040		
675	13469623	241	69	43	56	13950		
676 ^b	13511833	94	33	73	46	17320	Overexposed	

^a Partial picture.

The phase angle coverage is shown independently in Fig. 3. Within the constraints of the scan-platform this coverage is complete, making it possible to determine the photometric functions of the satellite surfaces.

Finally, in Figs. 4 and 5 the latitudes and longitudes of the subspacecraft points are plotted to indicate the completeness of the surface coverage.

3. STANFORD PROCESSING OF SATELLITE PICTURES

The television pictures were processed both at JPL's Image Processing Laboratory and at Stanford's Artificial Intelligence Laboratory. In both cases the data source was the Experimenter Data Record, or EDR (described by Levinthal *et al.*, 1972). The processing techniques at the

^b Overexposed picture.

^c West longitude.

TABLE IV
DEIMOS B-FRAMES

		Sub-spacecraft point		Approximate apparent			
Revolution	DAS time	Longitude	Latitude	Phase	diameter (Pixels)	Range (km)	Comments
25	02490320	20°	-14°	68°	52	8830	
63	03854625	7	-14	73	59	7770	
73	04212605	41	-4	22	46	10070	
111	05553378	27	-1	31	64	7220	
121	05918708	13	-22	44	30	15340	
149	06918168	355	27	65	85	5490	
159	07283428	3	-20	51	46	10060	
197^{b}	08647664	335	-2	73	63	7380	Overexposed
4374	11994749	323	46	28	54	8590	1

- ^a Partial picture.
- ^b Overexposed picture.
- ^c West longitude.

two institutions were similar, but not identical, and a brief description of each is given in this and in the following section.

- At Stanford several preliminary steps were carried out before the pictures were enhanced:
- (1) Numerous undesirable artifacts in the EDR data were searched for, found, and so indexed. Once a pixel was indexed as "bad", any subsequent calculation involving that pixel attempted to exclude it. For example, a calculation to determine the average intensity over an n by m pixel area would ignore those pixels which were indexed as bad. Eventually, a "fill" operation might be performed replacing bad points by an average of their neighbors.
- (2) The reseau marks on the vidicon were located by knowing their approximate locations and searching in that immediate area for the darkest group of points of the approximate size of the reseau. The center of these points was calculated and an n by m area (usually 5 by 5) centered there was marked as bad.
- (3) Single pixel transmission errors are characterized by isolated pixels which are either much brighter or much darker than their neighbors. A standard statistical technique was used to detect such errors. If a pixel differed from the mean of

its neighbors over an n by m area (usually 5 by 5) by more than 2 standard deviations from the mean calculated over the same area, then that pixel was replaced by the mean. This procedure, called "Custer", eliminated most of the single point errors in the EDR data.

(4) Finally, the dark current level was determined. When the TV camera looks into the relative black of space, the vidicon receives so little light that only the biasing current (called dark current) of the vidicon is seen. The intensity level (DN or data number value) of the dark current can be determined for the satellite images by examining their histograms for a very large peak in the low intensity portion of the histogram. All pixels with intensity values in the dark current portion of the histogram were marked as bad. Only the remaining pixels were subjected to enhancement.

Once these initial steps were performed, the data were improved sufficiently for enhancements to be performed without the introduction of artifacts due to areas of bad data points. This initial processing is particularly important for the high frequency filters. If high frequency filtering is performed on images which contain reseau marks, large bright vertical,

TABLE V
PHOBOS RANGE COVERAGE

TABLE VII
PHOBOS PHASE ANGLE COVERAGE

Range (km)	Revolution	DAS time	Phase angle	Revolution	DAS time
5710	34	02816310	18°	129	06209278
5720^a	34	02816240	19	129	06209628
5760	89	04790455	26	53	03501965
5980	57	03642245	34ª	41	03067265
6110	133	06350468	34	41	03067335
6450^{a}	43	03137335	41	221	09518254
6460	73	04215685	42	87	04720805
6950	207	09013274	43	675	13469623
7000°	80	04470485	45	131	06278438
7120	87	04720805	45	161	07360358
7170	80	04470625	49	48	03320875
7160	48	03320875	50	48	03320945
7180	48	03320945	52	57	03642245
7270	41	03067335	55	117	05773388
7380	43	03136565	57	73	04215685
7400^{a}	41	03067265	58ª	34	02816240
8130	77	04365205	59	34	02816310
9800	221	09518254	63	207	09013274
10000	161	07360358	64	150	06968708
10170	117	05773388	65	444	12159217
10410	131	06278438	66	43	03136565
10710	430	11801371	70	145	06781038
11880	53	03501965	71	171	07725968
12500	129	06209278	73ª	43	03137335
12650	129	06209628	73 ^b	676	13511833
13040	444	12159217	73	133	06350468
13590	171	07725968	7 6	31	02711170
13950	675	13469623	77	430	11801371
14510	150	06968708	80	77	04365205
14530	31	02711170	80	89	04790455
15260	145	06781038	81ª	80	04470485
17320 ^b	676	13511833	83	80	04470625

^a Partial picture.

TABLE VI DEIMOS RANGE COVERAGE

Revolution	DAS time
149	06918168
111	05553378
197	08647664
63	03854625
437	11994749
25	02490320
159	07283428
73	04212605
121	05918708
	149 111 197 63 437 25 159

^a Overexposed picture.

horizontal or rectangular artifacts, depending on the type of the filter, are introduced.

The stretch enhancement used is a simple linear rescaling (ax+b) based on the histogram of the image. It rescales the data so that the significant part of the histogram (central 90%) covers the entire dynamic range of the film. The stretch enhancement is comparable to turning the brightness and contrast controls on a TV set to maximize contrast without saturating the bright areas and without losing the dark areas.

The purpose of high frequency filtering

^b Overexposed picture.

^a Partial picture.

^b Overexposed picture.

TABLE VIII
DEIMOS PHASE ANGLE COVERAGE

Phase angle	Revolution	DAS time
22°	73	04212603
28	437	11994749
31	111	05553378
44	121	05918708
51	159	07283428
65	149	06918168
68	25	02490320
73	63	03854625
73ª	197	08647664

Overexposed picture.

is to enhance small scale intensity variations from the local mean intensity. This technique is particularly valuable when there is a gradual, but large, intensity gradient across the image. Images near the terminator and images which contain both bright and dark areas are best enhanced with high frequency filtering. All satellite images have terminators and large intensity gradients.

The high frequency filters are calculated as follows: subtract from the intensity of each pixel the average intensity around it calculated over an n by m area; stretch (see above) the result.

In the satellite enhancements contained in this paper, the typical values for n by m are 11 by 11, 21 by 21, and 31 by 31.

Since the satellite images are so small, it was desirable to expand or magnify them by a factor of 2 to 4. At first, the procedure was to double the size of the image by replicating each pixel in a 2 by 2 (or 3 by 3) square. This technique produced a disturbing checkerboard effect. The expanded images included here were produced by a refined magnification technique which avoids this checkerboarding by linearly interpolating the values of the intermediate pixels.

The Stanford processing of the satellite images is known to contain several deficiences. When the dark current level is determined, parts of the satellite image near the terminator (or in the shadow of a crater wall) may be considered dark current and marked as bad data. Most of the raggedness of the satellite terminators is due to this artifact.

An MTF (Modulation Transfer Function) correction can produce a substantial improvement in the very high frequency detail of the images. This processing was not implemented at Stanford.

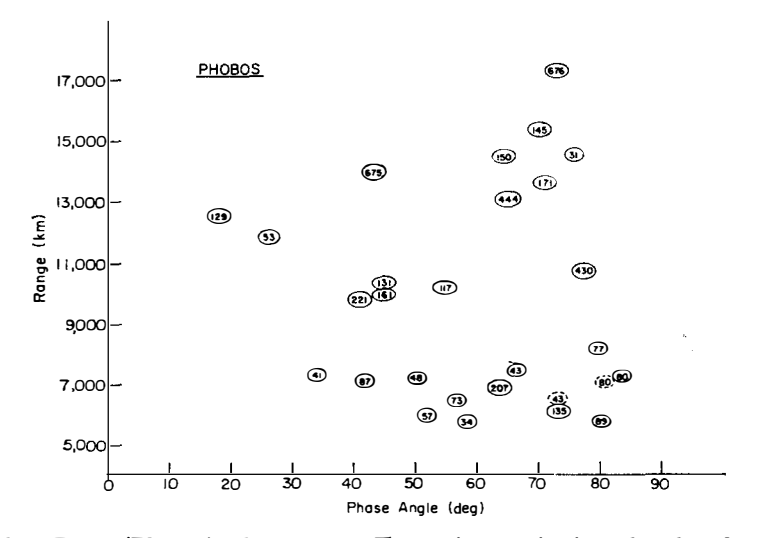


Fig. 1. Phobos. Range/Phase Angle coverage. For optimum viewing of surface features the range should be small and the phase angle large. The numbers refer to the Revolution on which the picture was taken. Dashed symbols indicate partial frames in which most of the satellite image is missing.

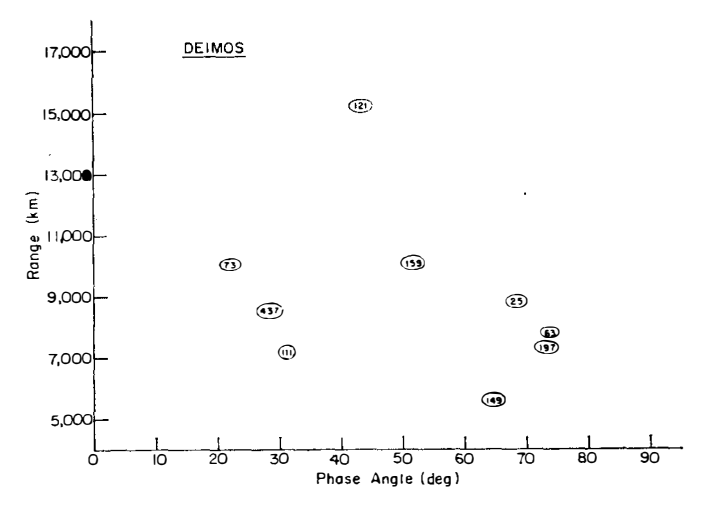


Fig. 2. Deimos. Range/Phase Angle coverage.

Finally, no geometric corrections were attempted to remove camera distortions. Since the satellites cover only a small portion of the 832×700 pixel TV images, geometric distortions over a satellite image are small if the image occurs in the central part of the camera's field of view. Near the corners of the frame significant shape distortions of up to 30% can occur.

4. IPL Processing of Satellite Pictures

The enhanced images of the satellites produced at JPL's Image Processing Laboratory (IPL) were processed as follows: First, the frame segment containing the satellite was extracted from the original

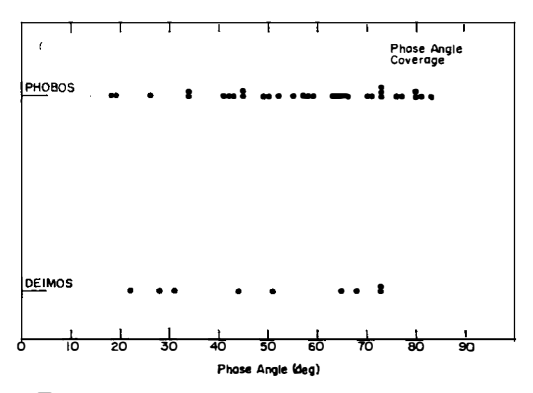
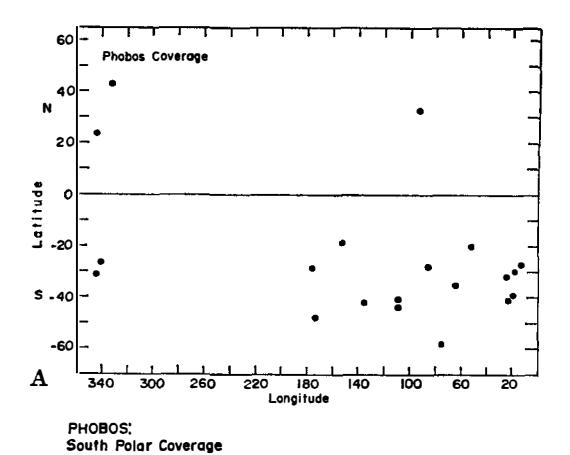


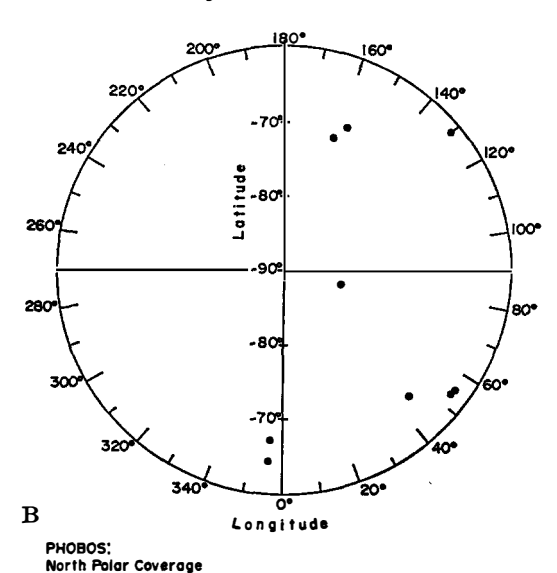
Fig. 3. Phase angle coverage of Phobos and Deimos.

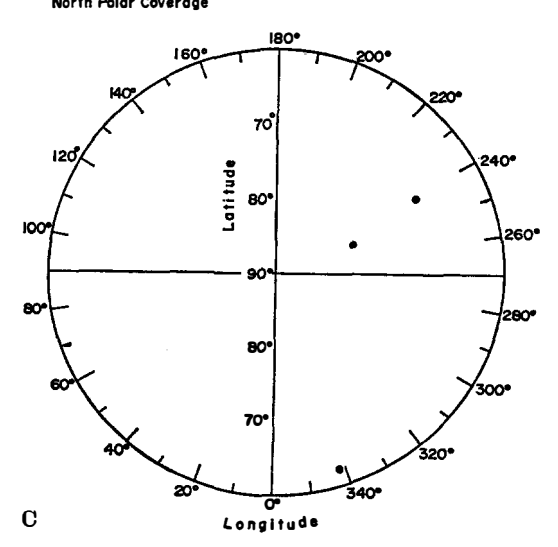
image. Telemetry bit errors cause anomalous picture element values to occur either singly or in pairs in the image, and these were removed using a simple algorithm that searches for picture element intensity values that deviate significantly from vertical neighbors. Anomalous picture element values were replaced by the average of the two vertical neighbors. Frames were also processed to replace missing image lines, using a vertical interpolation to "fill in" missing lines. Both of these procedures improve the appearance of the image.

The frame segment containing the satellite was then filtered digitally. The filter was a two dimensional convolution filter that is based on the inverse of the camera subsystem Modulation Transfer Function (MTF). The MTF is a measure of the camera system resolution as a function of spatial frequency within the image. The filtering serves to restore the high frequency degradation that occurs due to electronic sampling of the image.

The filtered frame segment was then enlarged using digital techniques. The enlargement was typically a factor of three or four times. The algorithm used in the magnification performs a bilinear interpolation to assign intensity values to the picture elements created by the magnification process. Digital enlargement of small sampled images is cosmetically superior to







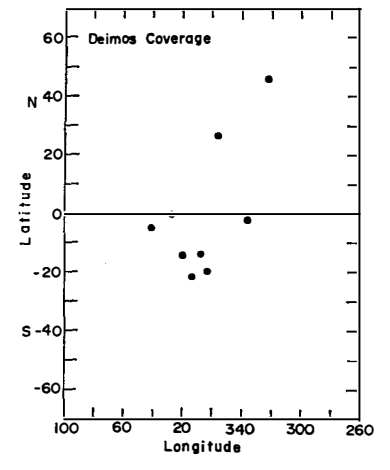


Fig. 5. High-resolution Mariner 9 coverage of Deimos. Shown are subspacecraft points.

photographic enlargement which produces very grainy images.

The final step in IPL processing was the generation of the following products:
(a) A series of contrast enhancements (designed to retain relative brightness information and display variation in several areas of the satellite); (b) application of a high pass filter designed to enhance local topographic detail and suppress large scale albedo variations, followed by a contrast enhancement; and (c) a contoured version, achieved by truncating a number of most significant bits. Examples of (a) and (b) are found throughout the picture catalog. An example of process (c) is shown in Fig. 6.

As in the case of the Stanford processing, no geometric correction was applied during IPL processing.

5. Computer Drawn Coordinate Grids

For each satellite picture the catalog gives a coordinate grid of the satellite indicating latitudes, longitudes, the subsolar and subspacecraft points, and the

Fig. 4 (A, B, C). High-resolution Mariner 9 coverage of Phobos. Shown are subspacecraft points.





Fig. 6. Example of "bit-clipping" to bring out isophotes: Revolution 25. Deimos. Left: IPL 144007. Stretched. Right: IPL 144035. Nine-bit data truncated to 4 bits.

terminator. These grids were computer drawn, assuming that the satellites are in perfect synchronous rotation about Mars and that the effects of satellite orbit eccentricity and solar perturbations on satellite orientation are negligible. A bodyfixed coordinate system (Fig. 7) is defined in which the x-axis points from the satellite center toward Mars, the z-axis is parallel to the satellite orbit angular momentum vector, and the y-axis is in the orbit plane and completes a righthanded, orthogonal coordinate system. Given the position vector **p** and the velocity vector **v** of a satellite in a Mars-centered, inertial reference system (e.g., 1950.0 Earth Equator), the body-fixed coordinate axes in the

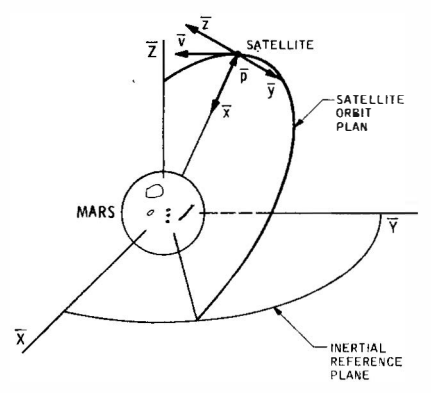


Fig. 7. Definition of coordinate axes and notation. See text for details.

inertial reference system are given by

$$\begin{aligned} \mathbf{x} &= -\mathbf{p}/|\mathbf{p}|, \\ \mathbf{z} &= \mathbf{p} \times \mathbf{v}/|\mathbf{p} \times \mathbf{v}|, \\ \mathbf{y} &= \mathbf{z} \times \mathbf{x}. \end{aligned} \tag{1}$$

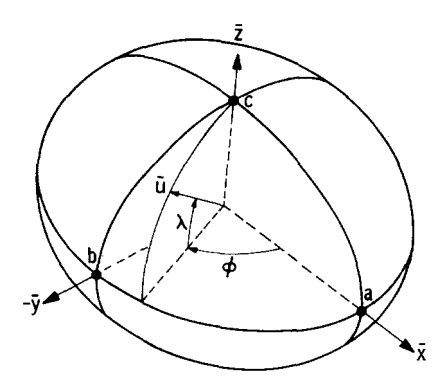
The computer drawn coordinate grids were computed assuming the satellites are ellipsoidal. A point on the surface of an ellipsoid (Fig. 8) is defined relative to the body fixed (x, y, z) system by

$$\mathbf{u} = u \begin{bmatrix} \cos \lambda \cos \phi \\ -\cos \lambda \sin \phi \\ \sin \lambda \end{bmatrix} = u \begin{bmatrix} u_x \\ u_y \\ u_z \end{bmatrix}, \quad (2)$$

where ϕ is the longitude of the point (measured positive west), λ is the latitude of the point, u is the distance from the center of figure to the point on the surface and u_x , u_y , u_z are the direction cosines of u in (x, y, z). For an ellipsoid whose major axes a, b and c are along x, y and z, respectively, the radius u (for a given ϕ and λ) is given by

$$u = (abc)/(b^2 c^2 u_x^2 + a^2 c^2 u_y^2 + a^2 b^2 u_z^2)^{1/2}.$$
 (3)

The three axes a, b and c were initially varied until a good match was obtained between the overlays and a variety of pictures. The three axes (Table I), determined for both Phobos and Deimos, show the satellites to be in dynamically stable orientations with a > b > c.



x - LONGEST AXIS - TOWARD MARS

- y INTERMEDIATE AXIS IN ORBIT PLANE
- z SHORTEST AXIS NORMAL TO ORBIT PLANE

Fig. 8. Definition of latitude (λ) and longitude (ϕ) on the reference triaxial ellipsoid.

The grid computation used the Mars ephemeris, Mariner 9 trajectory, and TV pointing data, supplied by the Mariner Navigation Team, to determine the viewing geometries.

A preliminary map of Phobos (Duxbury, 1974) is shown in Fig. 9. Seven of the craters shown have received official IAU names which are listed in Table 9. In addition, the long ridge emanating from Crater No. 47 (Stickney) is known as Kepler Ridge. Two of the craters on Deimos have also been named (Swift and Voltaire; see Fig. D6). The IAU nomenclature committee for features on Phobos and Deimos was chaired by C. Sagan.

6. Cautions to Users

This paper provides a complete set of the best enhancements of Mariner 9 high resolution pictures of Phobos and Deimos. The aim is to display clearly all topographic and albedo features on the satellite surfaces.

In using the information in this paper several facts must be kept in mind:

- (1) Relative contrasts within a single frame have meaning only for the "stretched" products.
- (2) The "filtered" products are intended to bring out small scale detail at

TABLE IX

IAU Phobos Nomenclature^a

Crater number (Fig. 9)	Name
1	Todd
3	Sharpless
13	D'Arrest
21	\mathbf{W} endell
34	\mathbf{Hall}
47	Stickney
48	\mathbf{Roche}

^a Official designations chosen by the IAU subcommittee on Phobos-Deimos Nomenclature (C. Sagan, Chairman).

the expense of large scale information (see above). Large scale contrast differences can be misleading in these products.

- (3) No attempt was made to retain photometric accuracy among the different pictures. Thus the fact that a given area appears darker relative to its surroundings on one orbit compared to its appearance on another orbit is not necessarily significant. Nor is it meaningful to compare photometrically the IPL and Stanford versions of a given product.
- (4) Satellite photometry should be carried out *only* on the basis of the EDR digital data.
- (5) Most pictures in this collection have been expanded by numerical bilinear interpolation (see above). One result of this procedure is to make the satellites appear smoother than they probably are at the limiting resolution. Consider a 2×2 pixel area of the original picture. It may appear smooth even though there exists a 1×1 pixel crater in this area. Expanding this picture by a factor of 3 yields a bland area 6×6 pixels across, whereas in fact it should contain a 3×3 pixel crater.
- (6) No geometric corrections were applied to the products. There are, therefore, camera-induced geometrical distortions in the pictures given in this paper, and these distortions are different for each image since the satellites were imaged in varying locations of the field of view. Since the satellites cover only a small fraction of

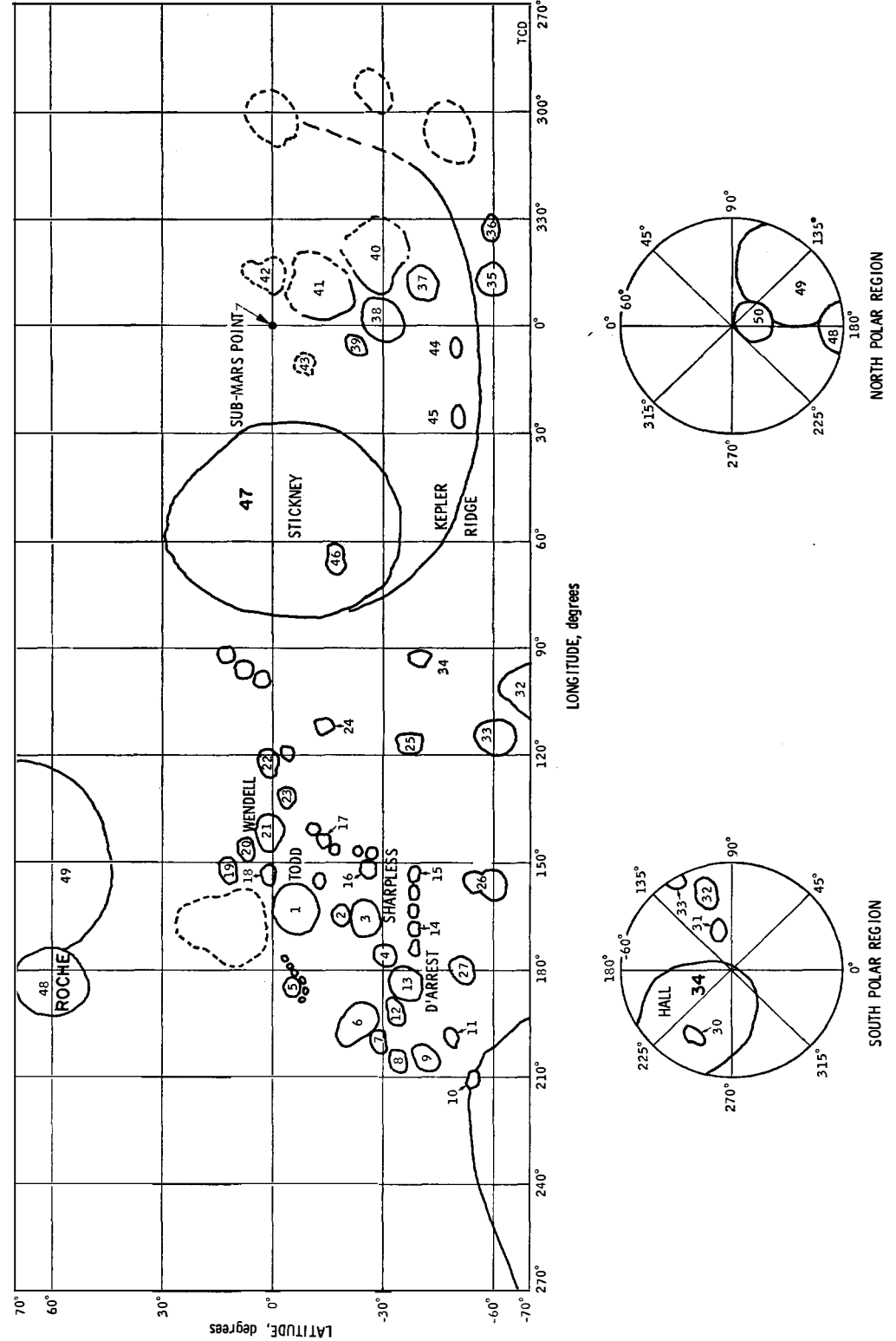


Fig. 9. Preliminary sketch map of Phobos. A list of IAU named craters is given in Table IX. From Duxbury, 1974.

- the total area of the original 700×832 pixel frame, the geometric distortions are not severe in general. For most pictures given in this catalog the shape distortion is less than 10%.
- (7) Accurate satellite geodesy should not be attempted on the basis of the pictures presented here. Such studies should be based on the EDR data (see, e.g., Duxbury, 1974).
- (8) The latitude—longitude grids given in this paper are intended for the approximate location of surface features. In the case of Phobos, the sketch map (Fig. 9) can be used to locate these features more precisely. No comparable map of Deimos has been produced, due to the limited coverage of that satellite.

ACKNOWLEDGMENTS

We thank the many individuals at the Jet Propulsion Laboratory and elsewhere who participated in the Mariner 9 mission. Special thanks are due to W. K. Hartmann, D. Milton, B. A. Smith, J. Seidman, R. Ruiz, A. Schwartz, T. Thorpe, R. Becker, and especially S. Soter for comments on an earlier version of this paper. This research was supported by grant NGR 33-010-220, Planetology Program Office, Office of Space Research, NASA Headquarters.

REFERENCES

- Burns, J. A. (1972). Dynamical characteristics of Phobos and Deimos. *Rev. Geophys. Space Physics* **10**, 463–483.
- Duxbury, T. (1974). Control network analysis of Phobos. *Icarus* 23, 290.
- Gatley, I., Kieffer, H., Miner, E., and Neugebauer, G. (1974). Infrared observations of Phobos from Mariner 9. Astrophys. J. 190, 497-503.
- HARRIS, D. L. (1961). Photometry and colorimetry of planets and satellites. Chapter 8 in "Planets and Satellites" (Kuiper and Middlehurst, eds.). University of Chicago Press, Chicago.
- LEVINTHAL, E. C., GREEN, W. B., CUTTS, J. A., JAHELKA, E. D., JOHANSEN, R. A., SANDER, M. J., SEIDMAN, J. B., YOUNG, A. T., AND SODERBLOM, L. A. (1973). Mariner 9 Image processing and products. *Icarus* 18, 75.
- MASURSKY, H., BATSON, R. M., McCAULEY, J. F., SODERBLOM, L. A., WILDEY, R. L., CARR, M. H., MILTON, D. J., WILHELMS, D. E., SMITH, B. A., KIRBY, T. A., ROBINSON, J. C.,

- Leovy, C. B., Briggs, G. A., Young, A. T., Duxbury, T. C., Acton Jr., C. H., Murray, B. C., Cutts, J. A., Sharp, R. P., Smith, Susan, Leighton, R. B., Sagan, C., Veverka, J., Noland, M., Lederberg, J., Levinthal, E., Pollack, J. B., Moore, Jr., J. T., Hartmann, W. K., Shipley, E. N., De Vaucouleurs, G., and Davies, M. E. (1972). Mariner 9 television reconnaissance of Mars and its satellites: Preliminary results. Science 175, 294.
- Pascu, D. (1973). Photographic photometry of the Martian satellites. A. J. 78, 794–798.
- Pollack, J. B., Veverka, J., Noland, M., Sagan, C., Hartmann, W. K., Duxbury, T. C., Born, G. H., Milton, D. J., and Smith, B. A. (1972). Mariner 9 television observations of Phobos and Deimos. *Icarus* 17, 394.
- POLLACK, J. B., VEVERKA, J., NOLAND, M., SAGAN, C., DUXBURY, T. C., ACTON, C. H., BORN, G. H., HARTMANN, W. K., AND SMITH, B. A. (1973). Mariner 9 television observations of Phobos and Deimos. II. JGR 78, 4313-4326.
- SINCLAIR, A. T. (1972). The motions of the satellites of Mars. Mon. Not. Roy. Ast. Soc. 155, 249-274.
- SMITH, B. A. (1970). Phobos: Preliminary results from Mariner 7. Science 168, 828.
- SYNDER, L. M. (1971). Mariner 9 TV subsystem calibration report. Project Report No. 610-202 Jet Propulsion Laboratory, Pasadena, California.
- THORPE, T. (1972). Mariner 9 television imaging performance evaluation (Mariner 9 TV subsystem calibration report). Project Report No. 619-237, Vol. II. Jet Propulsion Laboratory, Pasadena, California.
- THORPE, T. (1973). Verification of performance of the Mariner 9 television cameras. Appl. Opt. 12, 1775–1784.

APPENDIX: MARINER 9 HIGH RESOLUTION COVERAGE OF PHOBOS AND DEIMOS

General Remarks

For each high resolution picture of Phobos and Deimos obtained by Mariner 9, the following catalog contains two IPL enhancements, a computer drawn coordinate grid showing the viewing geometry, and four Stanford enhancements.

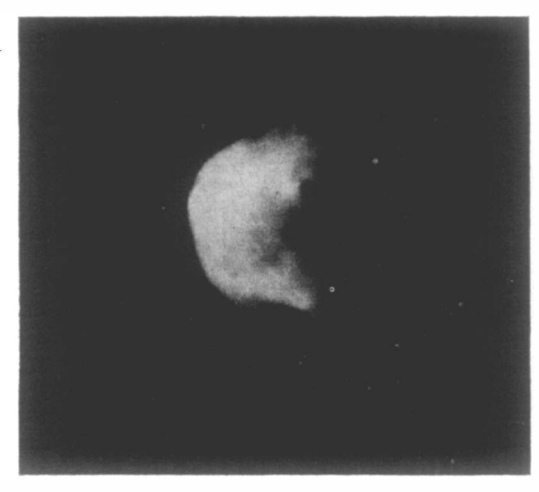
On the coordinate grids the asterisk indicates the subsolar point (called SUN in the caption); the cross represents the subspacecraft point (S/C in the caption). Δ LAT and Δ LONG in the grid caption represent the latitude and longitude grid increments.

Note that for reasons which are of no consequence in the present context the DAS time designation of a given picture can differ by almost 30 DAS counts in different data sources. Generally DAS times given in the Appendix are 5 DAS

counts higher than those which occur in the main body of the paper.

The smallest division on the pixel (picture element) scales of the Stanford products equals 5 pixels. For convenience during processing some of the Stanford products have been rotated through 90° relative to the IPL products and to the grids. This rotation is obvious whenever it occurs.

Section 1: Catalog of Deimos Coverage



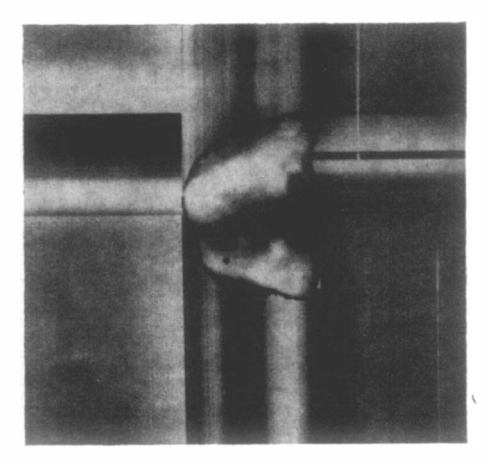
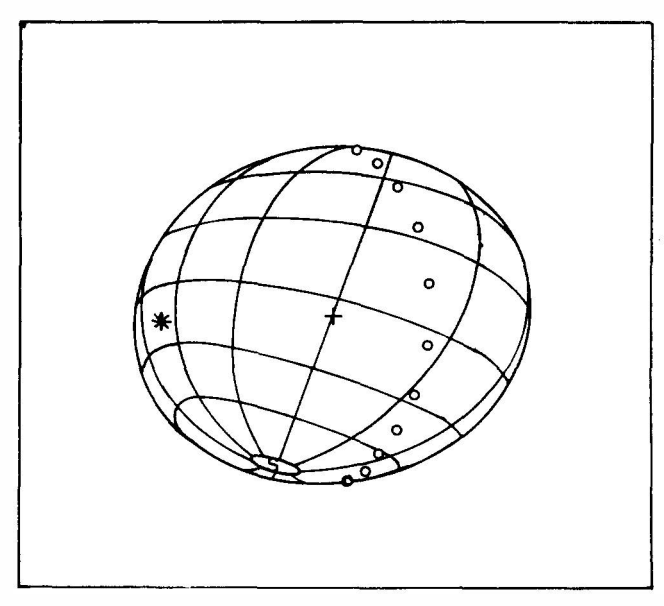
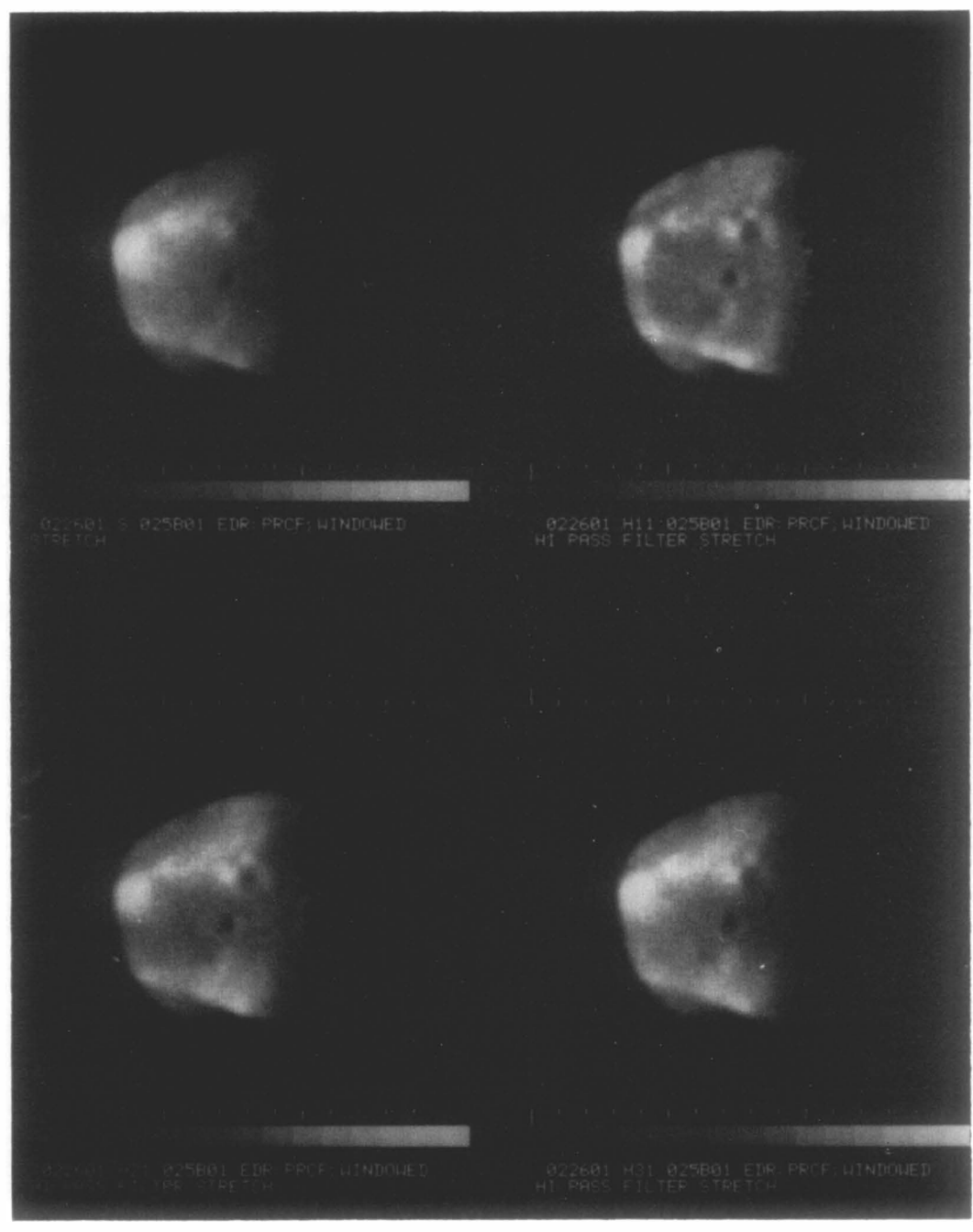


Fig. D1. Deimos. Revolution 25. DAS 02490325. Exposure = 24ms. I. Left: IPL 144007. Stretch. Mag $4\times$. Right: IPL 150839. High-pass filter and stretch. Mag $4\times$.



II. Phase = 68°. Range = 8830km. S/C = (14°.5 S, 20°.1 W). SUN = (21°.6 S, 91°.7 W). Δ LAT = 20°; Δ LONG = 30°.



III. Stanford AI product STN GS01-022601.



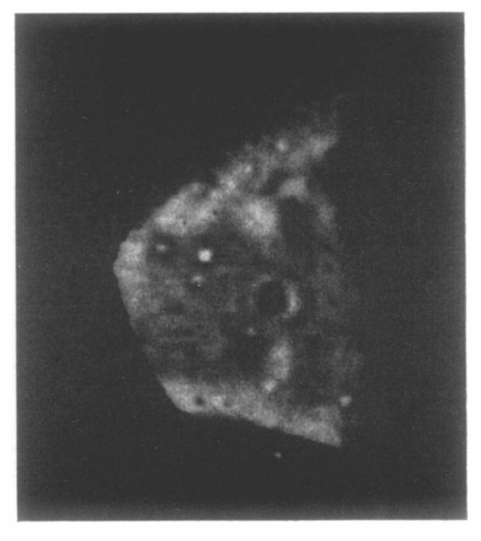
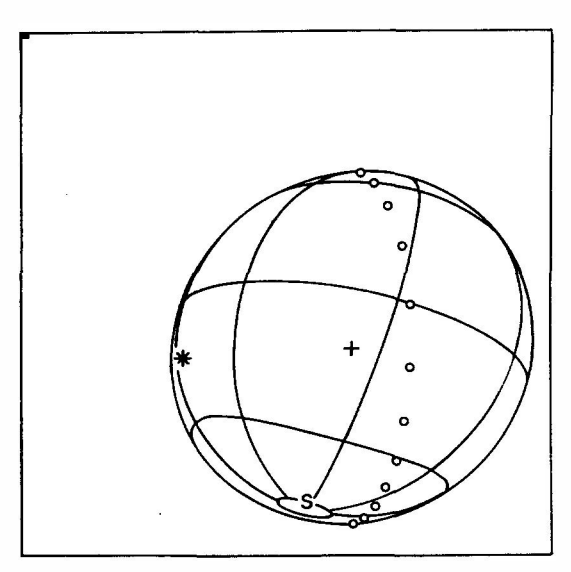
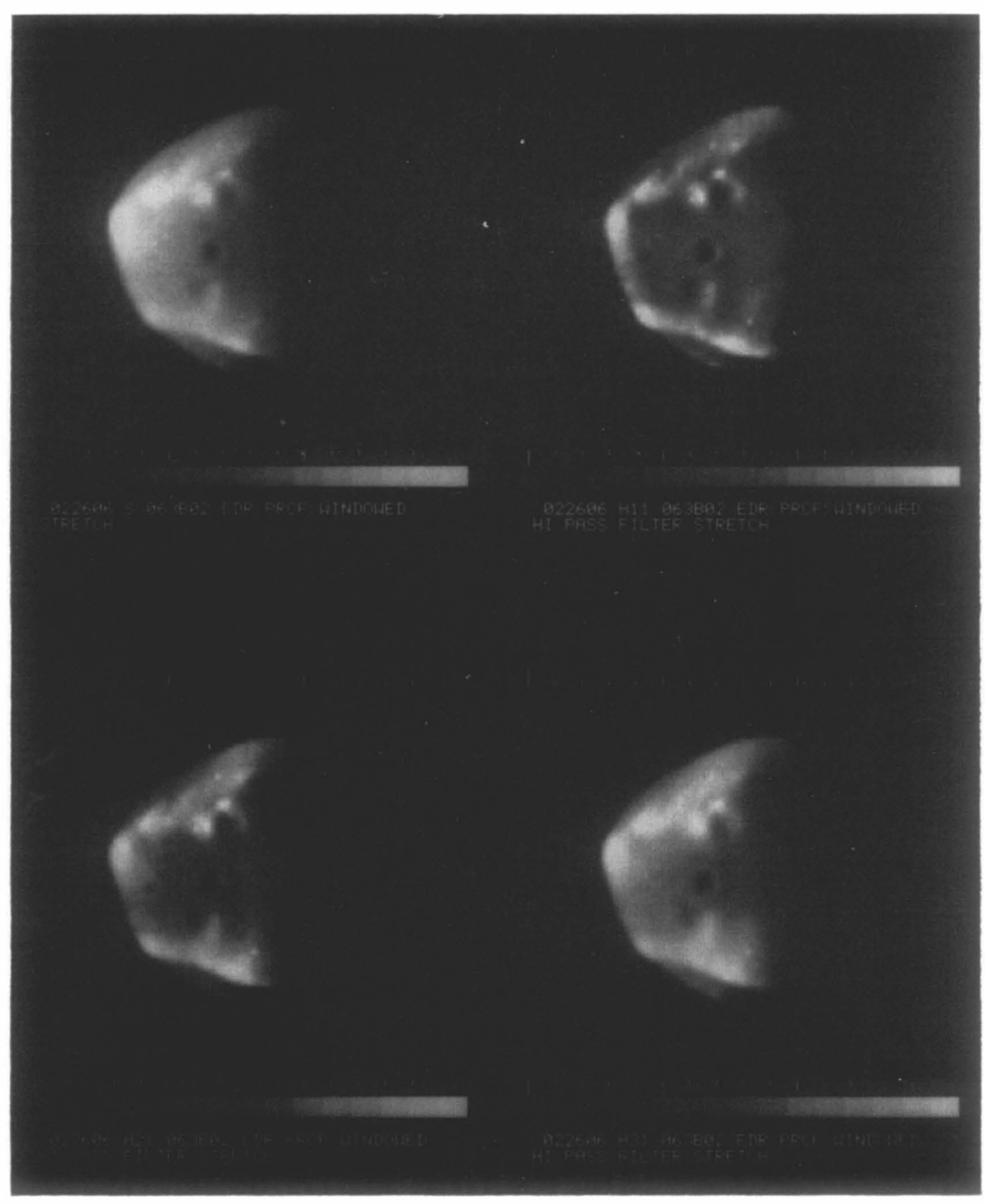


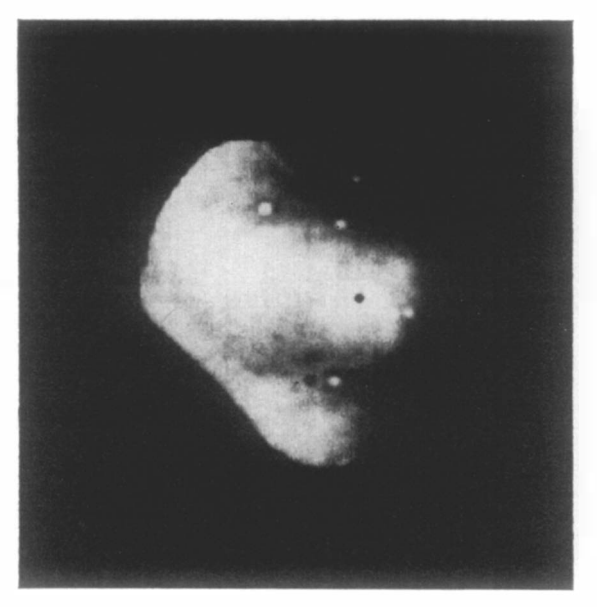
Fig. D2. Deimos. Revolution 63. DAS 03854630. Exposure = 48ms. I. Left: IPL 933/210148. Stretch. Mag $4\times$. Right: IPL 935/114431. High-pass filter and stretch. Mag $4\times$.



II. Phase = 73°. Range = 7770 km. $S/C = (13^{\circ}.5S, 7^{\circ}.3W)$. $SUN = (18^{\circ}.9S, 83^{\circ}.6W)$. $\Delta LAT = 40^{\circ}$; $\Delta LONG = 45^{\circ}$.



III. Stanford AI product STN GS01-022606.



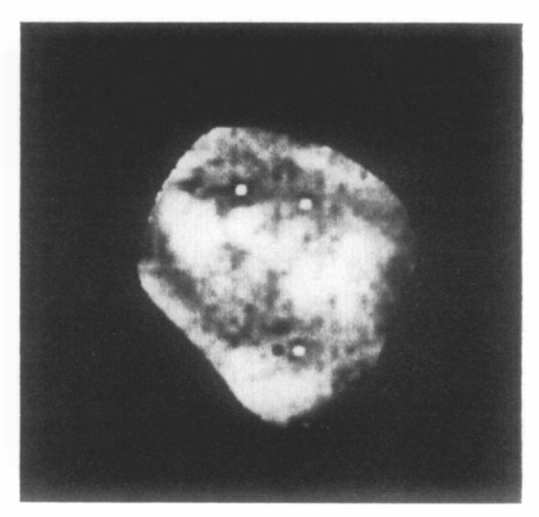
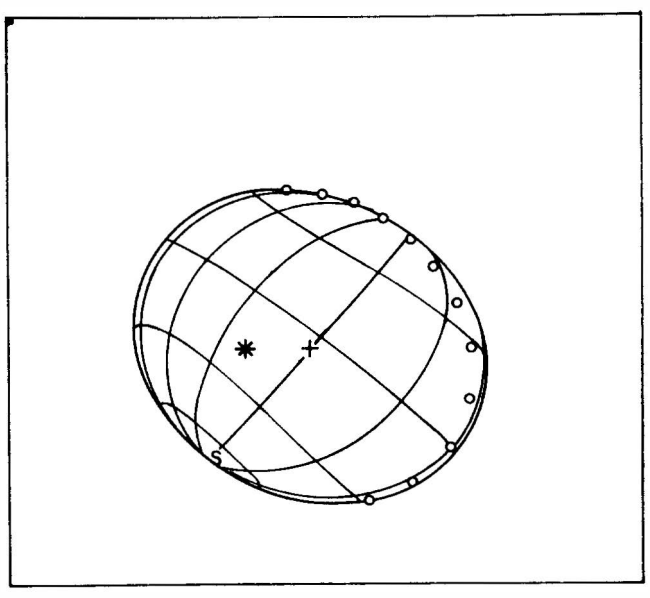
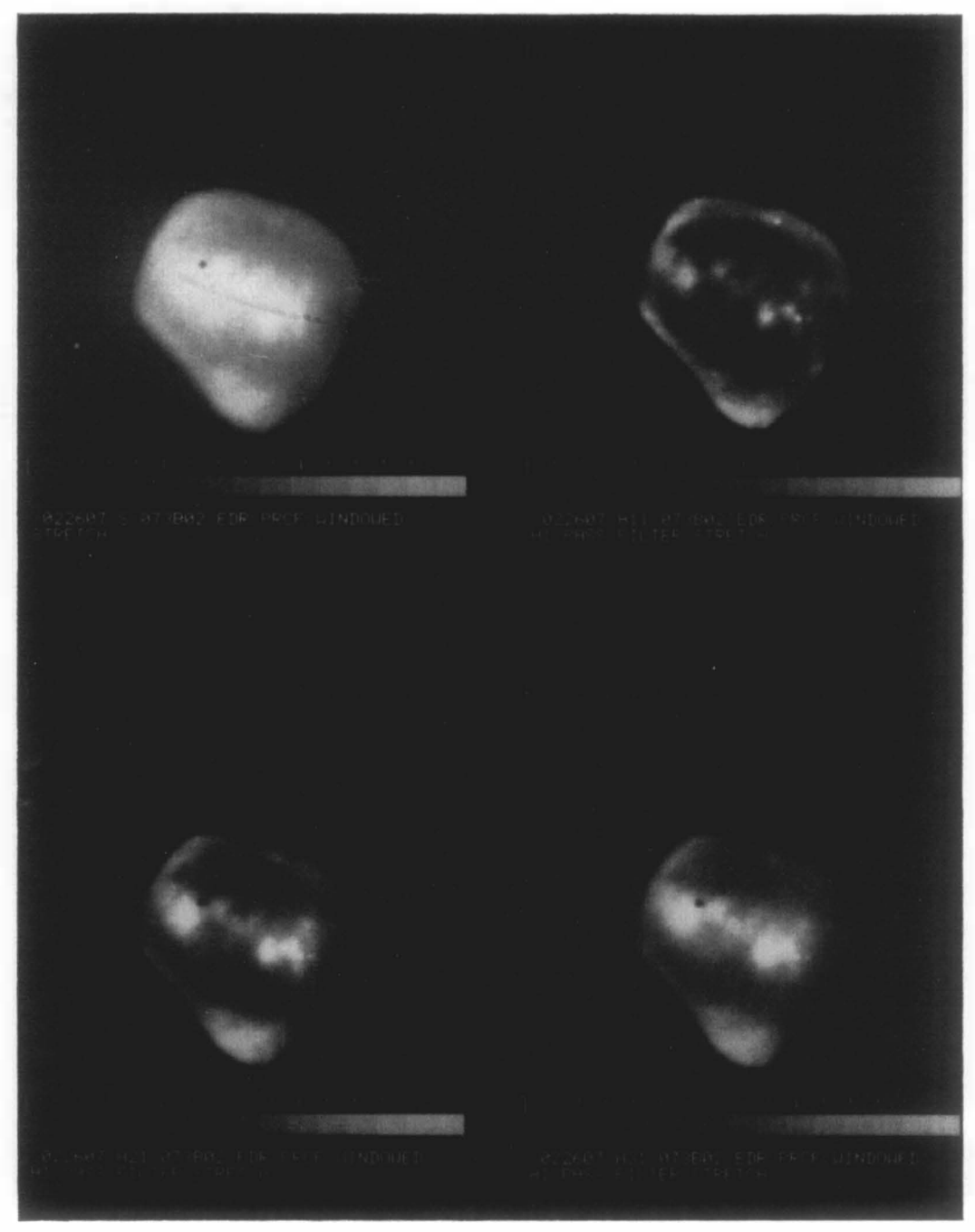


Fig. D3. Deimos. Revolution 73. DAS 04212610. Exposure = 24ms. I. Left: IPL 095905. Stretch. Mag $4\times$. Right: IPL 935/101703. High-pass filter and stretch. Mag $4\times$.



II. Phase = 22°. Range = 10070 km. $S/C = (4^{\circ}.5S, 40^{\circ}.6W)$. $SUN = (18^{\circ}S, 58^{\circ}.2W)$. $\Delta LAT = 30^{\circ}$; $\Delta LONG = 30^{\circ}$.



III. Stanford AI product STN GS01-022607.

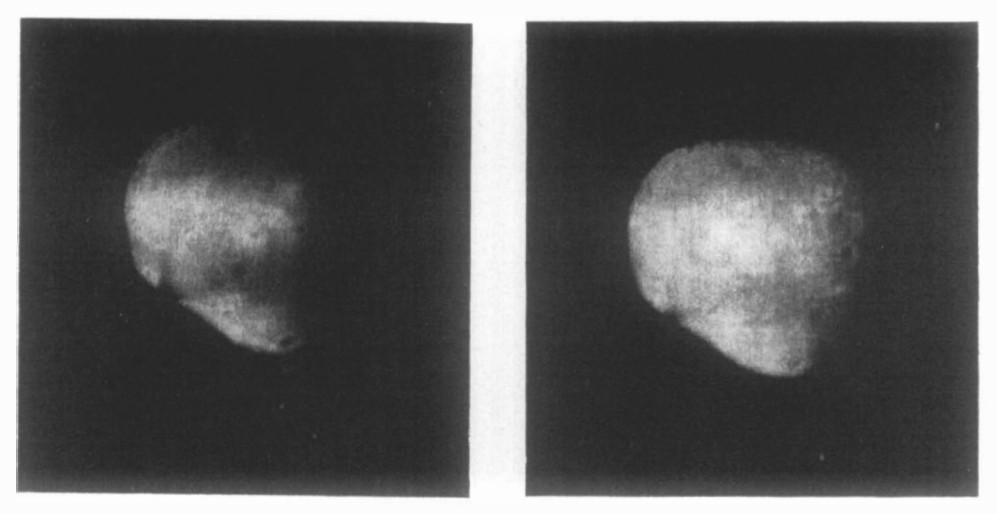
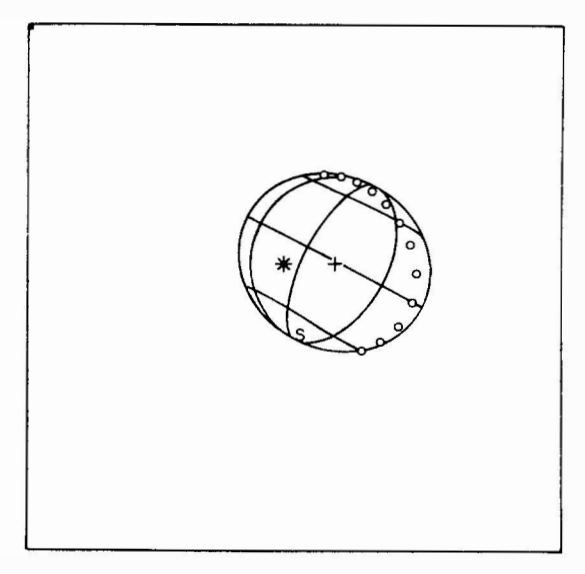
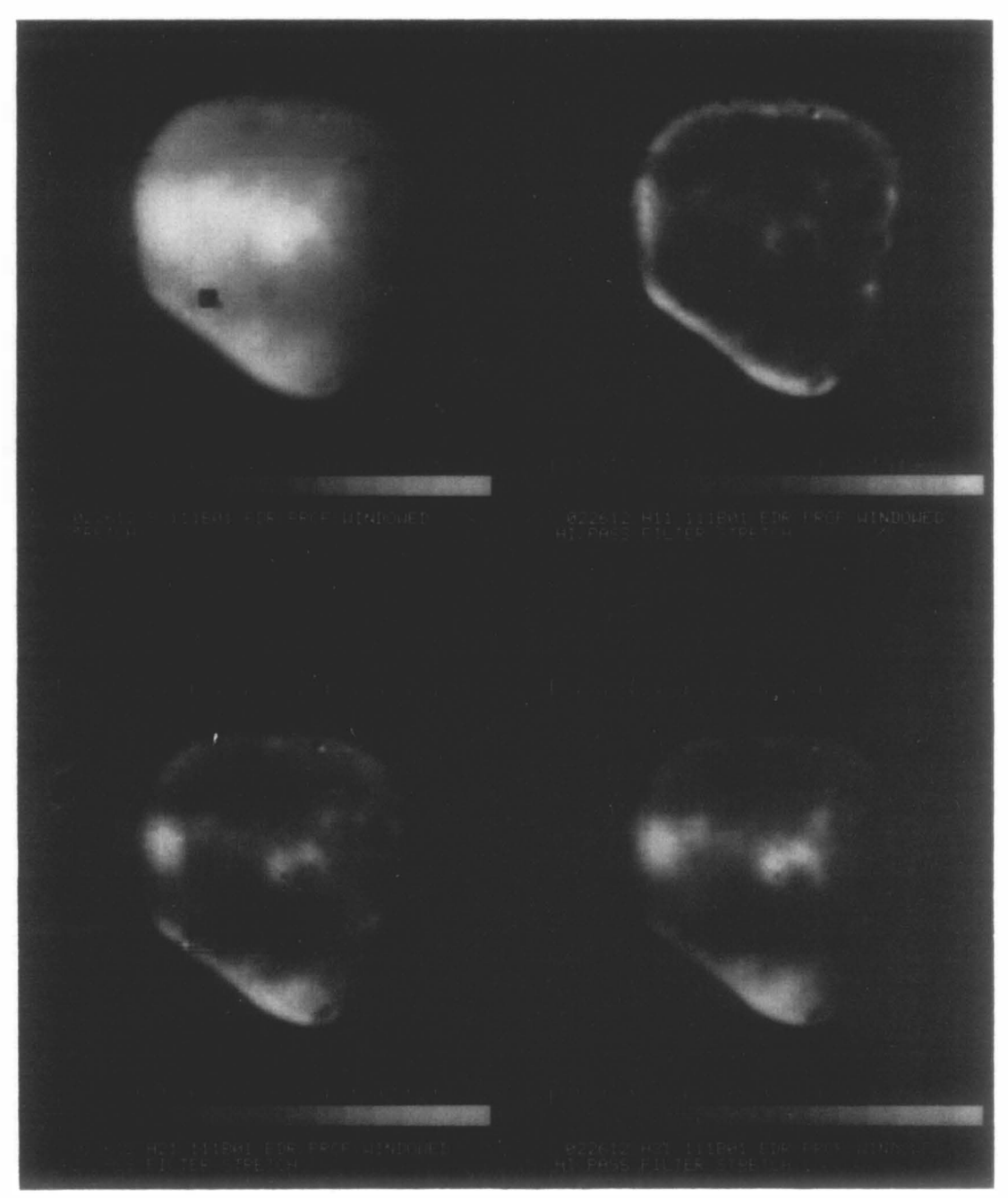


Fig. D4. Deimos. Revolution 111. DAS 05553383. Exposure = 48ms. I. Left: IPL 1792/063611 Stretch. Mag $4\times$. Right: IPL 1792/063344. Stretch. Mag $4\times$.



 $\begin{array}{ll} II. & Phase = 31^{\circ}. & Range = 7220\,km. & S/C = (1^{\circ}.l\,S, \\ 27^{\circ}.2\,W). & SUN = (14^{\circ}.6\,S, & 56^{\circ}.0\,W). & \varDelta LAT = 40^{\circ}; \\ \varDelta LONG = 45^{\circ}. & \end{array}$



III. Stanford AI product STNGS01-022612.

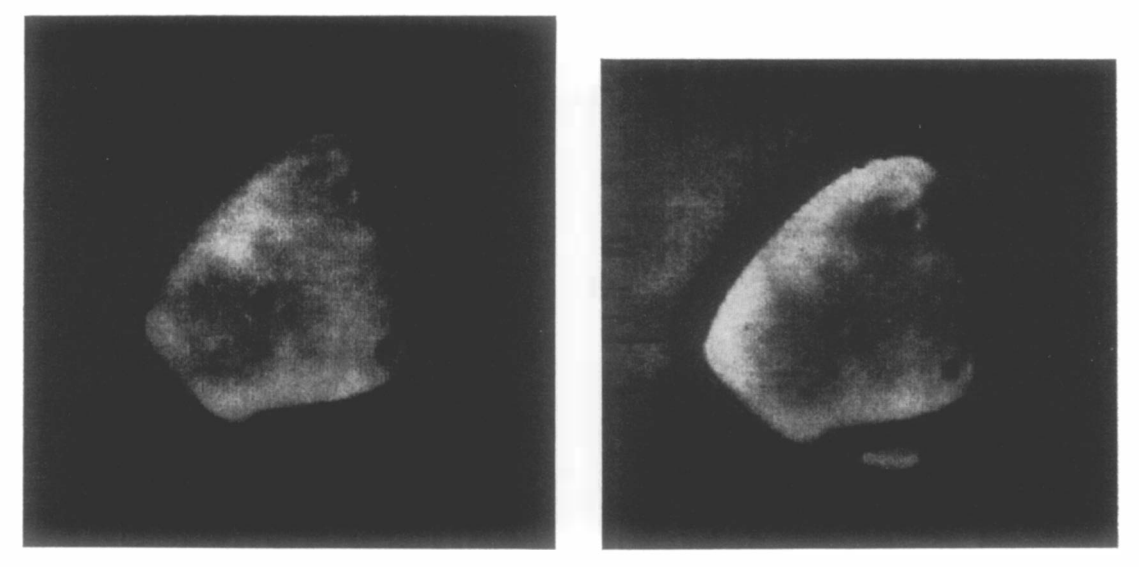
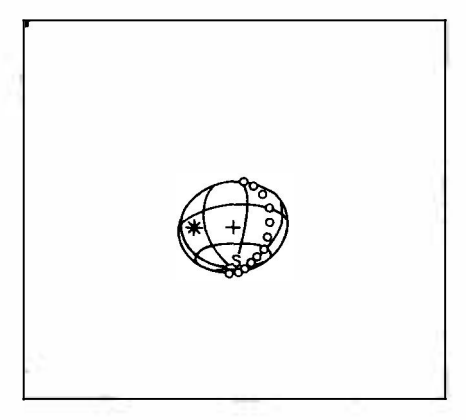
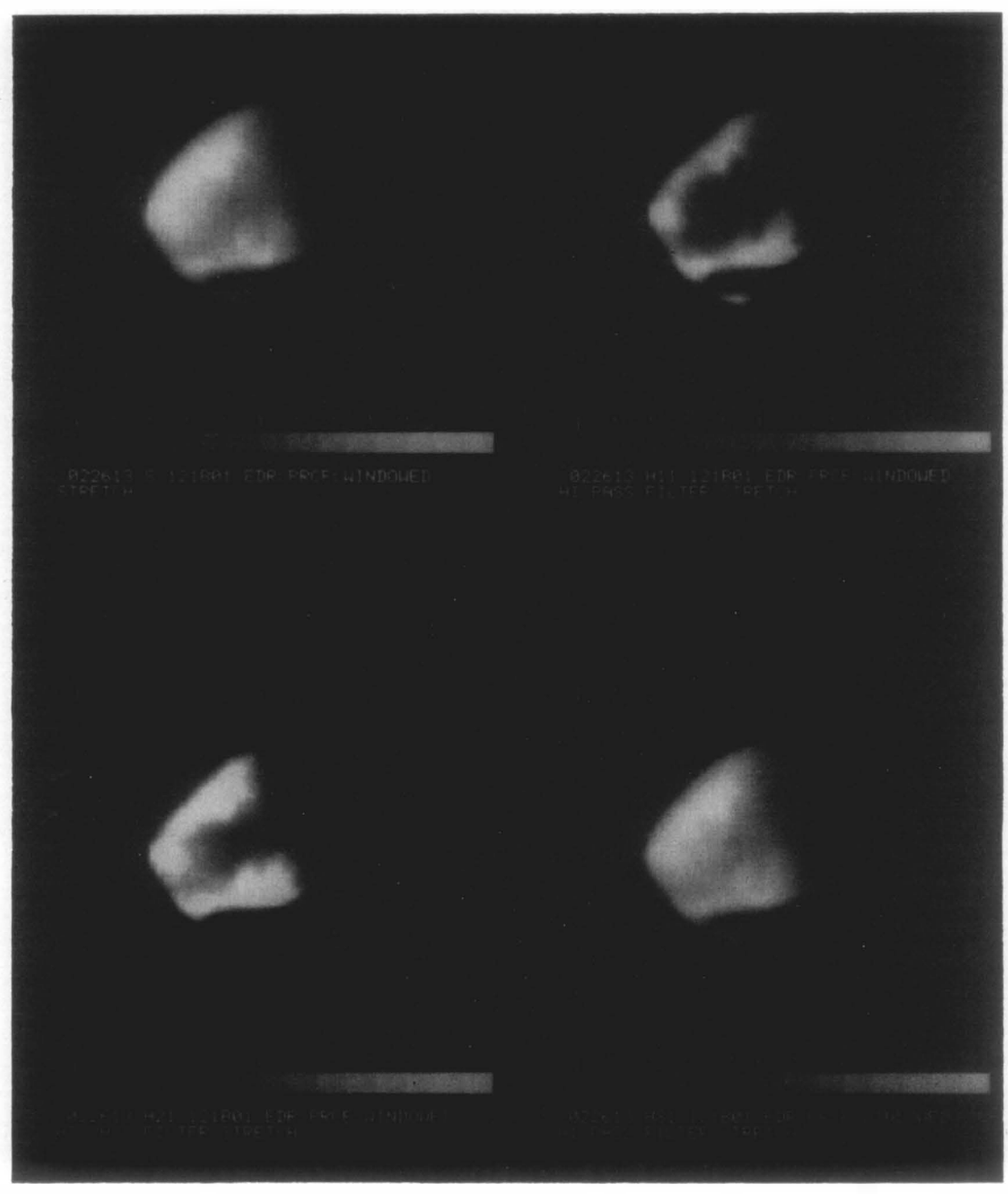


Fig. D5. Deimos. Revolution 121. DAS 05918713. Exposure = 48 ms. I. Left: IPL 315/201943. High-pass filter and stretch. Mag $4 \times$. Right: IPL 315/202327. High-pass filter and stretch. Mag $4 \times$.



II. Phase = 44°. Range = 15340 km. S/C = (21°.6S, 13°.2W). SUN = (13°.7S, 59°.3W). Δ LAT = 40°; Δ LONG = 45°.



III. Stanford AI product STN GS01-022613.

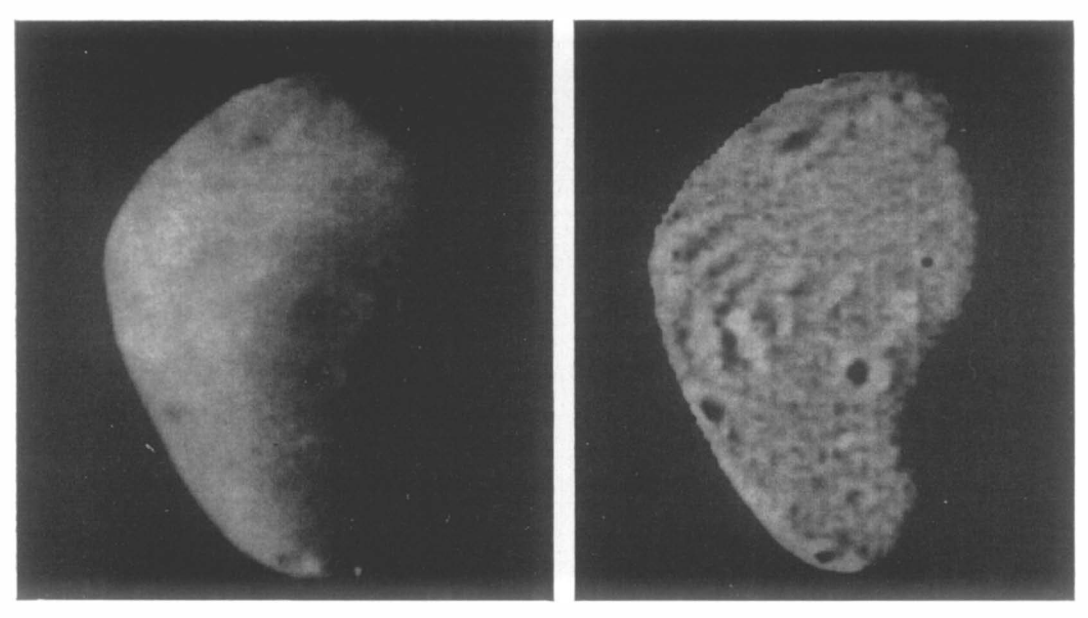
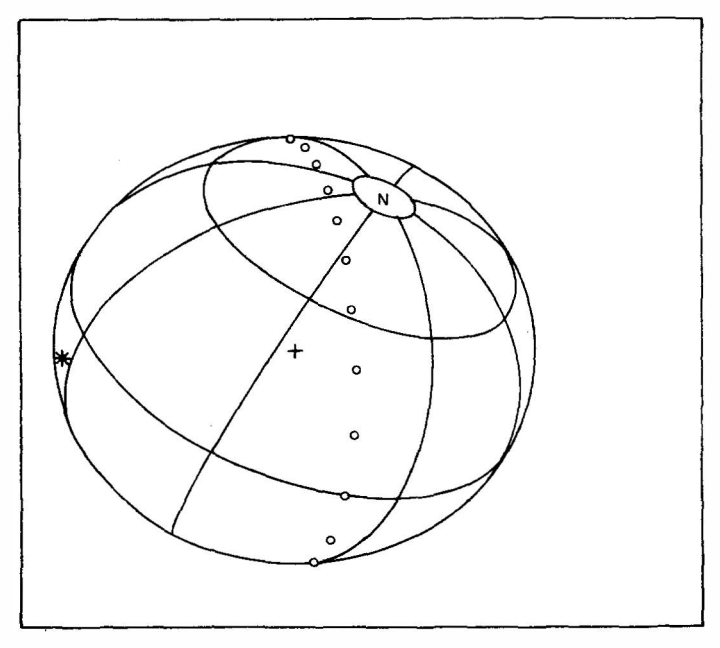
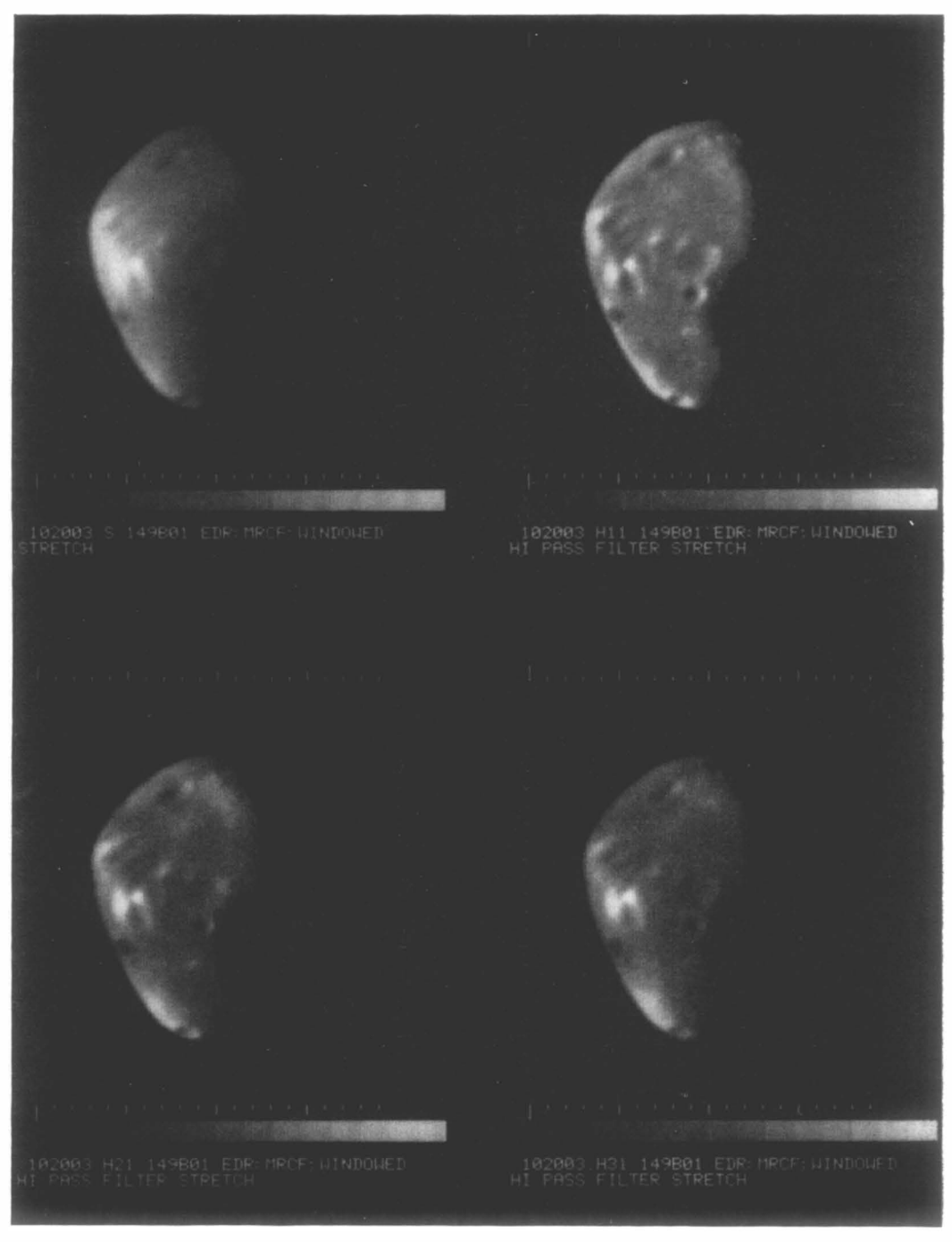


Fig. D6. Deimos. Revolution 149. DAS 06918173. Exposure = 48ms. I. Left: IPL 499/101033. High-pass filter and stretch. Mag $4\times$. Right: IPL 499/101518. High-pass filter and stretch. Mag $4\times$.

 a Note: The prominent round crater near the terminator is Swift; the larger more subdued crater immediately above it is Voltaire.



II. Phase = 65°. Range = 5490 km. S/C = (26°.9 N, 355°.5 W). SUN = (10°.8 S, 50°.4 W). Δ LAT = 40°; Δ LONG = 45°.



III. Stanford AI product STN GS01-102003.

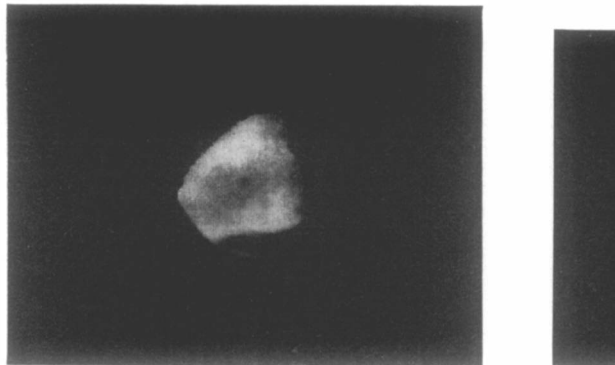
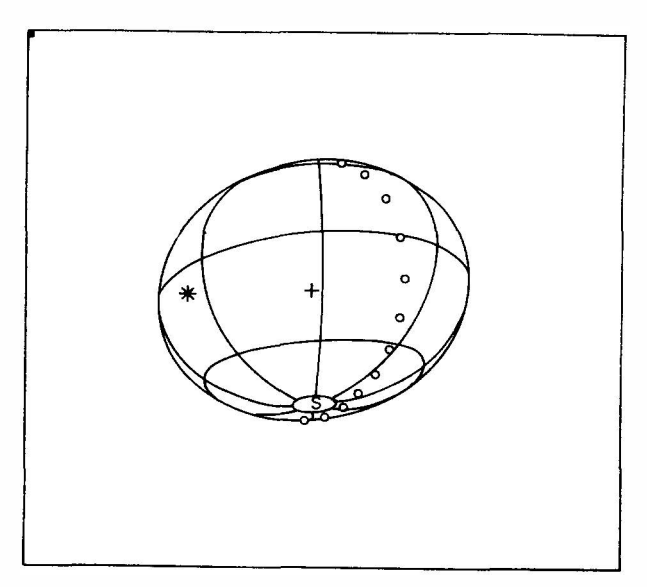
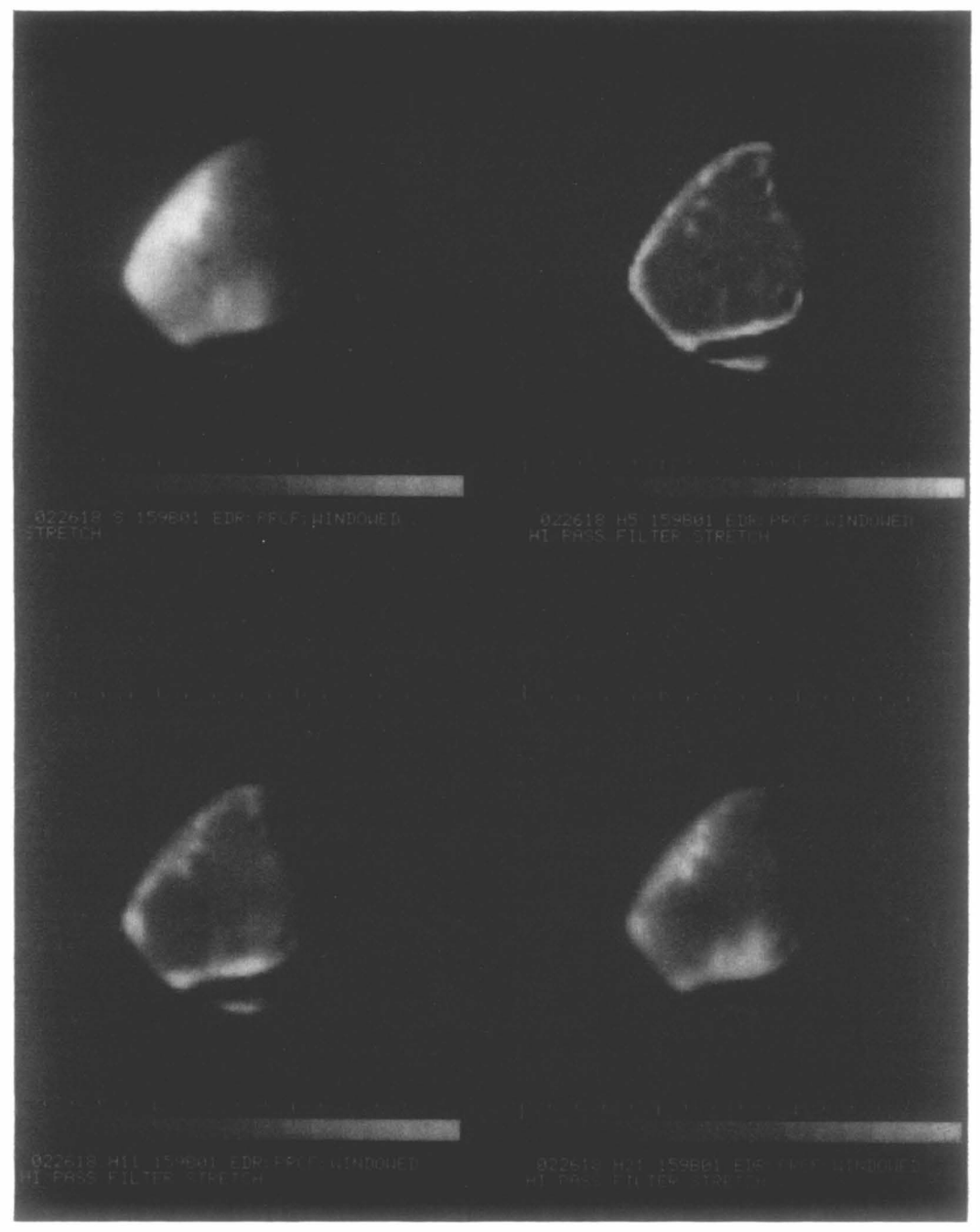




Fig. D7. Deimos. Revolution 159. DAS 07283433. Exposure = 48ms. I. Left: IPL 1111/175405. High-pass filter and stretch. Mag $4\times$. Right: IPL 1111/214305. High-pass filter and stretch. Mag $4\times$.



II. Phase = 51°. Range = $10060\,\mathrm{km}$. S/C = $(20^\circ.0\,\mathrm{S}, 3^\circ.0\,\mathrm{W})$. SUN = $(9^\circ.9\,\mathrm{S}, 54^\circ.6\,\mathrm{W})$. $\Delta\mathrm{LAT} = 40^\circ$; $\Delta\mathrm{LONG} = 45^\circ$.



III. Stanford AI product STN GS01-022618.

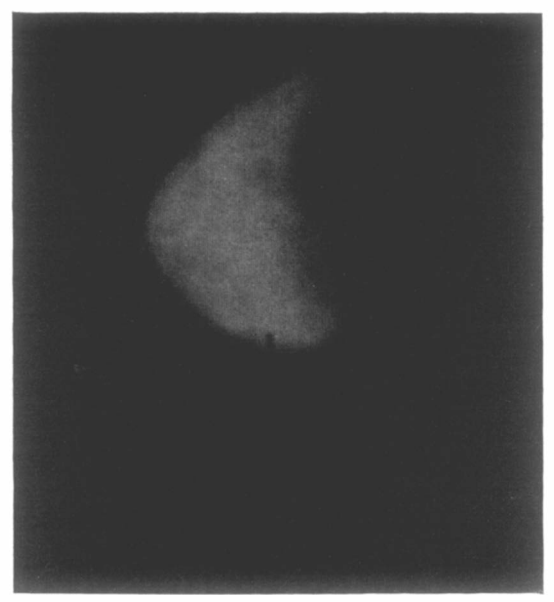
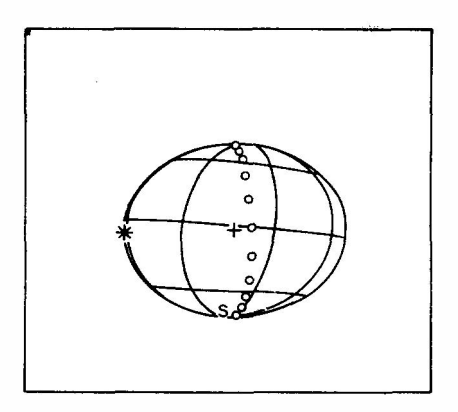
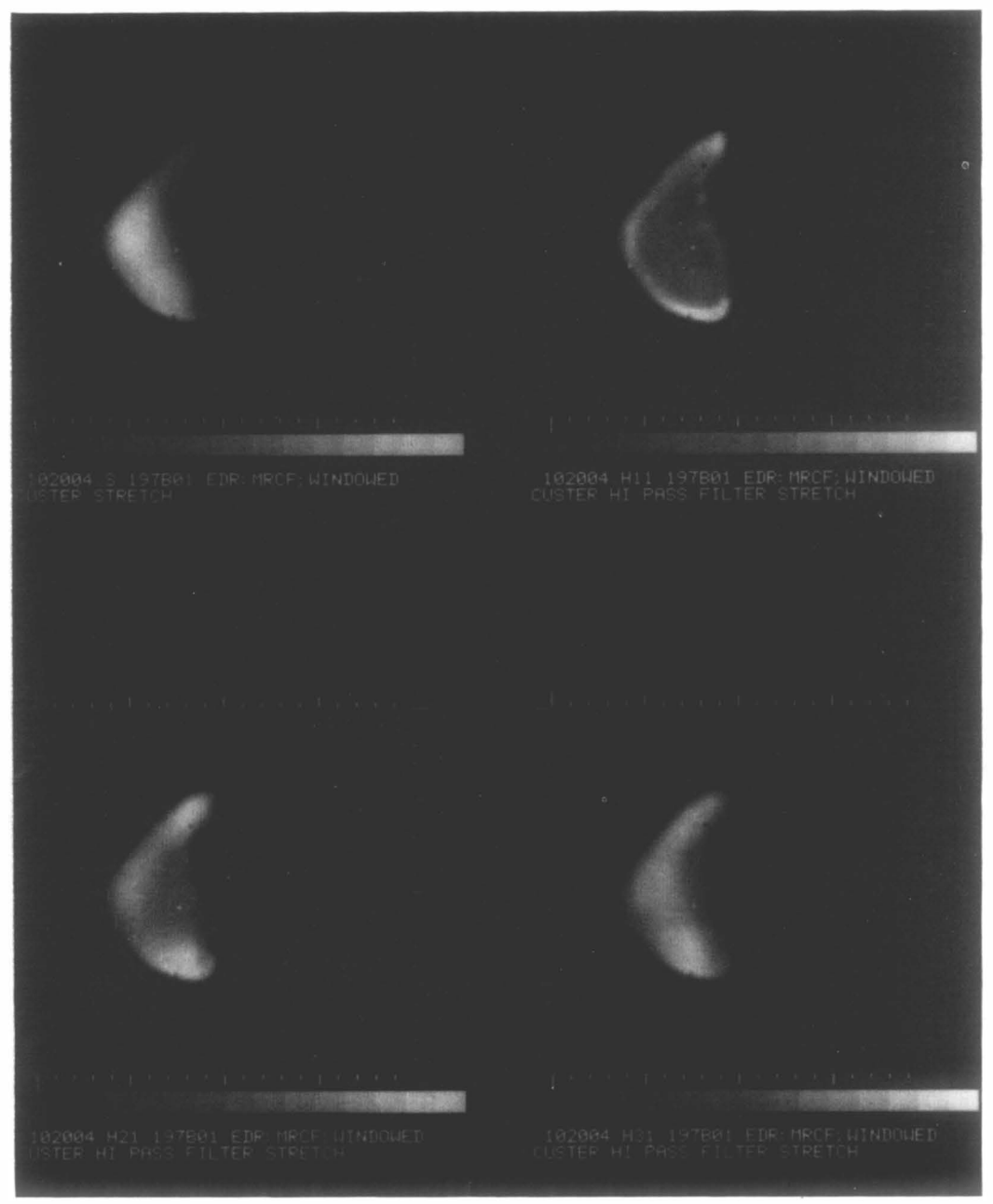


Fig. D8. Deimos. Revolution 197. DAS 08647669. Exposure = 192ms. I. IPL 1293/001340. Stretch. Mag $4 \times .a$

^a Note: Intentionally overexposed.



II. Phase = 73°. Range = 7380 km. S/C = (2°.1 S, 335°.1 W). SUN = (6°.0 S, 48°.5 W). Δ LAT = 40°; Δ LONG = 45°.



III. Stanford AI product GS01-102004.

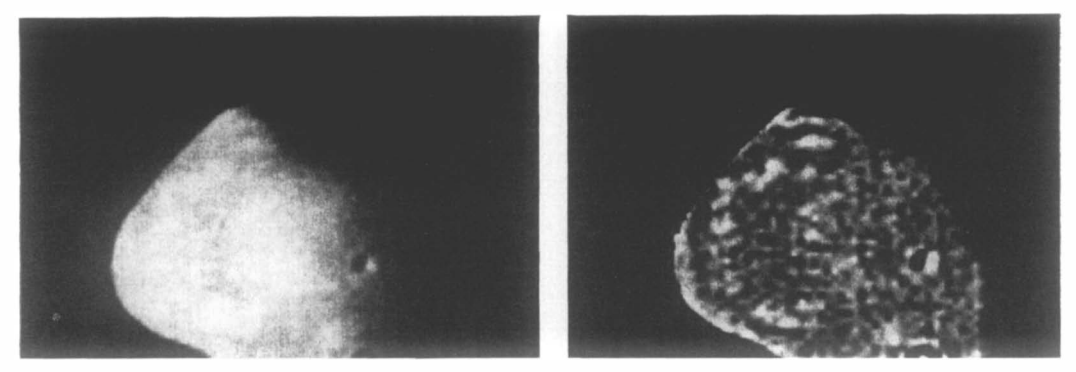
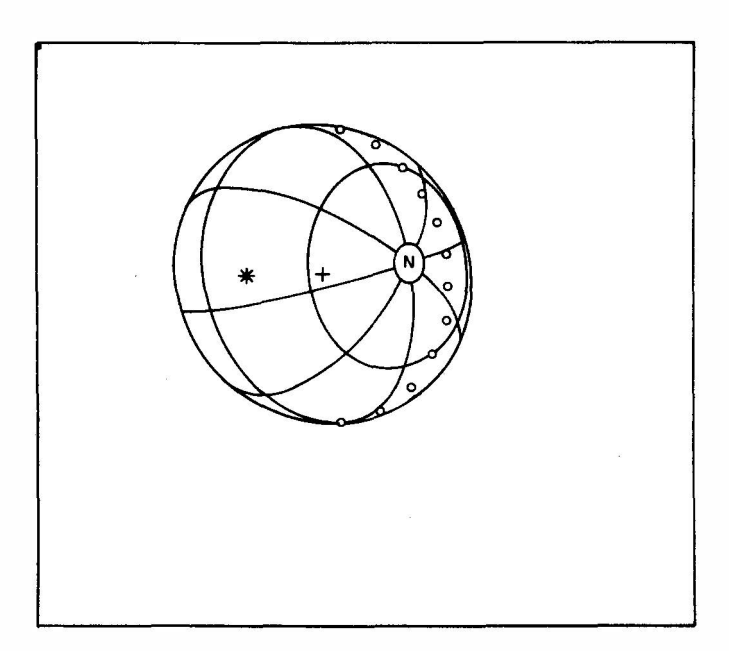
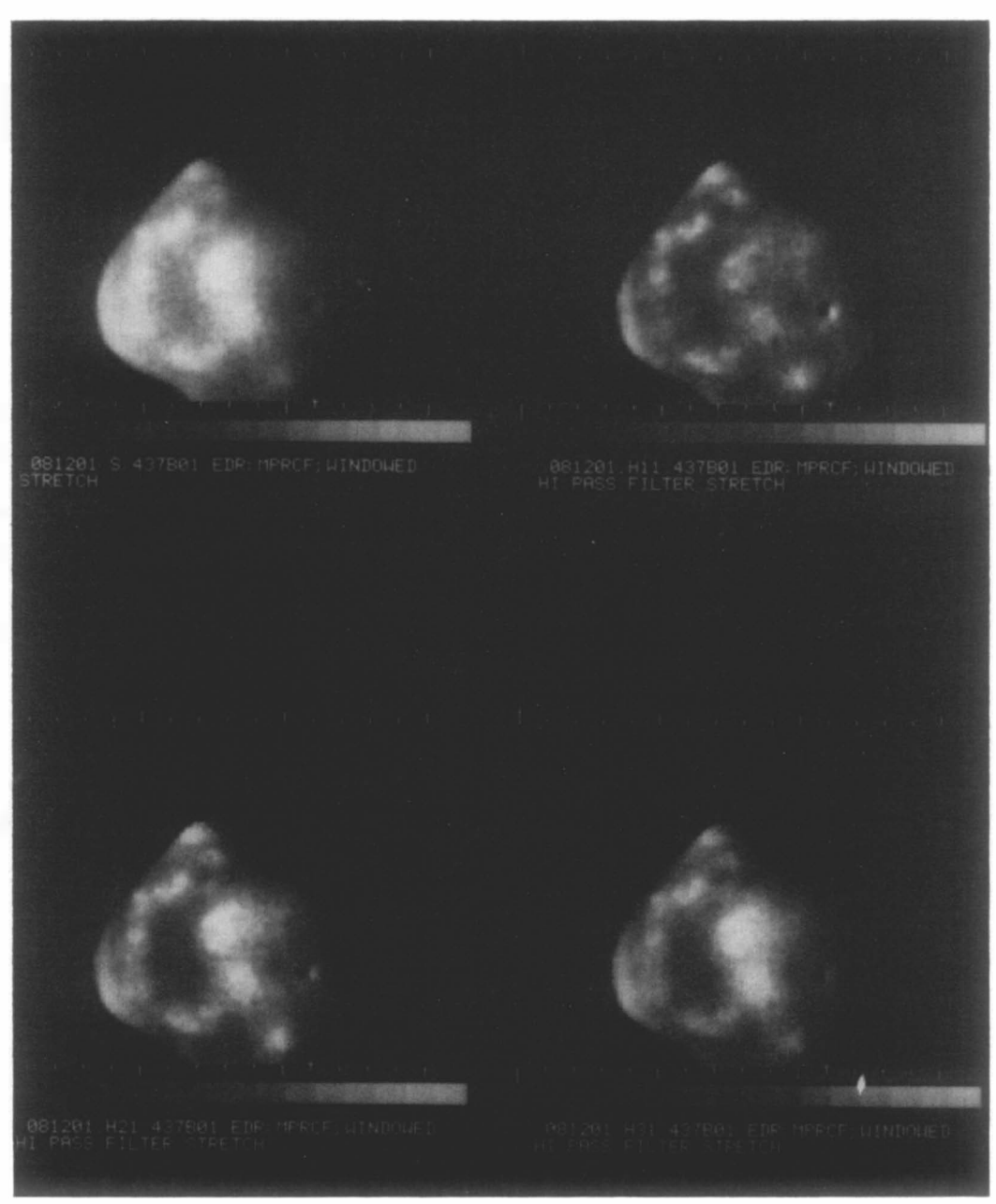


Fig. D9. Deimos. Revolution 437. DAS 11994754. Exposure = 24ms. I. Left: IPL 561/182746. Stretch. Mag $4\times$. Right: IPL 561/183051. High-pass filter and stretch. Mag $4\times$.



II. Phase = 28°. Range = 8590 km. S/C = (45°.6N, 323°.3W). SUN = (17°.5N, 326°.5W). Δ LAT = 40°; Δ LONG = 45°.



III. Stanford AI product GS01-081201.

 $Section\ 2: Catalog\ of\ Phobos\ Coverage$



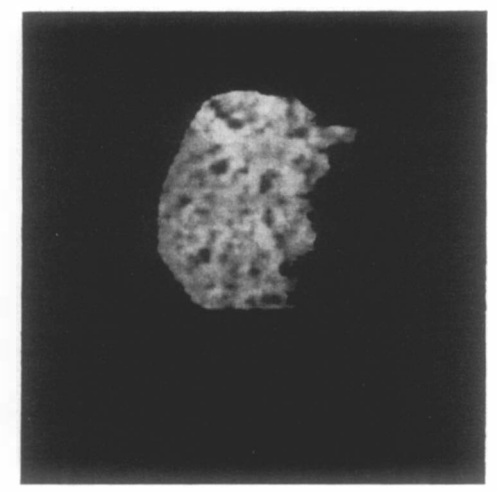
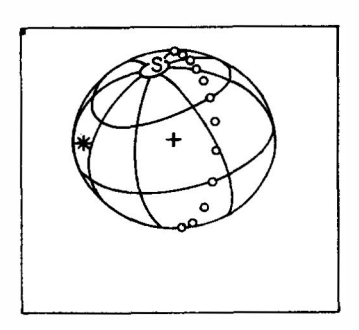
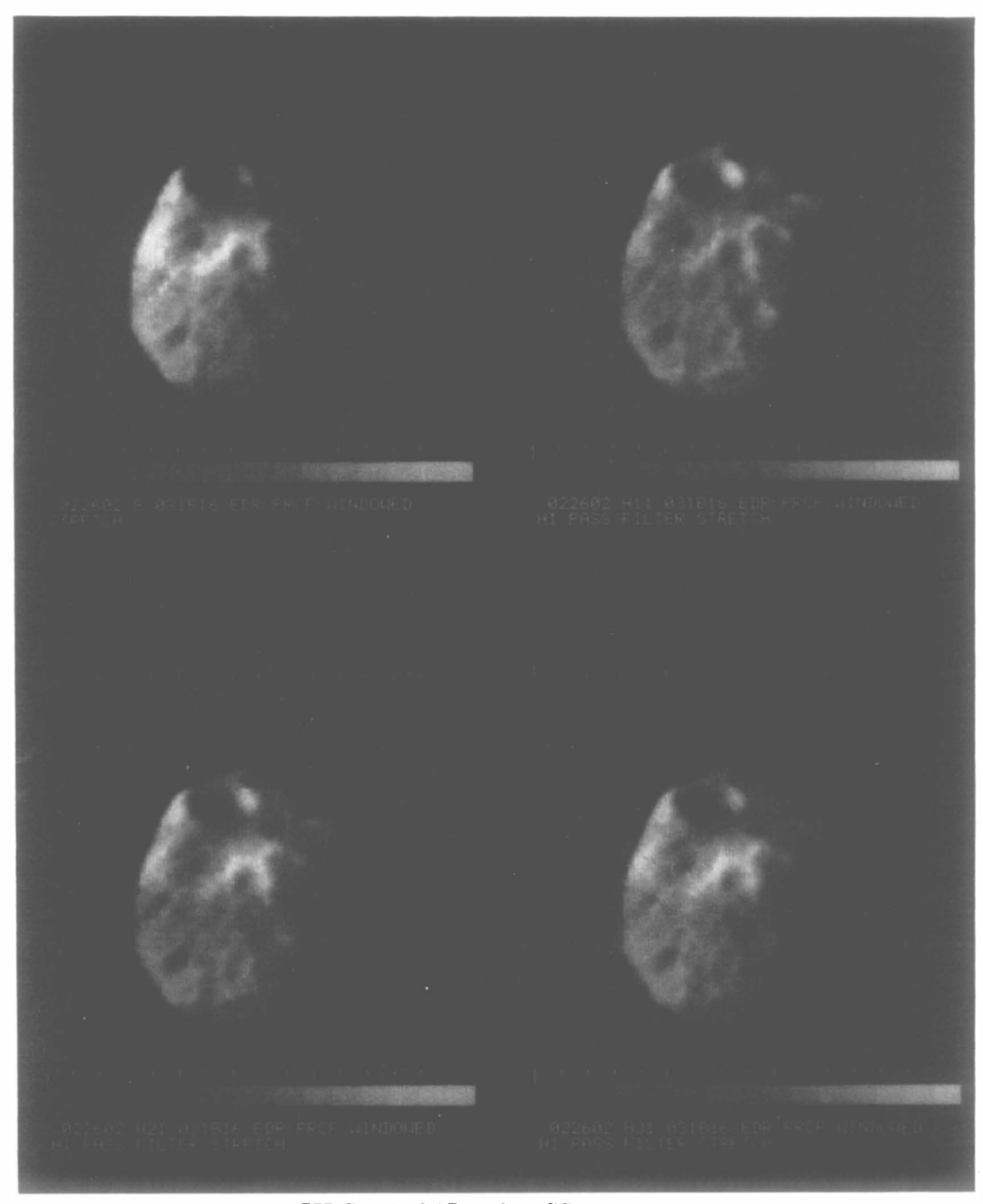


Fig. P1. Phobos. Revolution 31. DAS 02711175. Exposure = 24ms. I. Left: IPL 792/220312. Stretch. Mag $4\times$. Right: IPL 935/182504. High-pass filter and stretch. Mag $4\times$.

^a Note: The prominent crater at top is Hall.



II. Phase = 76°. Range = 14530 km. S/C = (26°.6 S, 340°.9 W). SUN = (21°.0 S, 256°.6 W). Δ LAT = 40°; Δ LONG = 45°.



III. Stanford AI product GS01-022602.



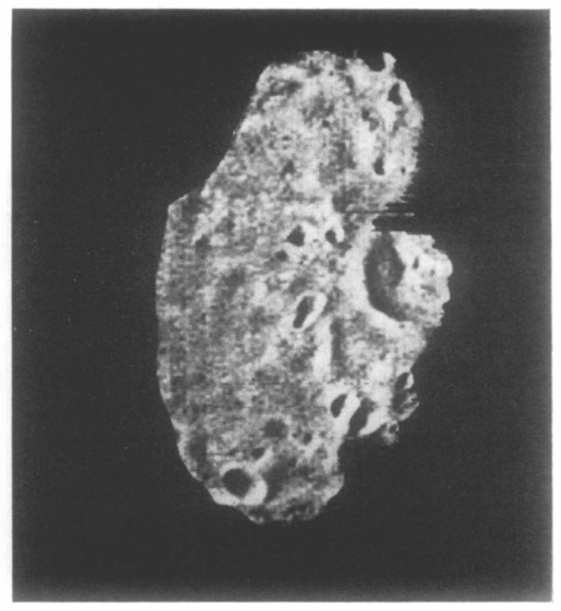
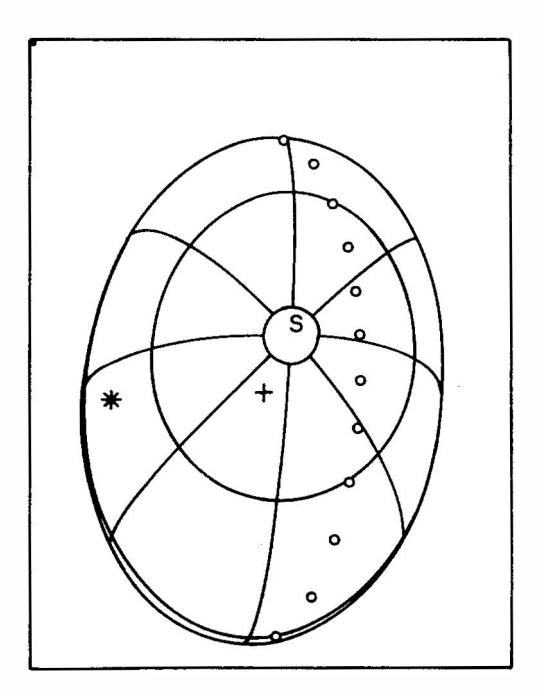
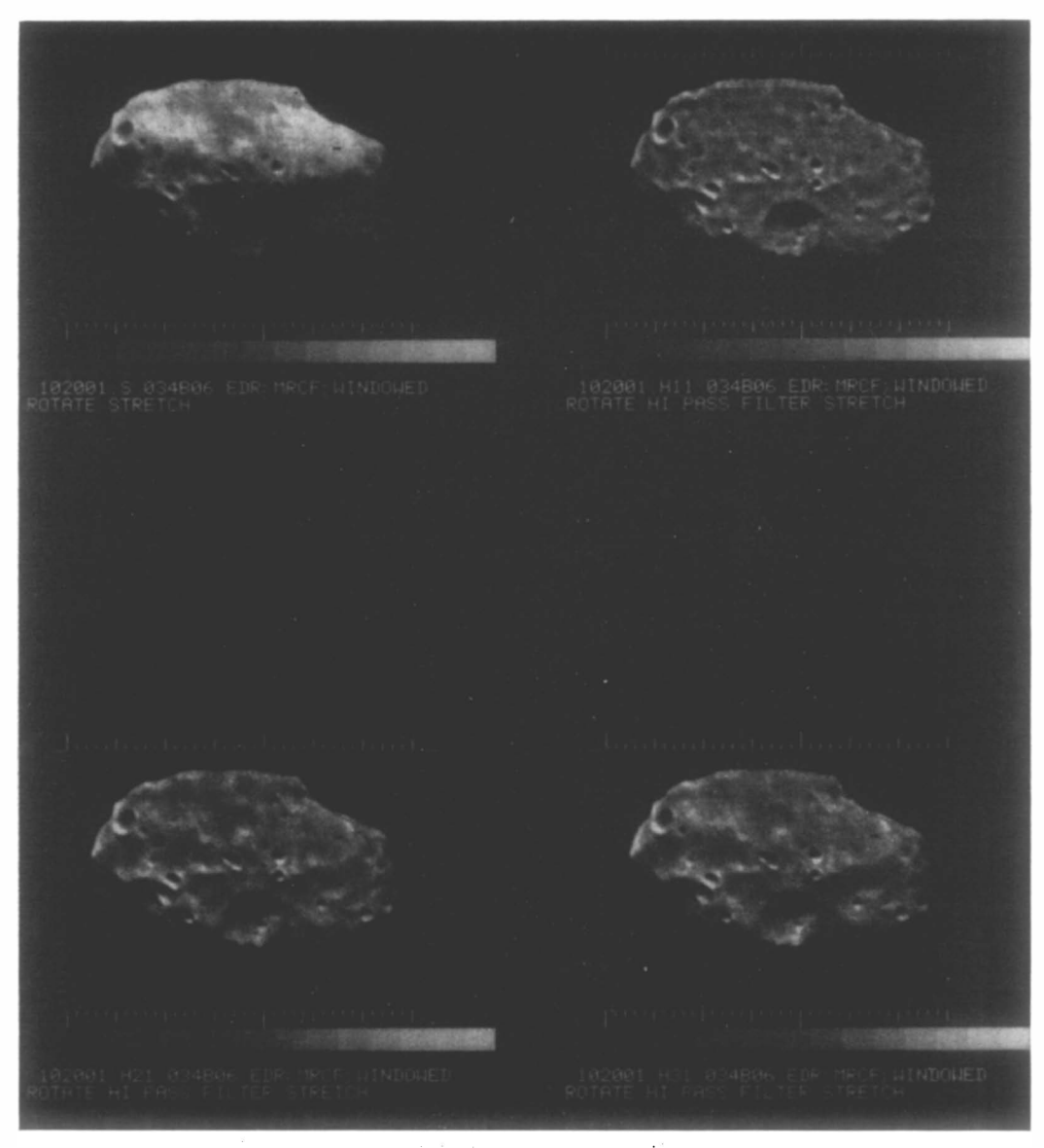


Fig. P2. Phobos. Revolution 34. DAS 02816315. Exposure = 24ms. I. Left: IPL 820/002025. Stretch. Mag $3\times$. Right: IPL 935/104056. High-pass filter and stretch. Mag $4\times$.

" Note: The large crater near the terminator is Hall.



II. Phase = 59°. Range = 5710km. S/C = (70°.9 S, 159°.8 W). SUN = (21°.2 S, 103°.2 W). Δ LAT = 40°; Δ LONG = 45°.



III. Stanford AI product GS01-102001.

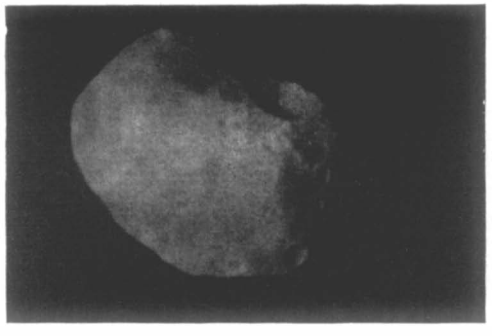
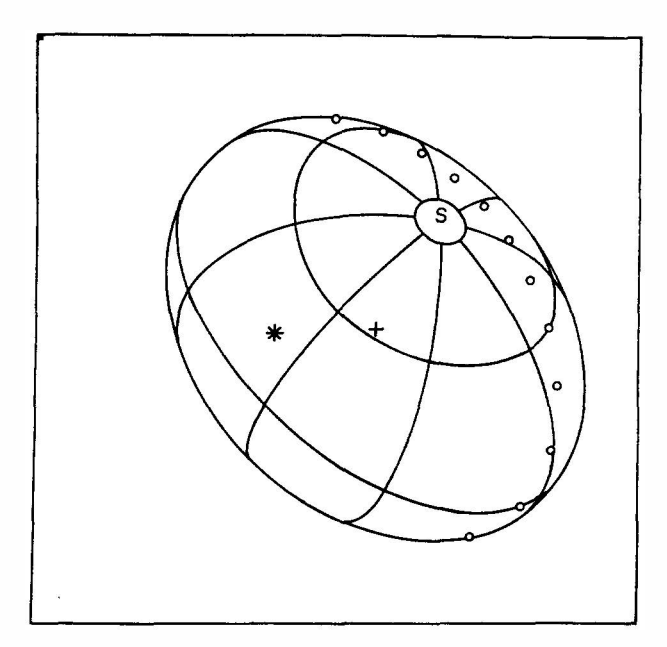




Fig. P3. Phobos. Revolution 41. DAS 03067340. Exposure = 24ms. I. Left: IPL 042039. Stretch. Right: IPL 183859. Stretch.

a Note: The large crater at top is Hall.



II. Phase = 34°. Range = 7270km. S/C = (43°.0S, 108°.2W). SUN = (20°.3S, 77°.5W). Δ LAT = 40°; Δ LONG = 45°.

III. No Stanford product.



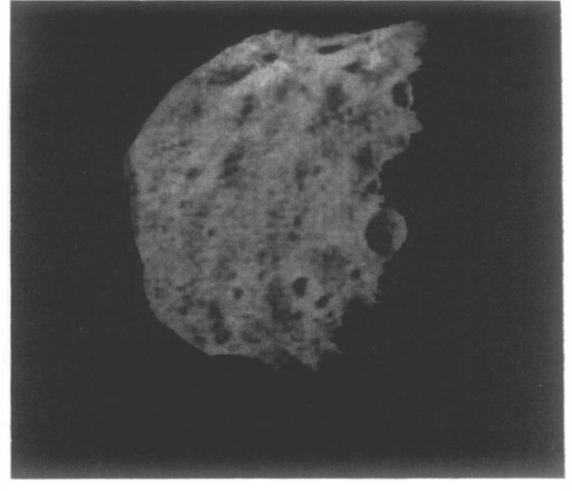
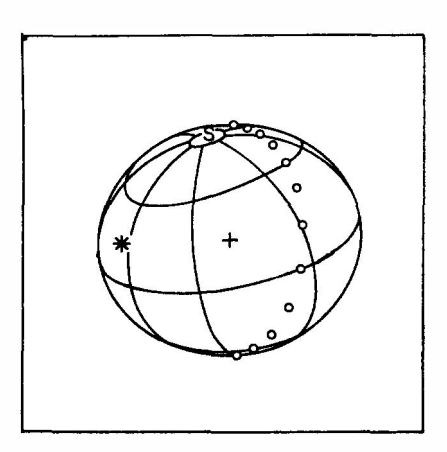
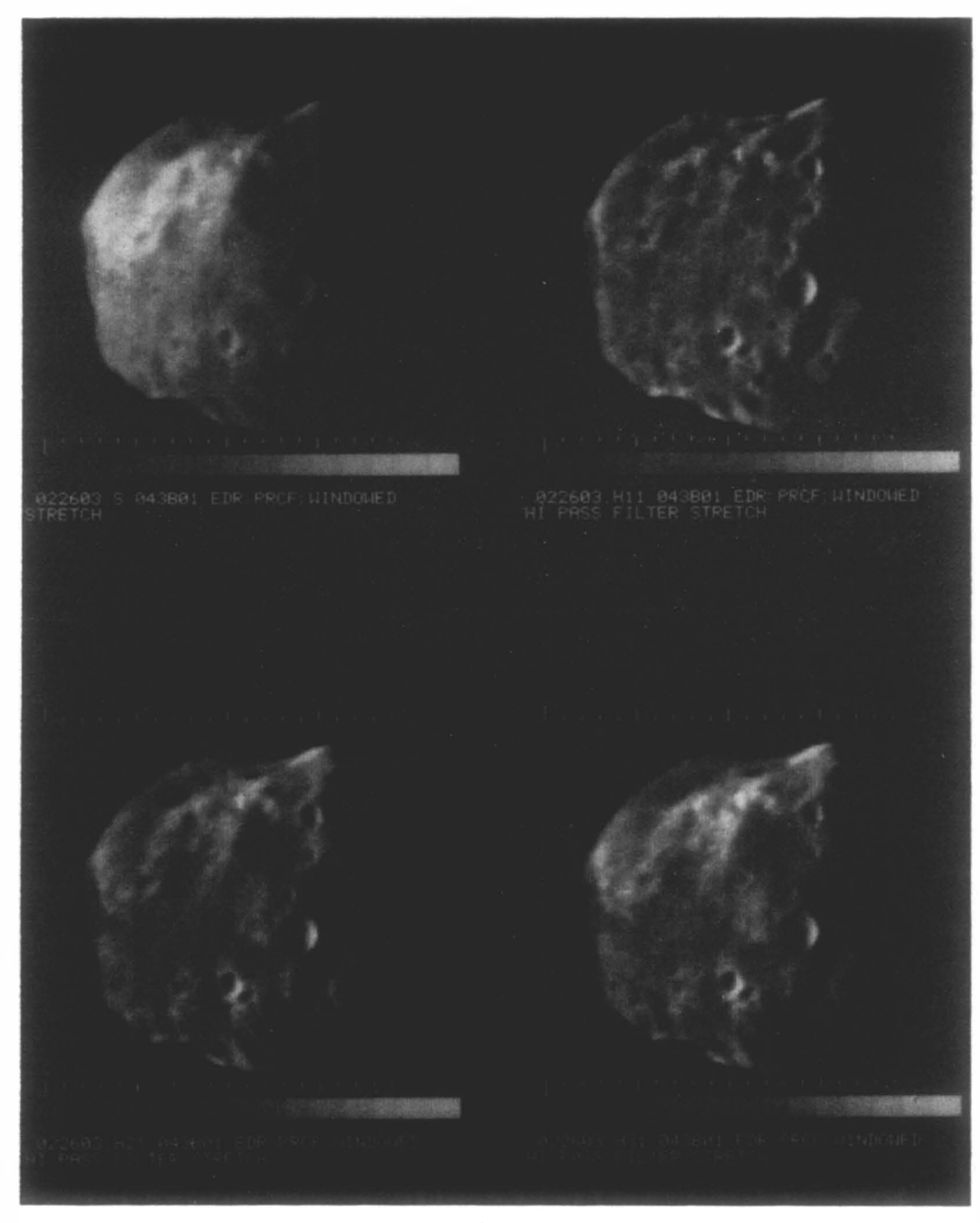


Fig. P4. Phobos. Revolution 43. DAS 03136570. Exposure = 24ms. I. Left: IPL 831/224914. Stretch. Mag $3\times$. Right: IPL 936/023029. High-pass filter and stretch. Mag $4\times$.

" Note: The crater Hall is on the limb at top.



II. Phase = 66°. Range = 7380km. S/C = (18°.6S, 152°.1 W). SUN = (20°.2S, 82°.1 W). Δ LAT = 40°; Δ LONG = 45°.



III. Stanford AI product GS01-022603.



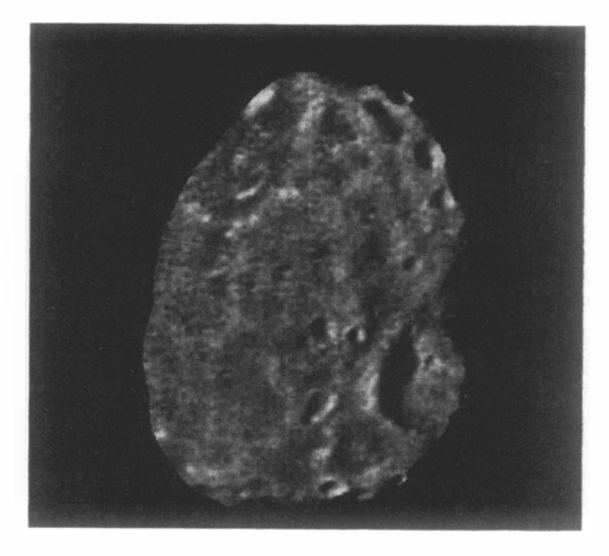
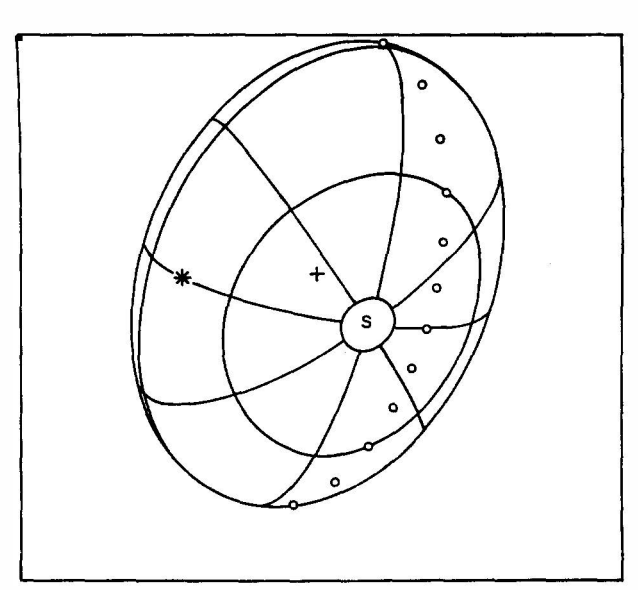
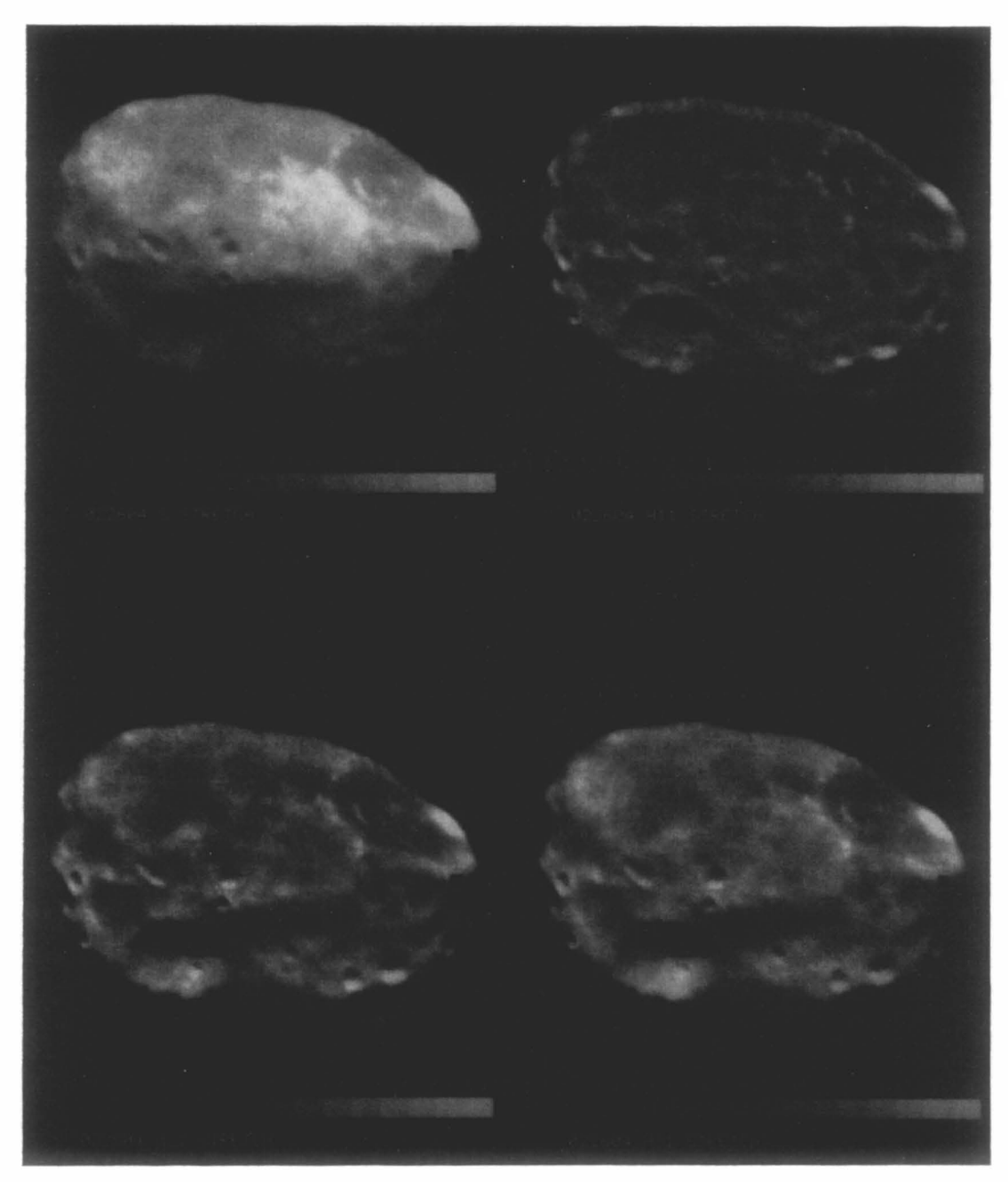


Fig. P5. Phobos. Revolution 48. DAS 03320880. Exposure = 24ms. I. Left: IPL 830/002836. Stretch. Mag $3\times$. Right: IPL 936/145516. High-pass filter and stretch. Mag $4\times$.

" Note: Hall is at lower right next to the terminator.



II. Phase = 49°. Range = 7160 km. S/C = (62°.2 S, 54°.7 W). SUN = (19°.9 S, 90°.0 W). Δ LAT = 40°; Δ LONG = 45°.



III. Stanford AI product GS01-022604.

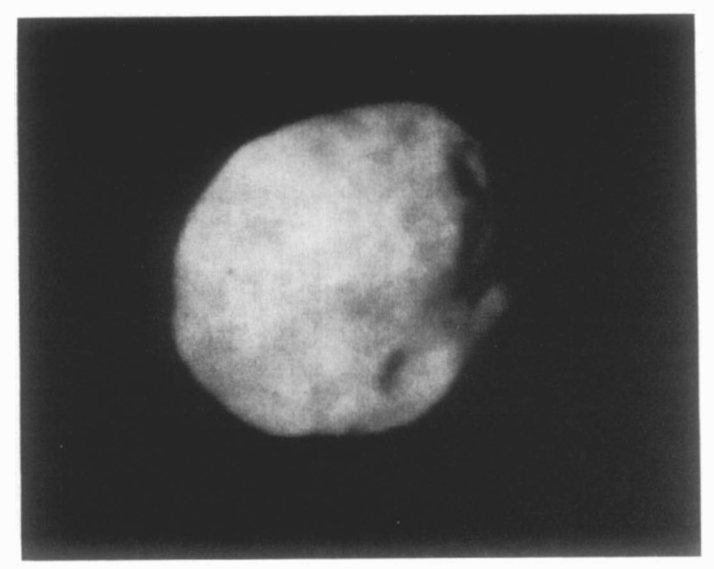
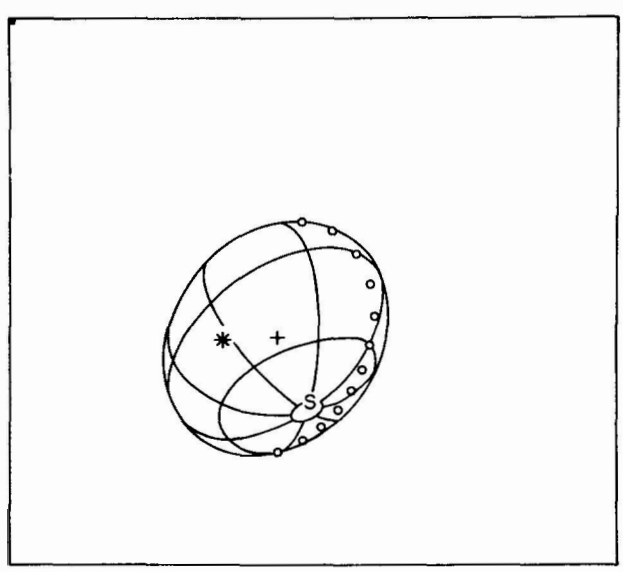
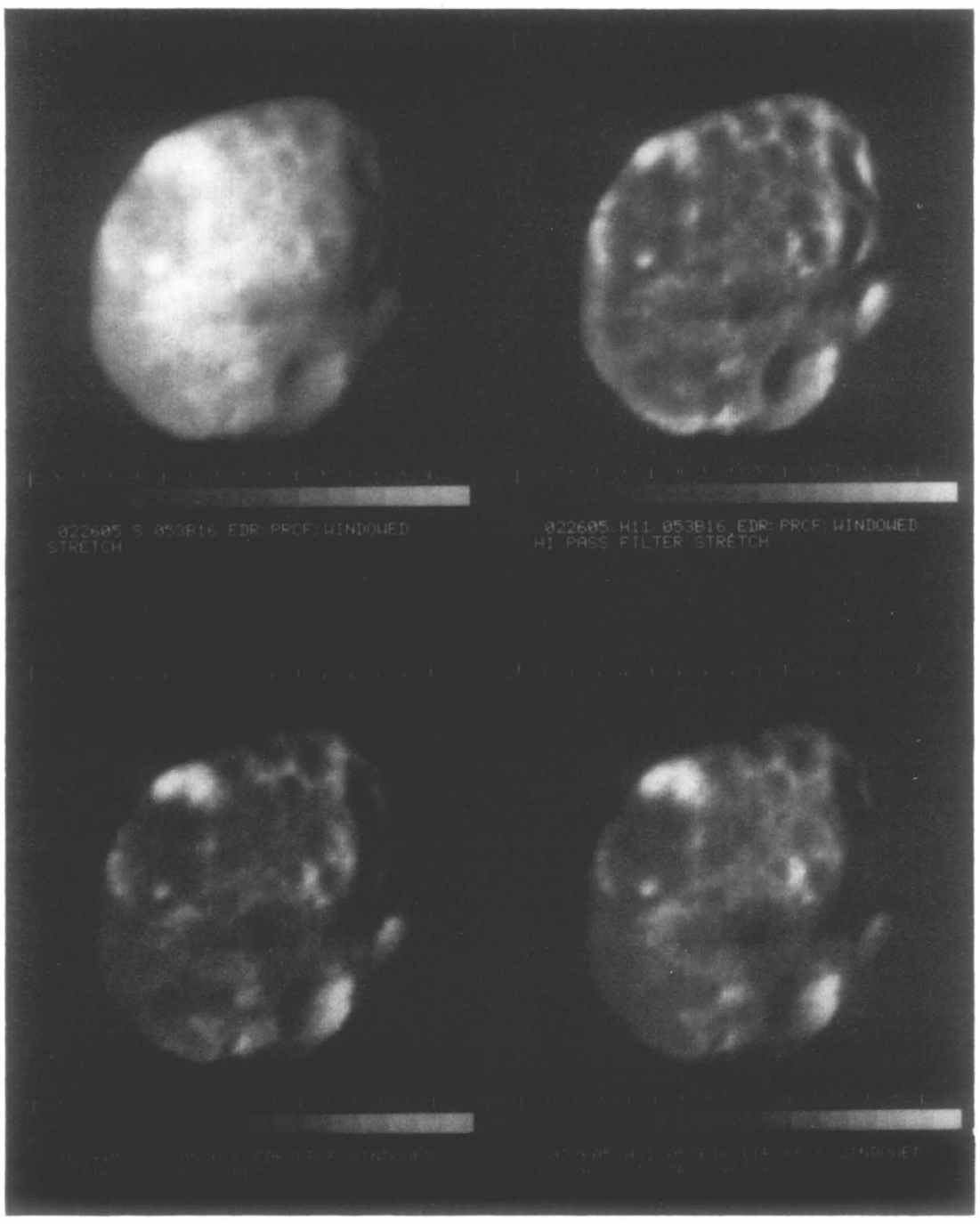


Fig. P6. Phobos. Revolution 53. DAS 035019770. Exposure = 24ms. I. IPL 573/230556. Stretch. Mag $4\times$.

" Note: Hall is at lower right next to the terminator.



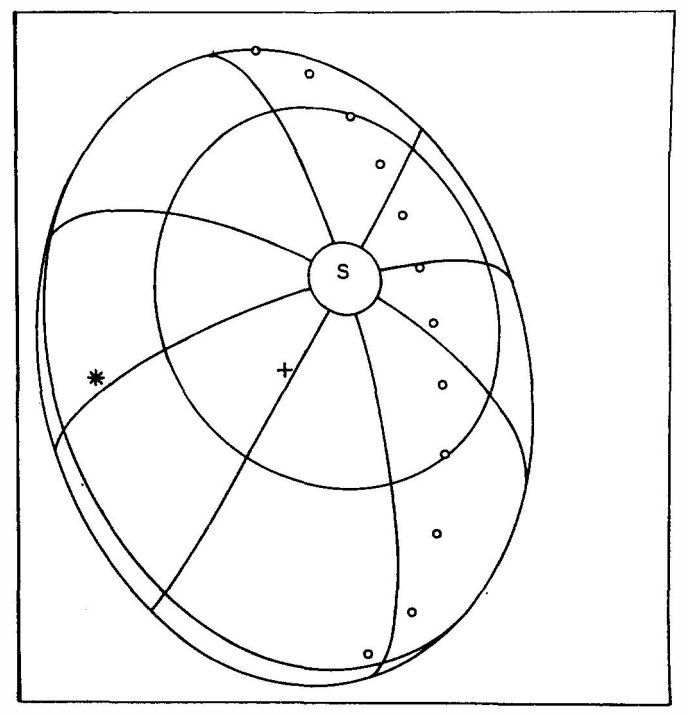
II. Phase = 26°. Range = 11880km. S/C = (32°.1 S, 23°.9 W). SUN = (18°.9 S, 49°.0 W). Δ LAT = 40°; Δ LONG = 45°.



III. Stanford AI product GS01-022605.



Fig. P7. Phobos. Revolution 57. DAS 03642250. Exposure = 24ms. I. IPL 573/012354. Stretch. Mag $4 \times$. Note: The crater Hall is near center next to the terminator.



II. Phase = 52°. Range = 5980km. S/C = (61°.58, 129°.8 W). SUN = (19°.28, 86°.0 W). Δ LAT = 40°; Δ LONG = 45°.

III. No Stanford product.



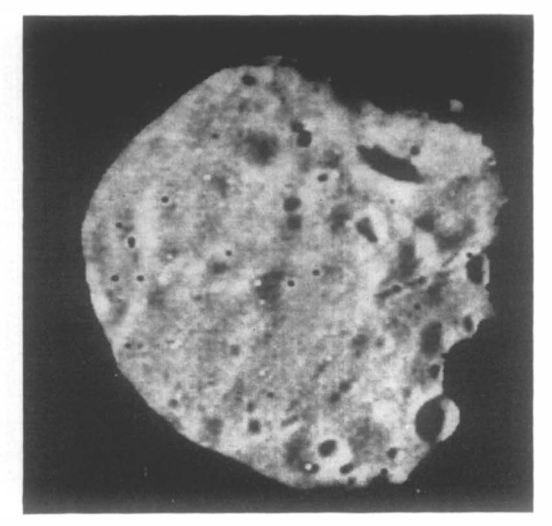
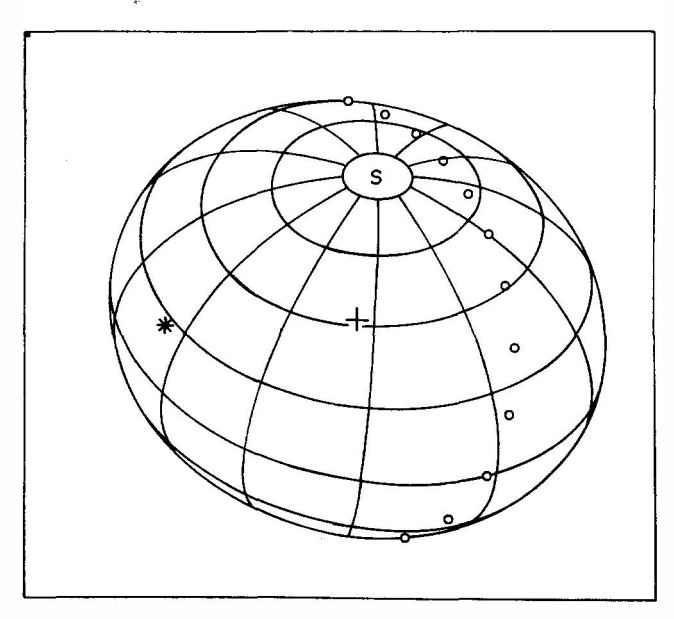
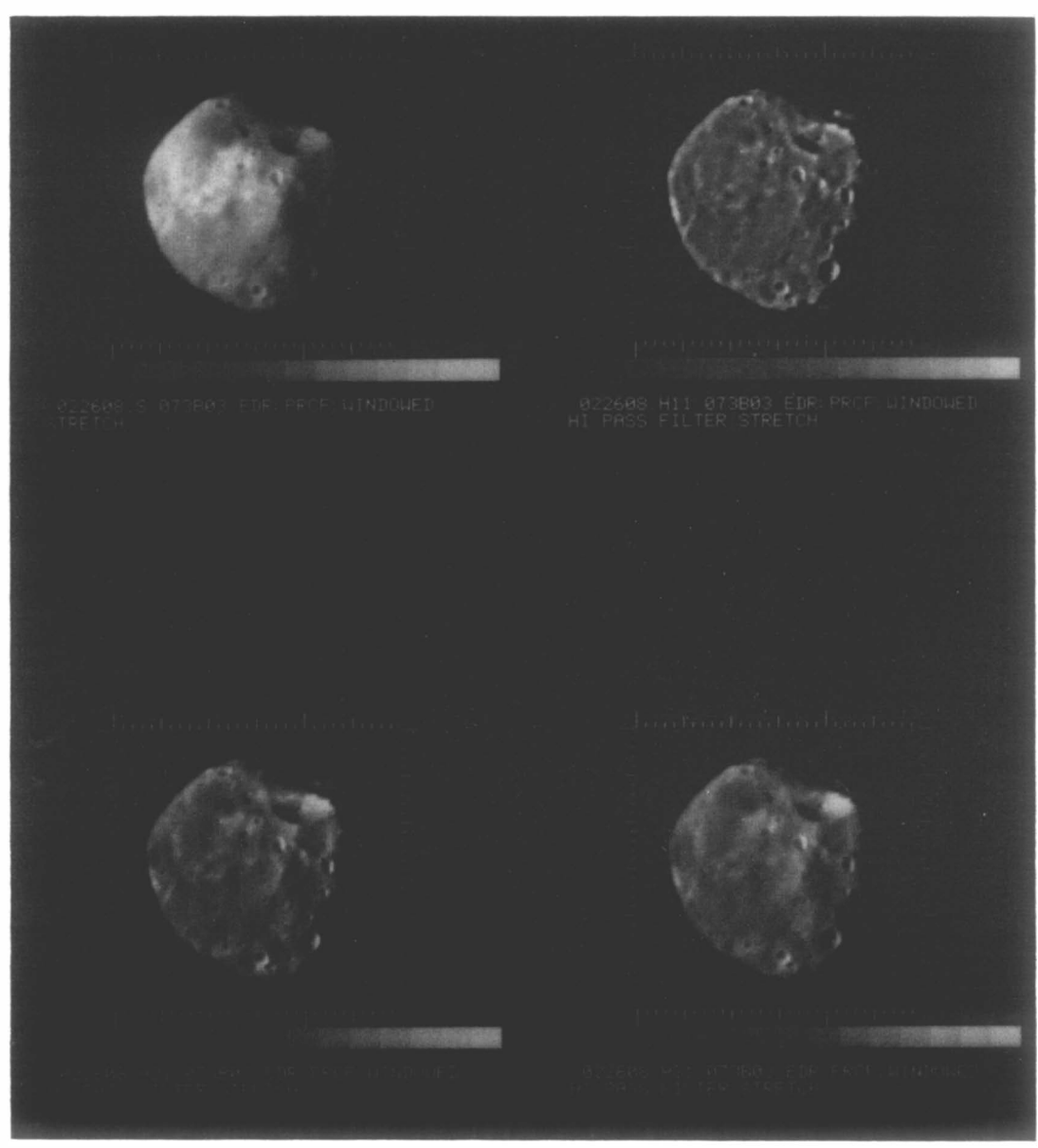


Fig. P8. Phobos. Revolution 73. DAS 04215690. Exposure = 48ms. I. Left: IPL 101203. Stretch. Mag $4\times$. Right: IPL 936/155531. High-pass filter and stretch. Mag $4\times$.

a Note: Hall is at top next to the terminator.



II. Phase = 57°. Range = 6460 km. S/C = (42°.0 S, 135°.0 W). SUN = (17°.0 S, 72°.0 W). Δ LAT = 20°; Δ LONG = 30°.



III. Stanford AI product GS01-022608.



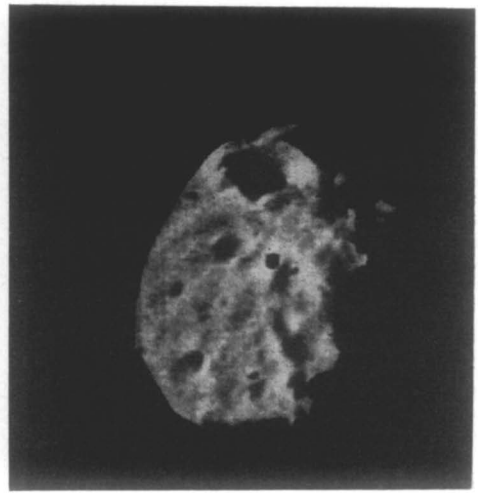
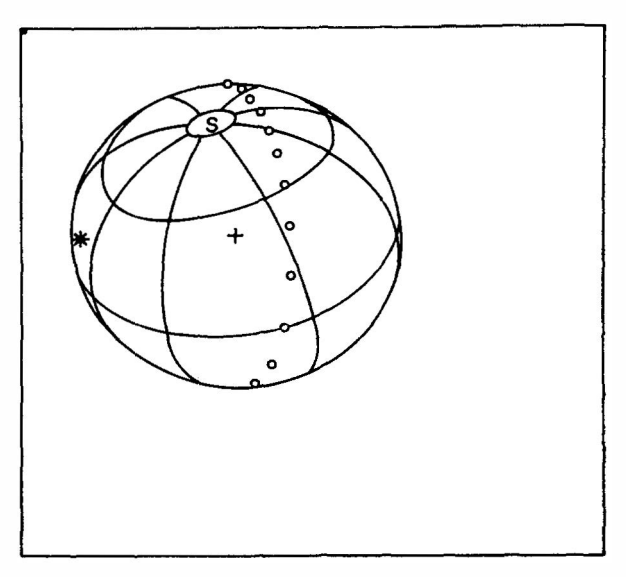
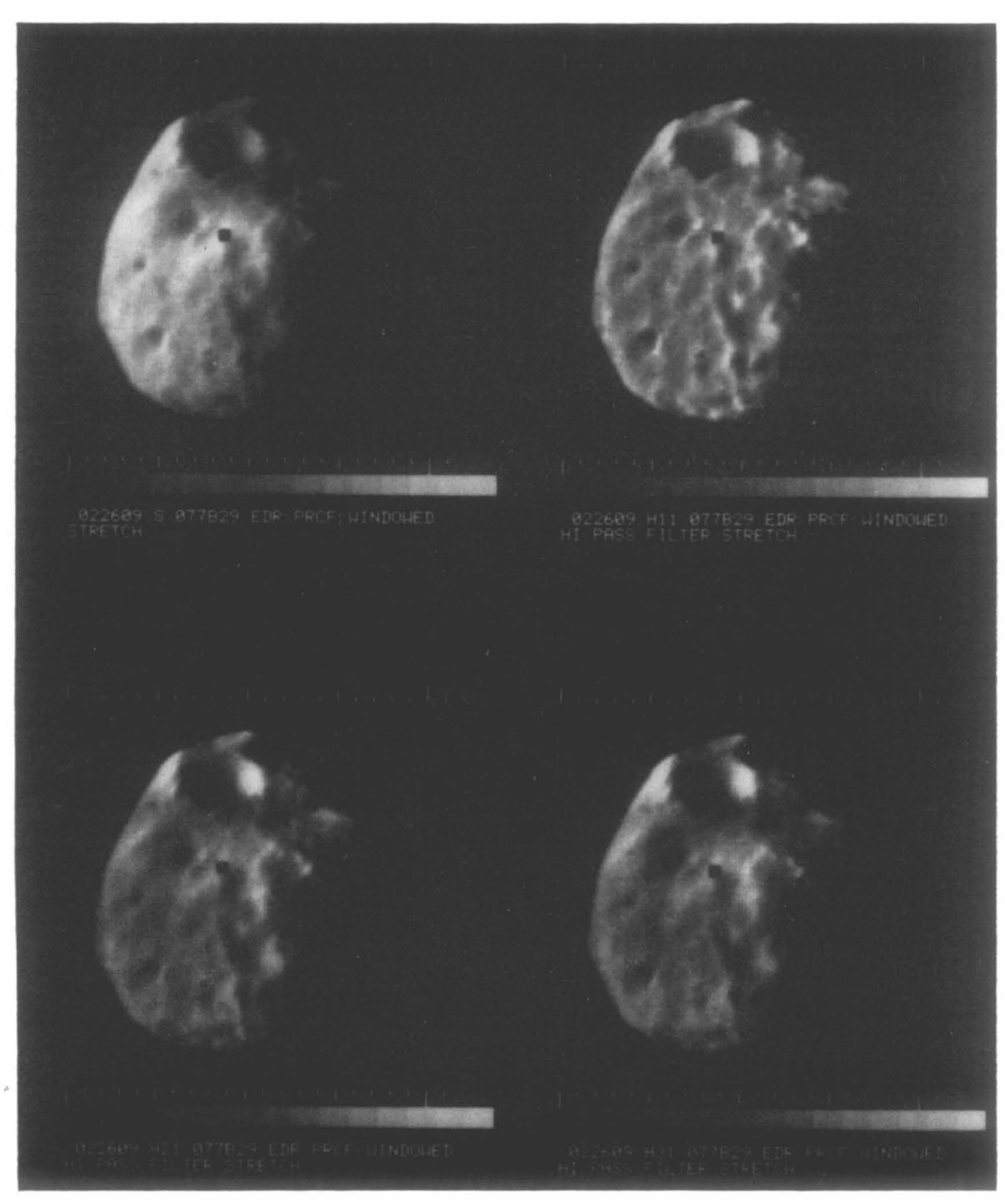


Fig. P9. Phobos. Revolution 77. DAS 04365210. Exposure = 48ms. I. Left: IPL 937/101629. Stretch. Mag $4\times$. Right: IPL 936/103925. High-pass filter and stretch. Mag $4\times$.

^a Note: The crater Hall is at top.



II. Phase = 80°. Range = 8130km. S/C = (30°.6S, 344°.2W). SUN = (17°.3S, 255°.6W). Δ LAT = 40°; Δ LONG = 45°.



III. Stanford AI product GS01-022609.

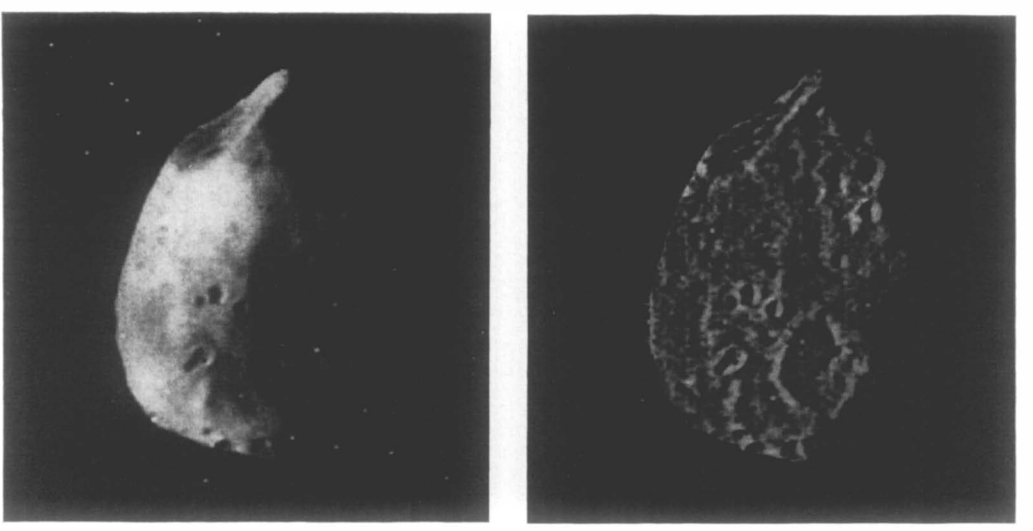
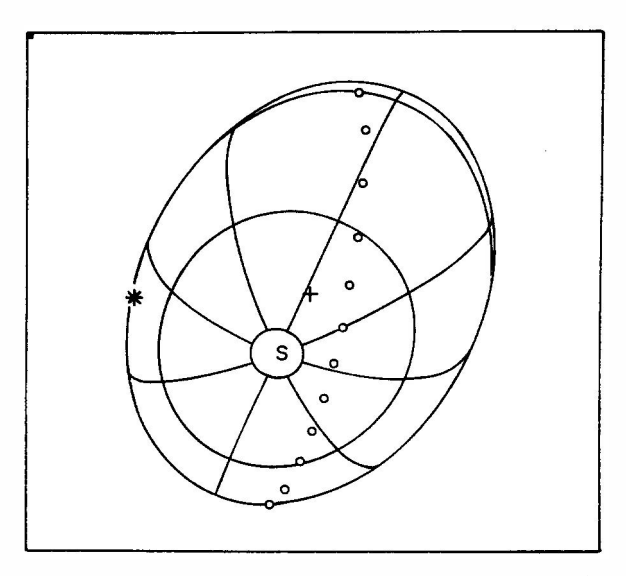
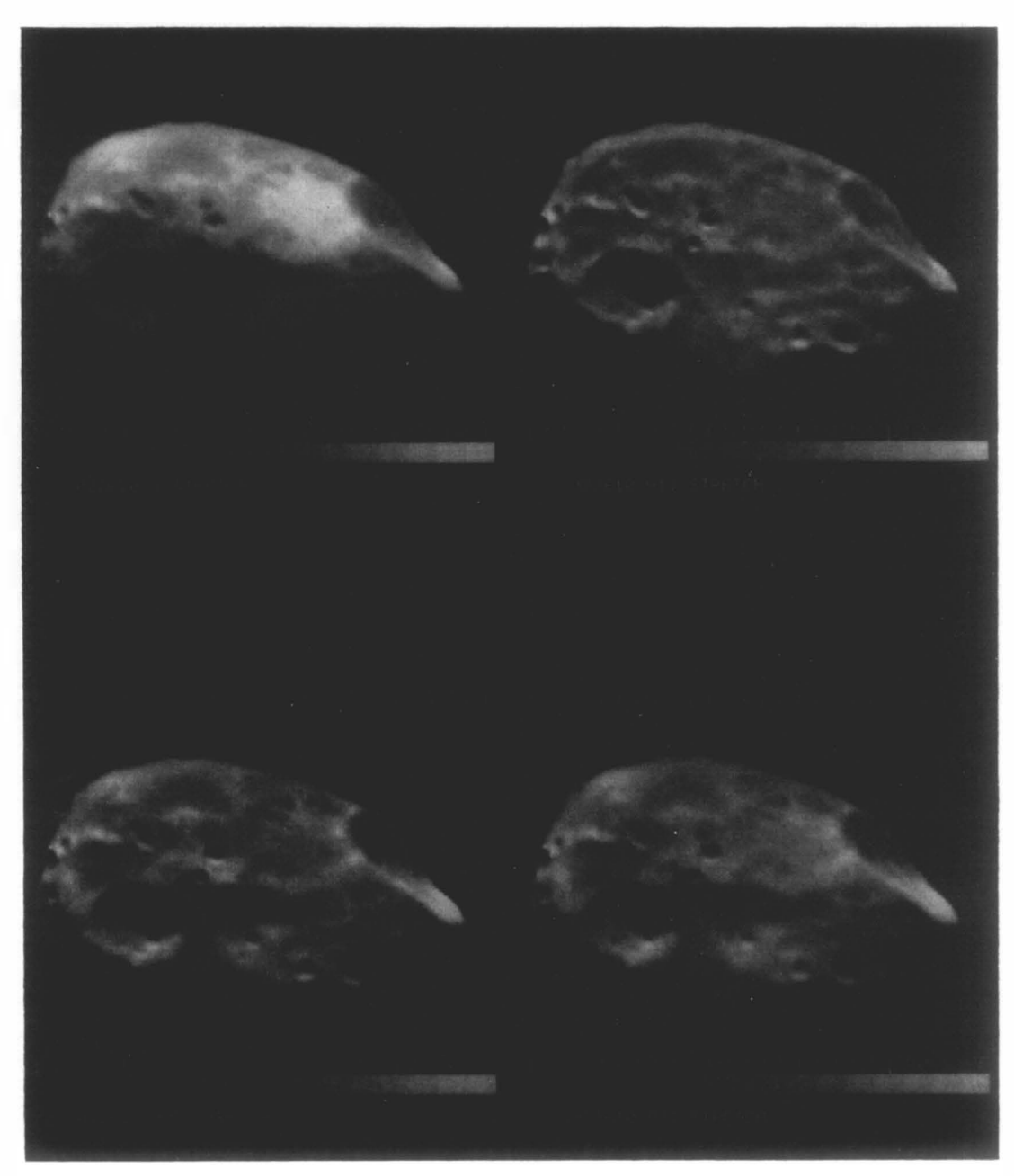


Fig. P10. Phobos. Revolution 80. DAS 04470630. Exposure = 48ms. I. Left: IPL 937/103305. Stretch. Mag $4\times$. Right: IPL 1110/191942. High-pass filter and stretch. Mag $4\times$.

a Note: Hall is at lower right next to the terminator.



II. Phase = 83°. Range = 7170 km. S/C = (64°.2 S, 356°.1 W). SUN = (17°.3 S, 106°.5 W). Δ LAT = 40°; Δ LONG = 45°.



III. Stanford AI product GS01-022610.



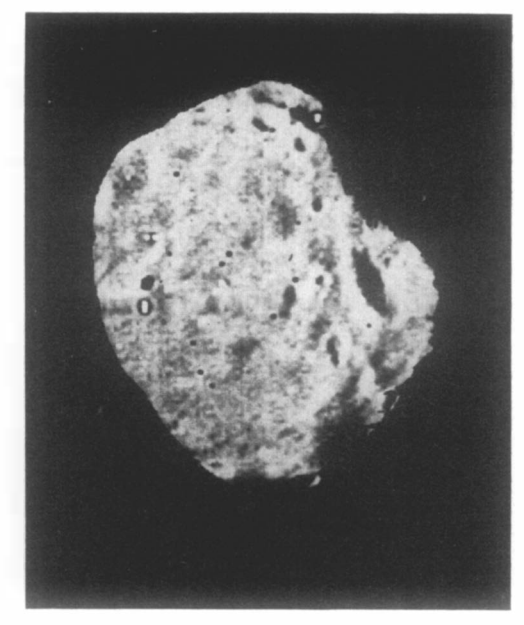
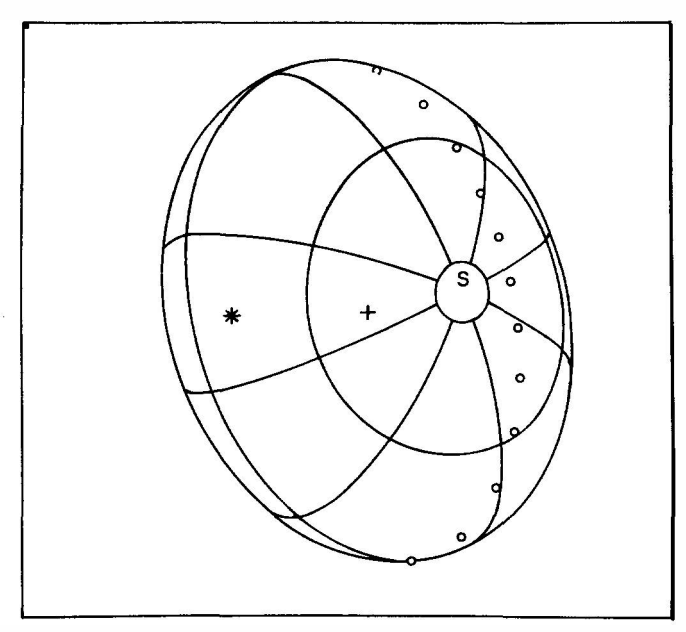
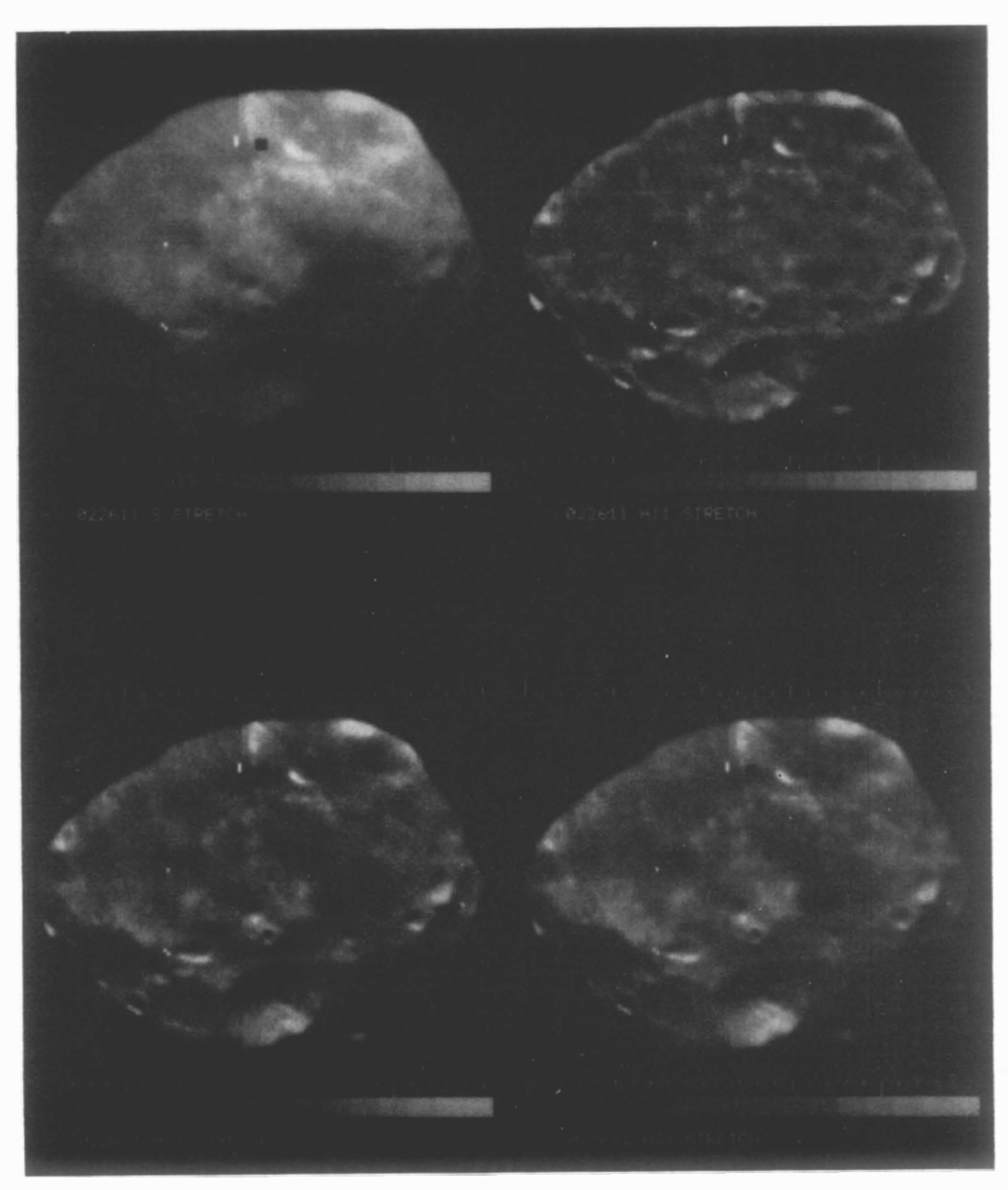


Fig. P11. Phobos. Revolution 87. DAS 04720810. Exposure = 24ms. I. Left: IPL 1009/093920. Stretch. Mag $4\times$. Right: IPL 1009/180740. High-pass filter and stretch. Mag $4\times$.

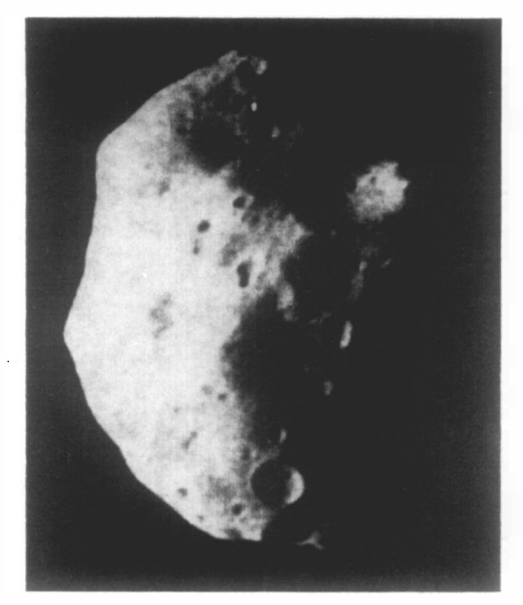
" Note: Hall is at center right next to the terminator.



II. Phase = 42°. Range = 7120 km. S/C = (57°.78, 75°.2 W). SUN = (16°.2 S, 68°.0 W). Δ LAT = 40°; Δ LONG = 45°.



III. Stanford AI product GS01-022611.



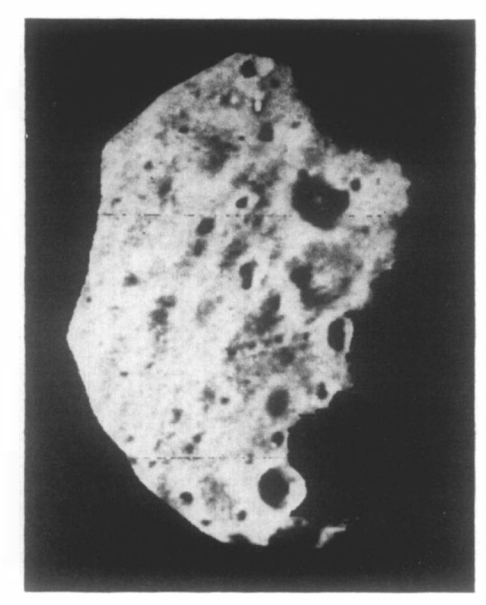
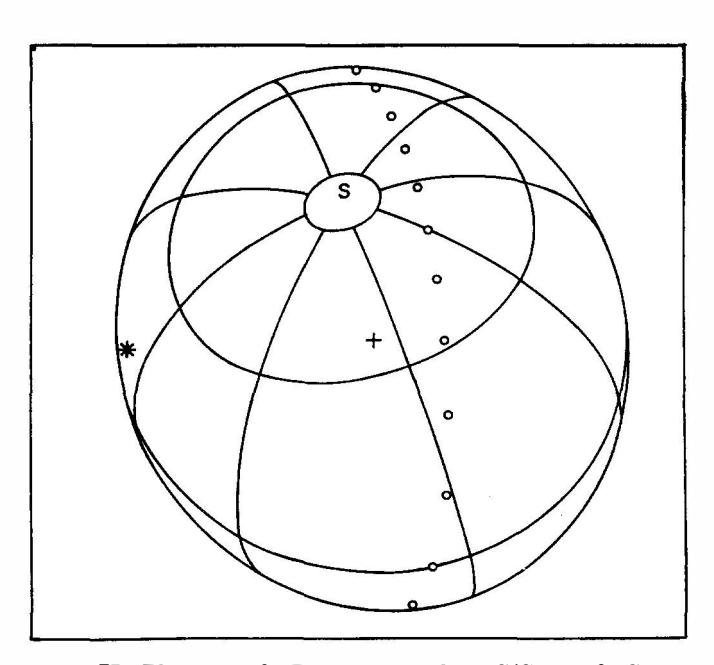
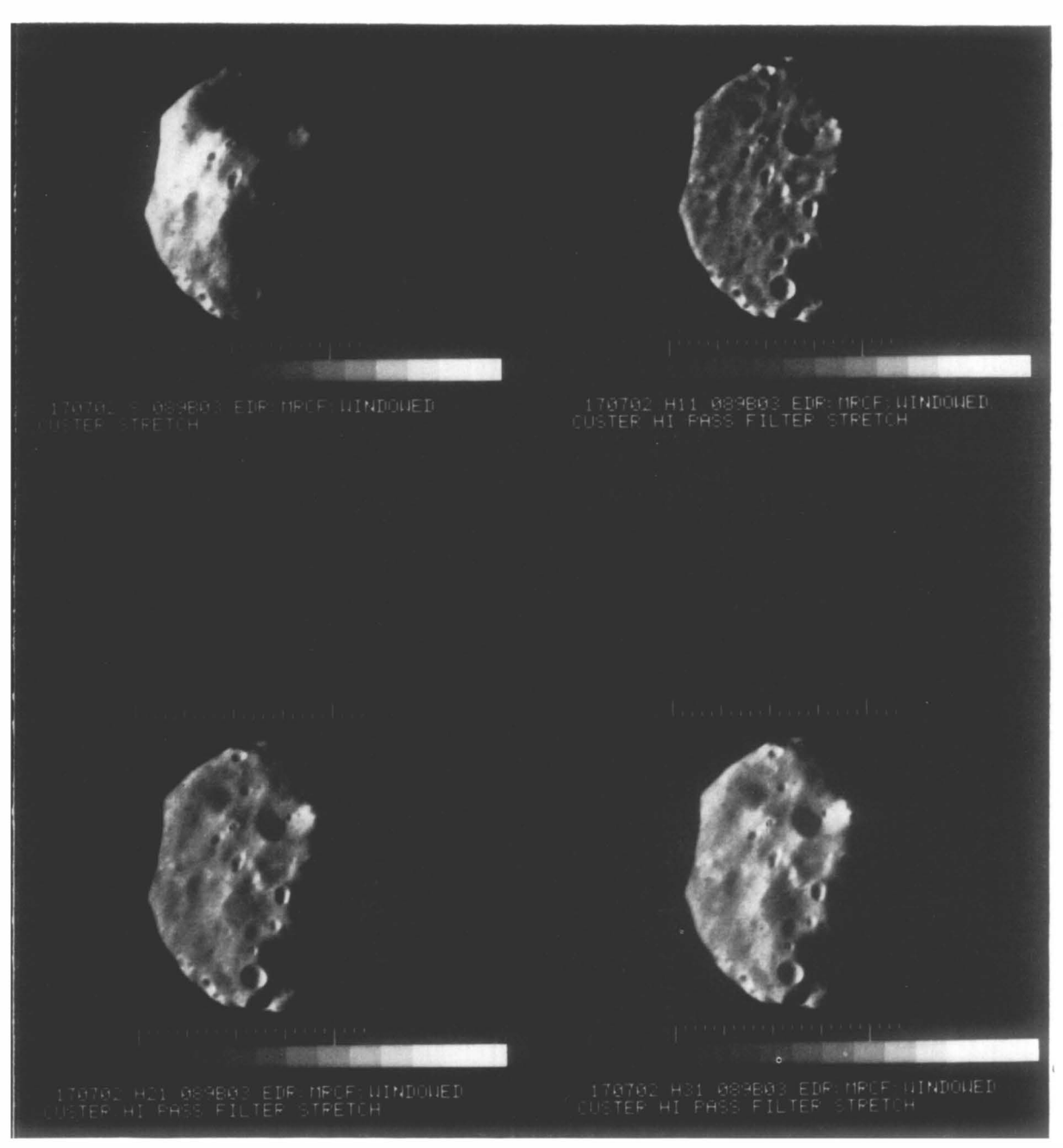


Fig. P12. Phobos. Revolution 89. DAS 04790460. Exposure = 48ms. I. Left: IPL 1008/082243. Stretch. Mag $4\times$. Right: IPL 1008/081607. High-pass filter and stretch. Mag $4\times$.

" Note: Hall is at upper right next to the terminator.



II. Phase = 80° . Range = $5760 \,\mathrm{km}$. S/C = $(47^{\circ}.9 \,\mathrm{S}, 171^{\circ}.9 \,\mathrm{W})$. SUN = $(16^{\circ}.2 \,\mathrm{S}, 79^{\circ}.1 \,\mathrm{W})$. $\Delta \mathrm{LAT} = 40^{\circ}$; $\Delta \mathrm{LONG} = 45^{\circ}$.



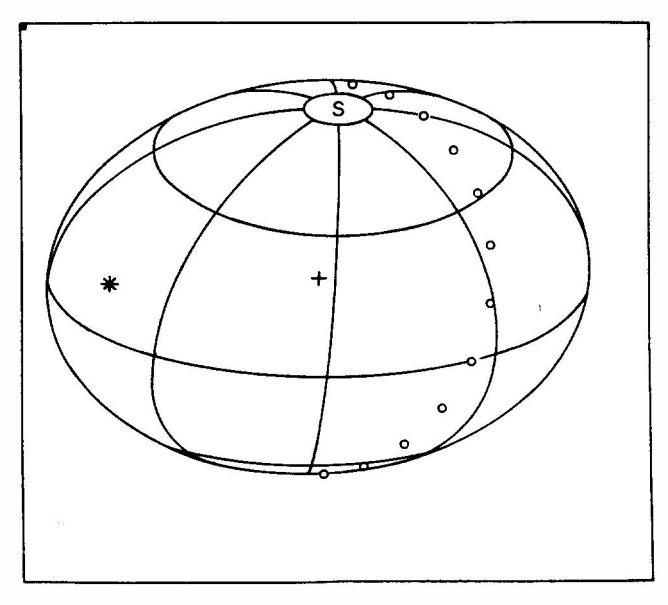
III. Stanford AI product STN 0200-170702.



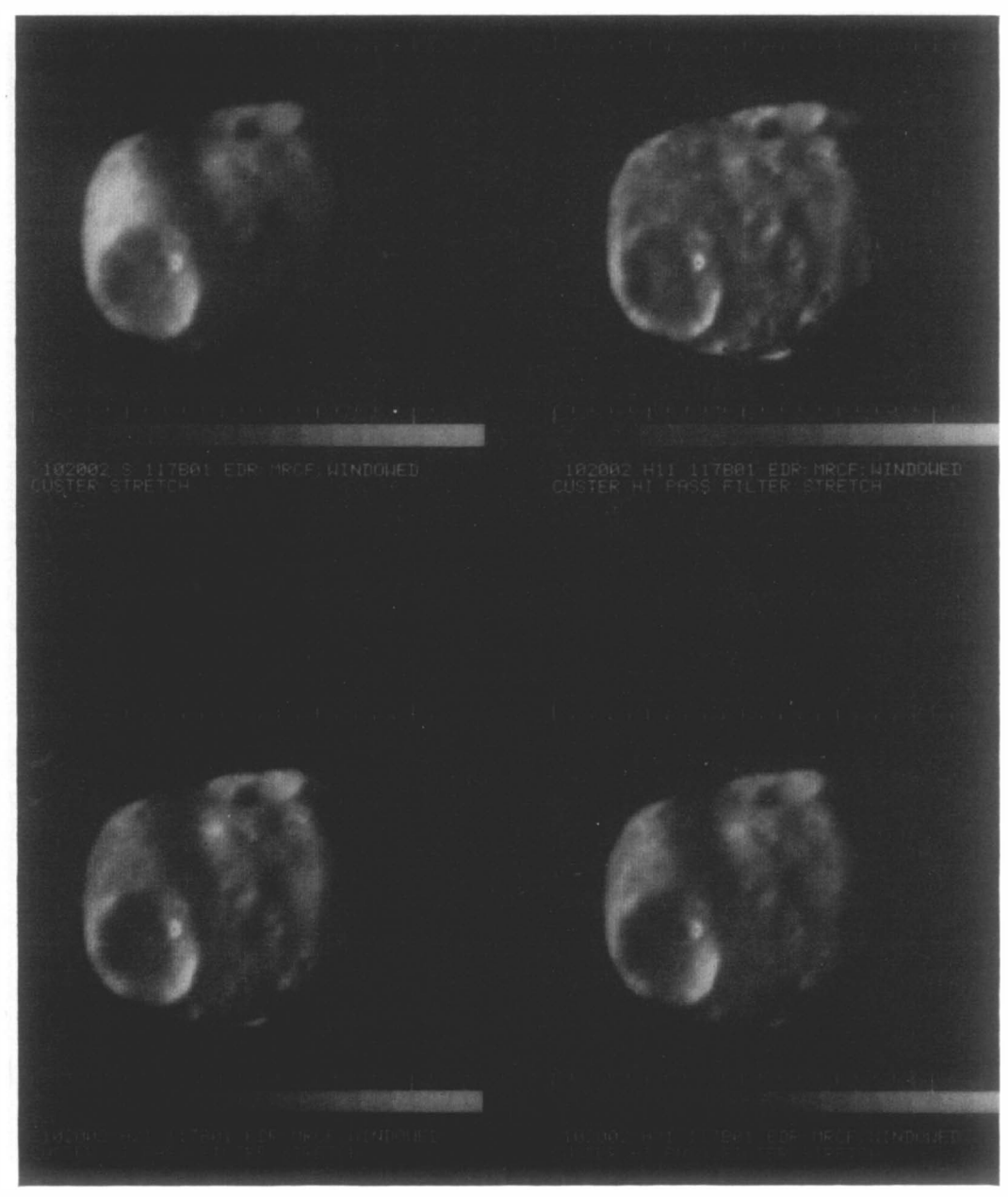


Fig. P13. Phobos. Revolution 117. DAS 05773393. Exposure = $48\,\text{ms}$. I. Left: IPL 315/0241319. High-pass filter and stretch. Mag $4\times$. Right: IPL 315/0241120. High-pass filter and stretch. Mag $4\times$.

 a Note: The crater Hall is on the limb at top.



II. Phase = 55°. Range = 10170 km. S/C = (28°.2 S, 85°.1 W). SUN = (12°.7 S, 28°.0 W). Δ LAT = 40°; Δ LONG = 45°.



III. Stanford AI product GS01-102002.



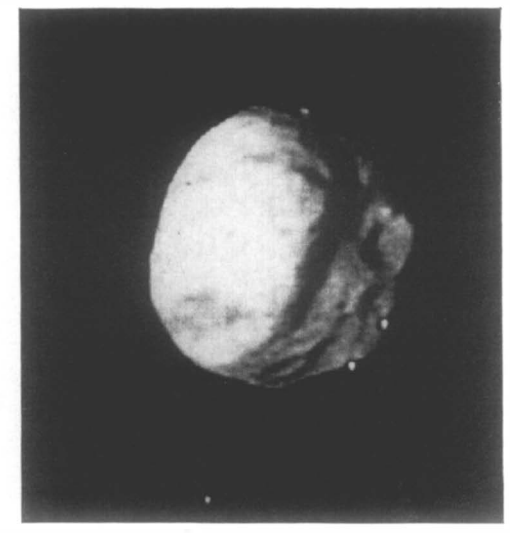
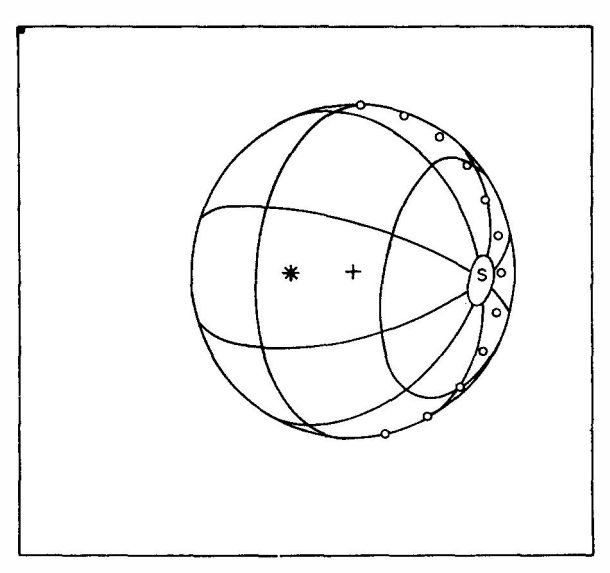
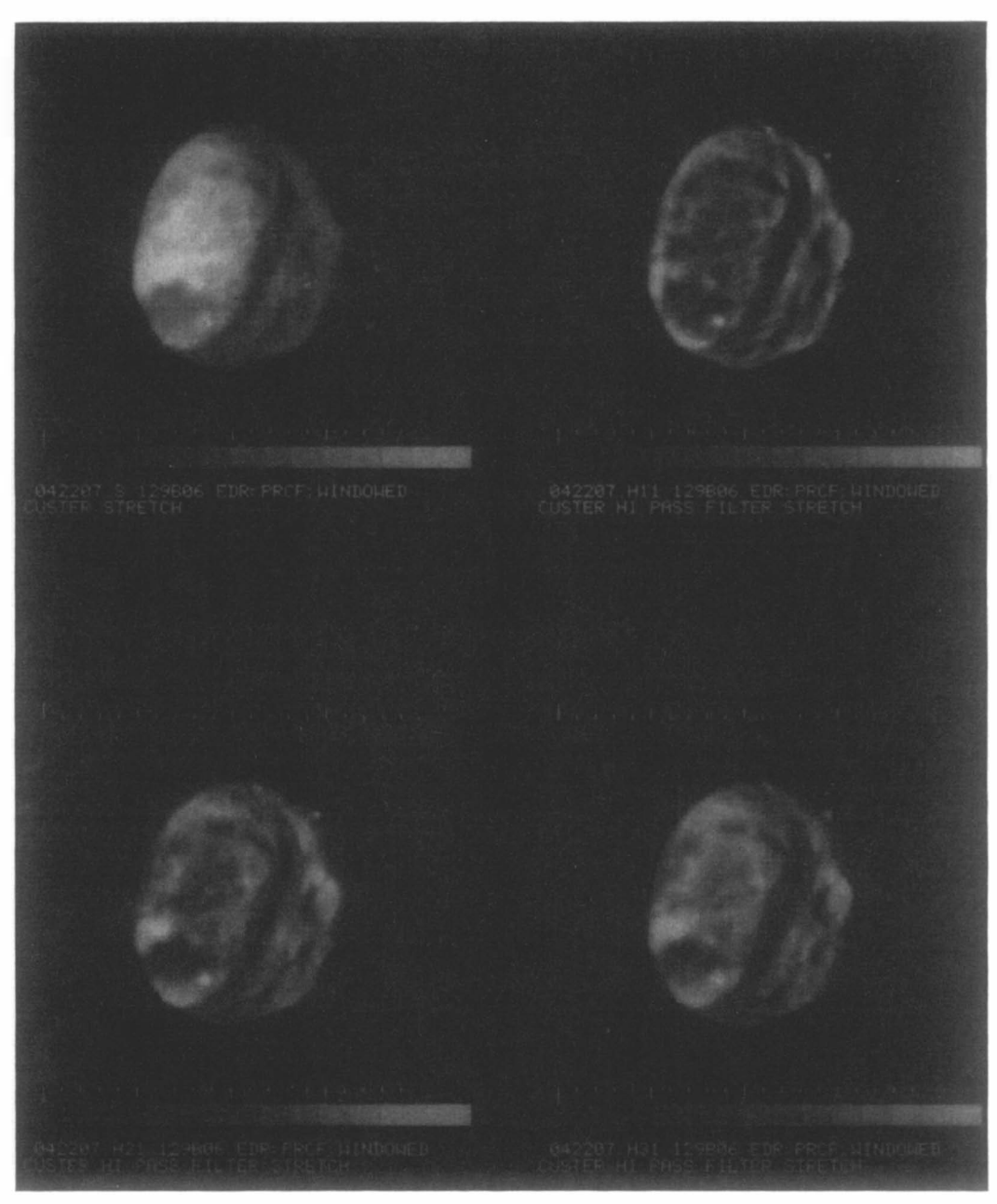


Fig. P14. Phobos. Revolution 129. DAS 06209283. Exposure = $24\,\mathrm{ms}$. I. Left: IPL 1114/172738. Stretch. Mag $4\times$. Right: IPL 1114/172919. Stretch. Mag $4\times$.

a Note: Hall is on the terminator.



II. Phase = 18°. Range = 12500 km. S/C = (29°.7 S, 17°.3 W). SUN = (11°.4 S, 19°.1 W). Δ LAT = 40°; Δ LONG = 45°.



III. Stanford AI product GS01-042207.

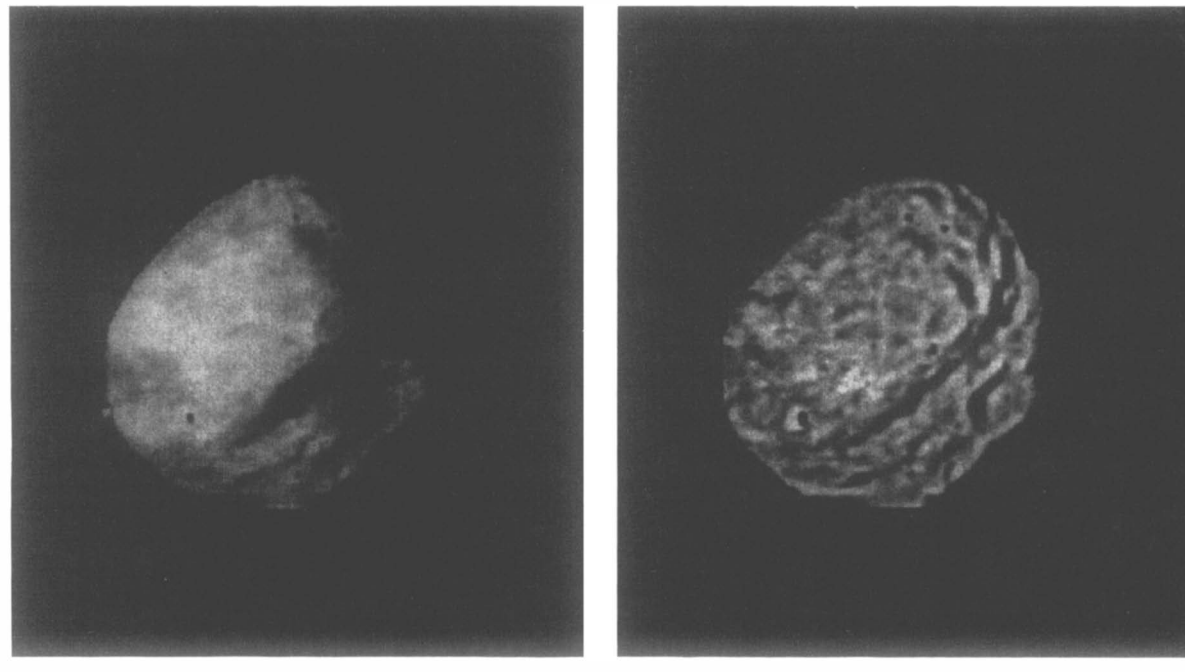
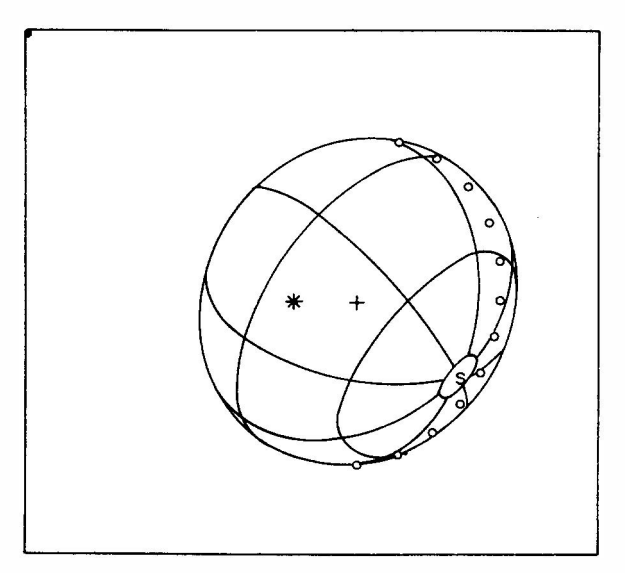
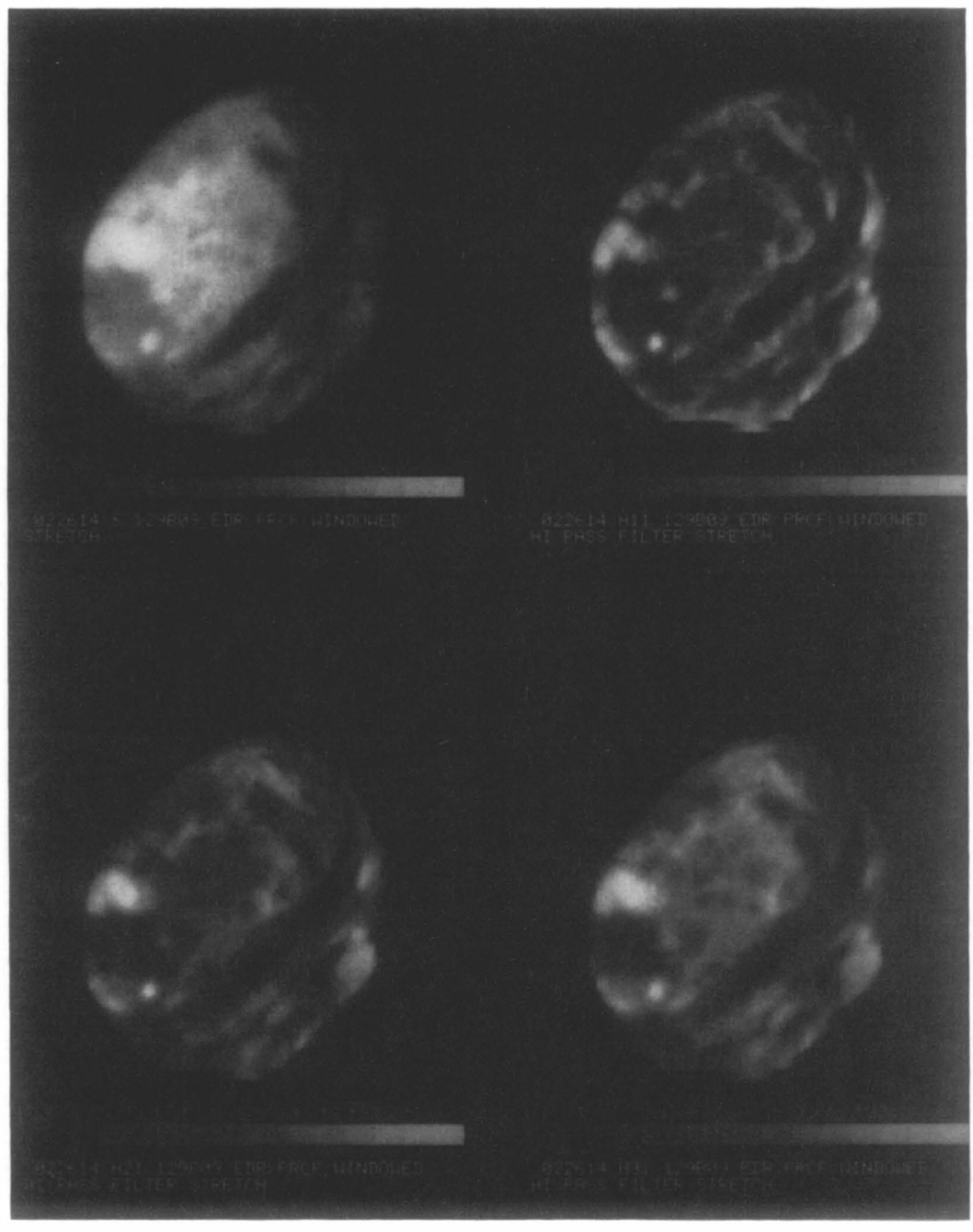


Fig. P15. Phobos. Revolution 129. DAS 06209633. Exposure = 24ms. I. Left: IPL 1114/174323. Stretch. Mag $4\times$. Right: IPL 1114/174504. High-pass filter and stretch. Mag $4\times$.

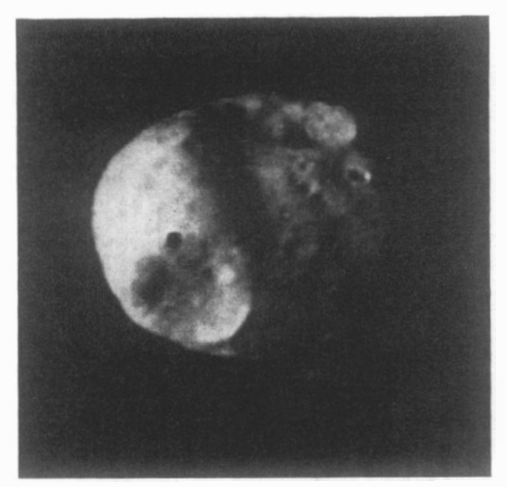
a Note: Hall is on the terminator at lower right.



II. Phase = 19°. Range = 12660 km. S/C = (27°.4 S, 12°.6 W). SUN = (11°.5 S, 24°.4 W). Δ LAT = 40°; Δ LONG = 45°.



III. Stanford AI product GS01-022614.



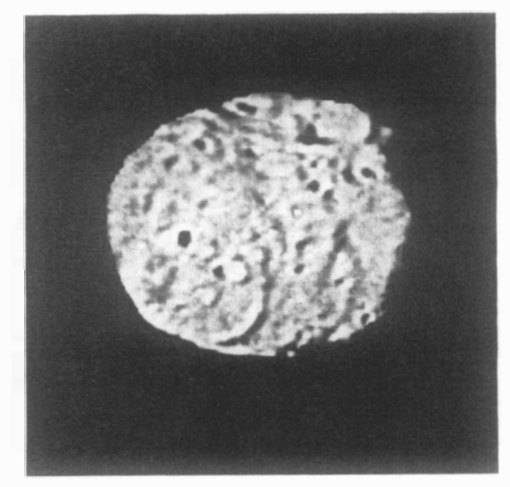
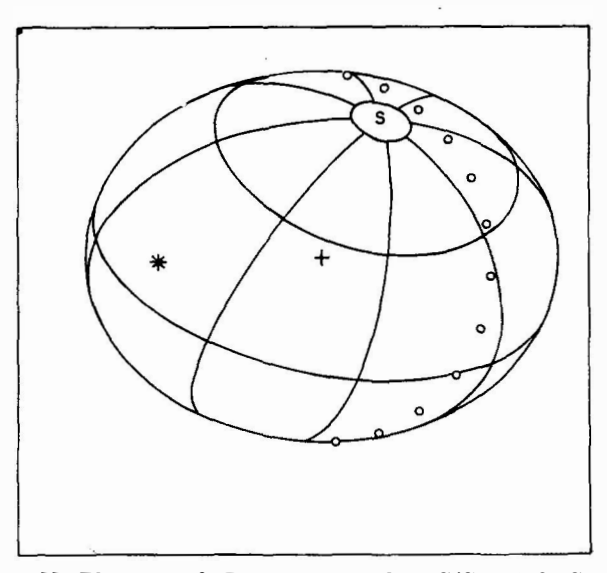
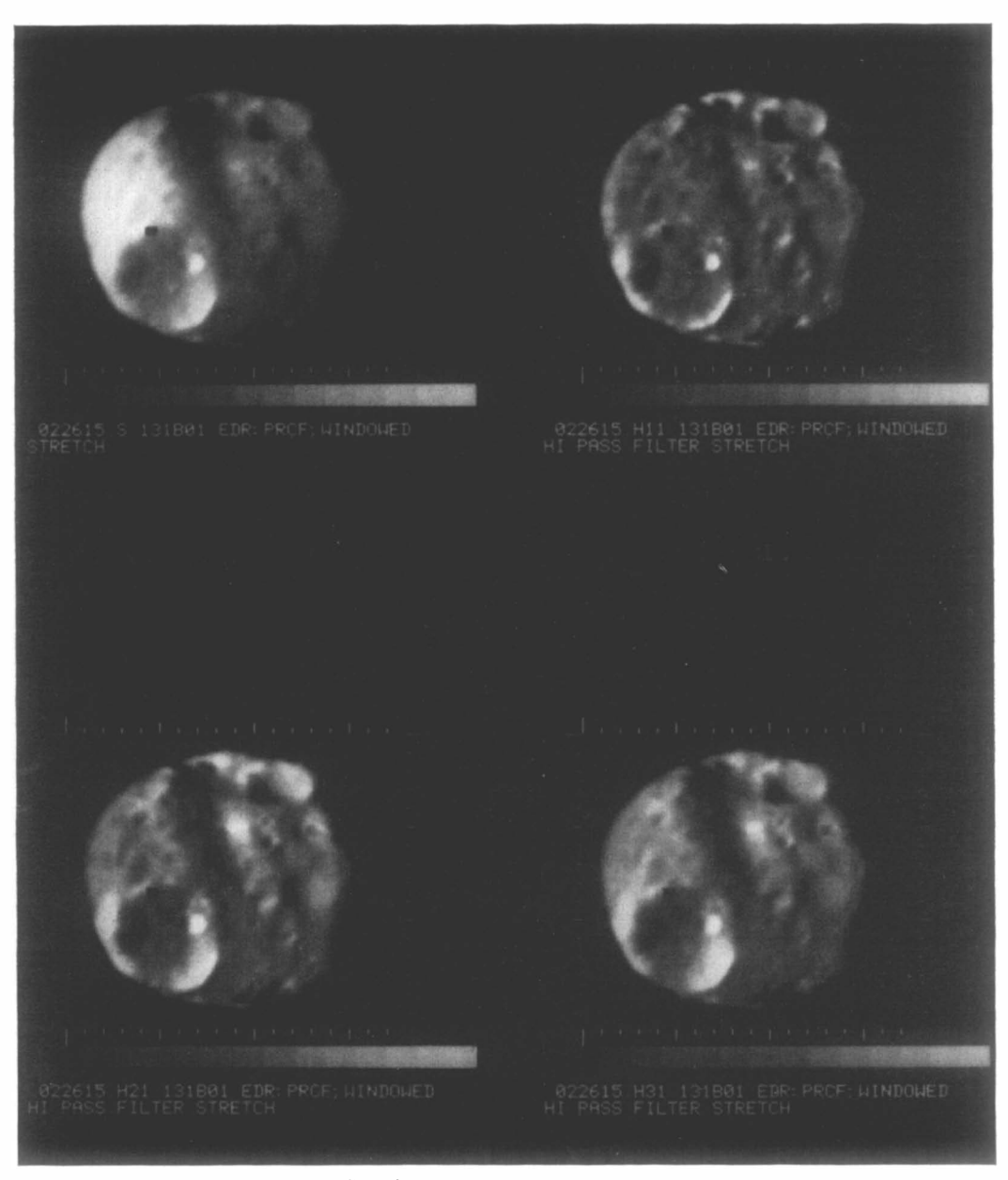


Fig. P16. Phobos. Revolution 131. DAS 06278443. Exposure = 48ms. I. Left: IPL 1114/175715. Stretch. Mag $4\times$. Right: IPL 1114/175947. High-pass filter and stretch. Mag $4\times$.

" Note: The crater Hall is at top next to the limb.



II. Phase = 45° . Range = $10410 \,\mathrm{km}$. S/C = $(35^{\circ}.0 \,\mathrm{S})$, $65^{\circ}.0 \,\mathrm{W})$. SUN = $(11^{\circ}.3 \,\mathrm{S})$, $22^{\circ}.8 \,\mathrm{W}$). $\Delta \mathrm{LAT} = 40^{\circ}$; $\Delta \mathrm{LONG} = 45^{\circ}$.

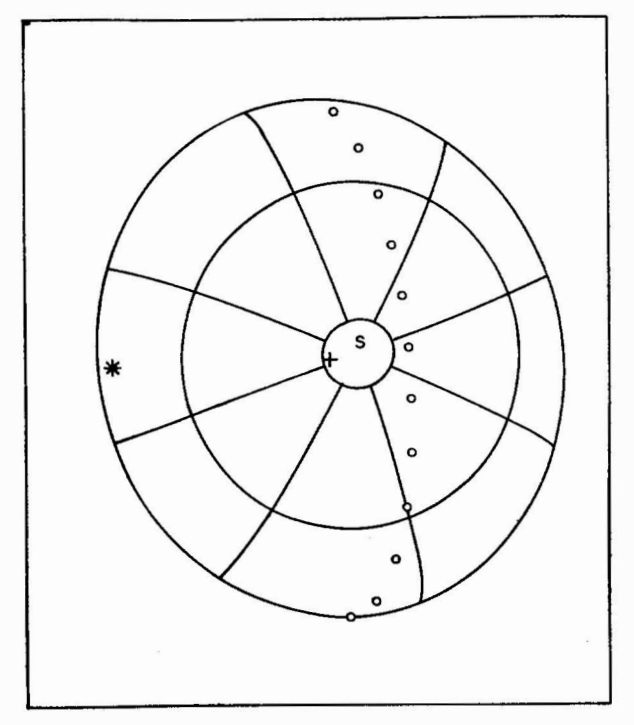


III. Stanford AI product GS01-022615.

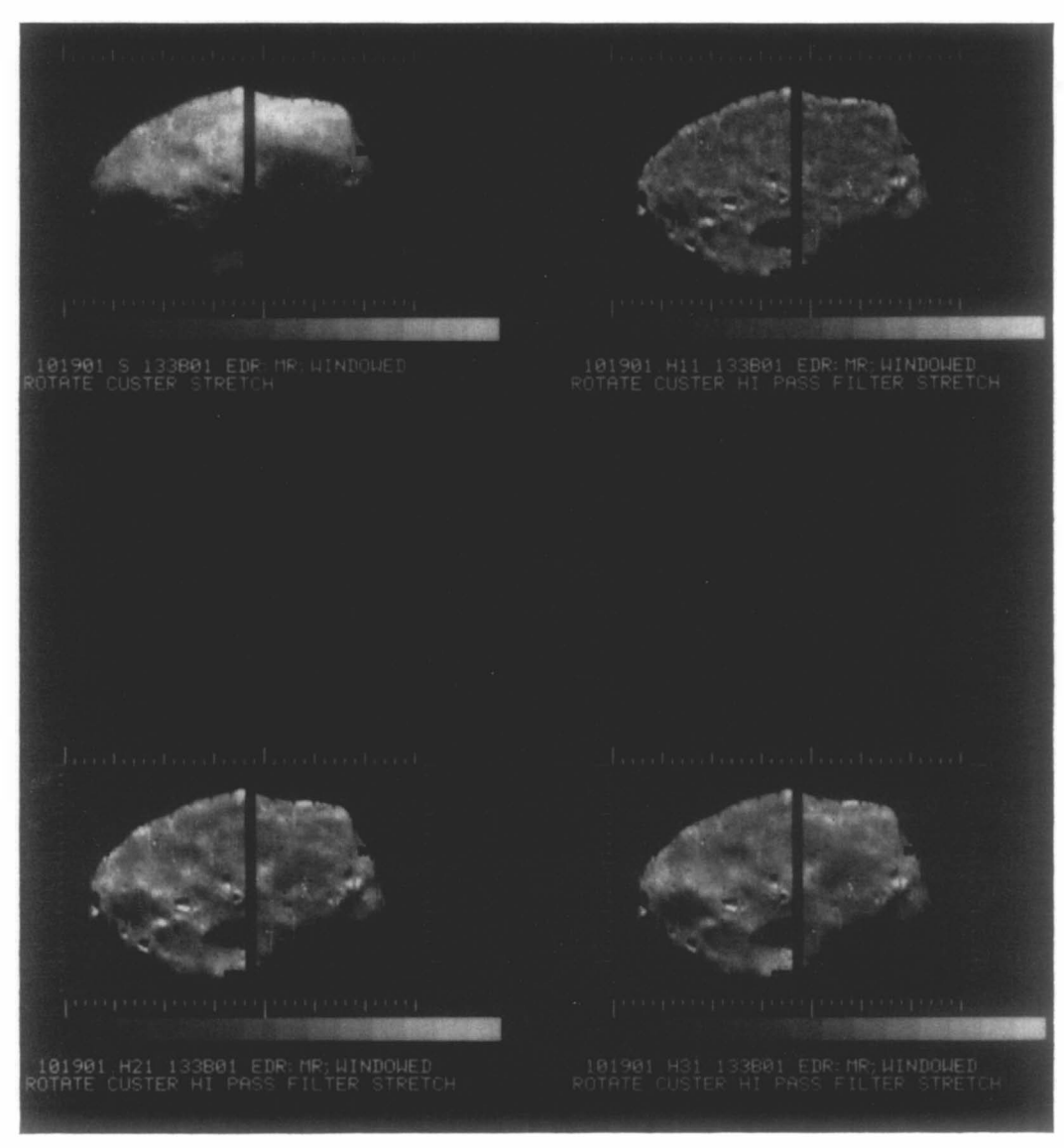


Fig. P17. Phobos. Revolution 133. DAS 06350468. Exposure = 48 ms. I. IPL 1182/011803. Stretch. Mag $4\times$.

Note: Hall is near center right next to the terminator.



II. Phase = 73°. Range = 6110 km. S/C = (82°.0 S, 79°.3 W). SUN = (11°.8 S, 70°.2 W). Δ LAT = 40°; Δ LONG = 45°.



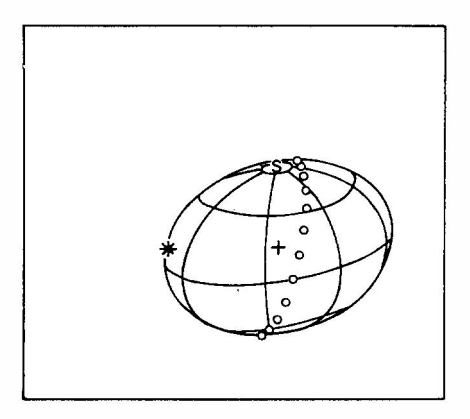
III. Stanford AI product GS01-101901.



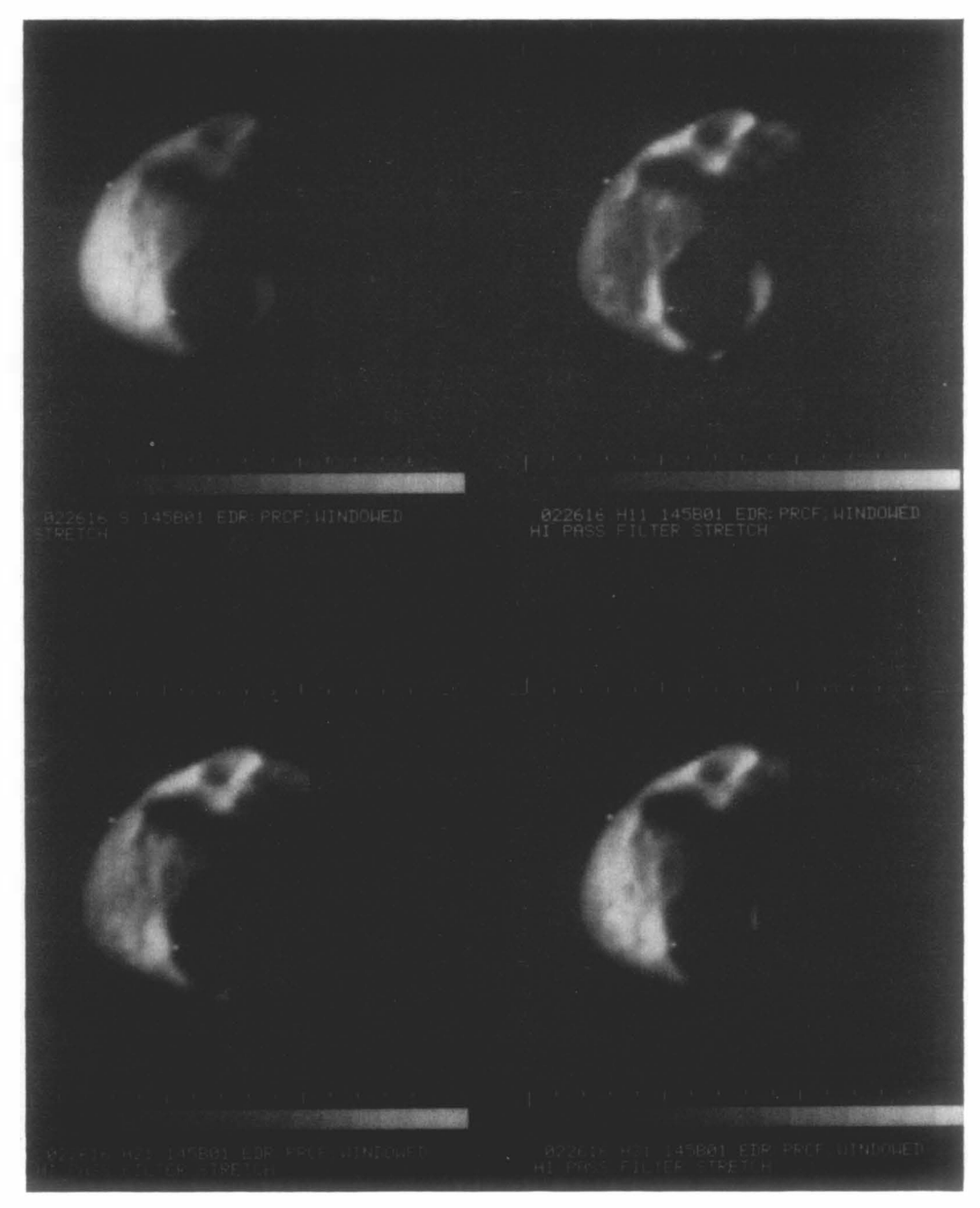


Fig. P18. Phobos. Revolution 145. DAS 06781043. Exposure = 48ms. I. Left: IPL 1792/142833. Stretch. Mag $4\times$. Right: IPL 1792/142720. Stretch. Mag $4\times$.

 a Note: The prominent crater next to the terminator is Stickney.



II. Phase = 70° . Range = $15260\,\mathrm{km}$. S/C = $(20^{\circ}.1\,\mathrm{S}, 52^{\circ}\mathrm{W})$. SUN = $(9^{\circ}.9\,\mathrm{S}, 339^{\circ}.8\,\mathrm{W})$. $\Delta\mathrm{LAT} = 40^{\circ}$; $\Delta\mathrm{LONG} = 45^{\circ}$.



III. Stanford AI product GS01-022616.



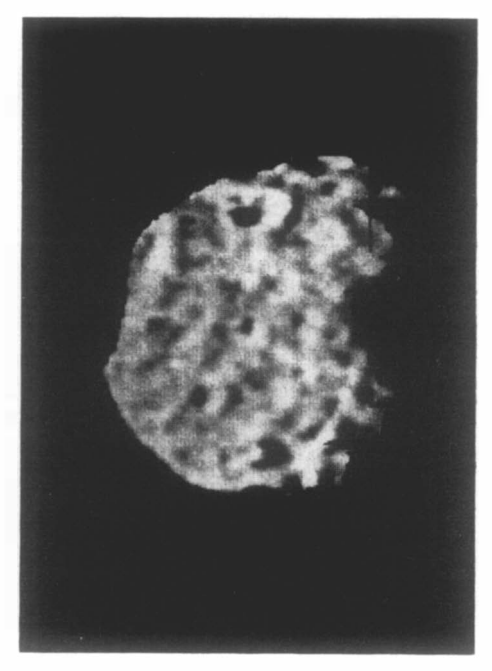
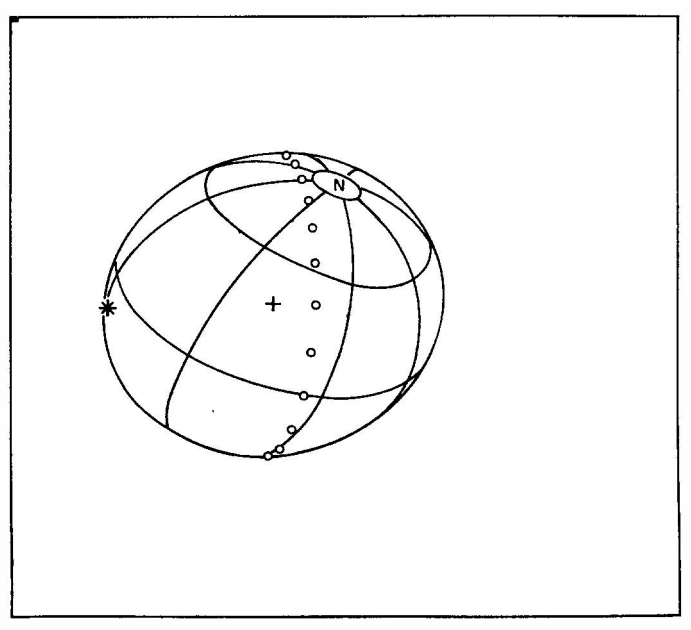
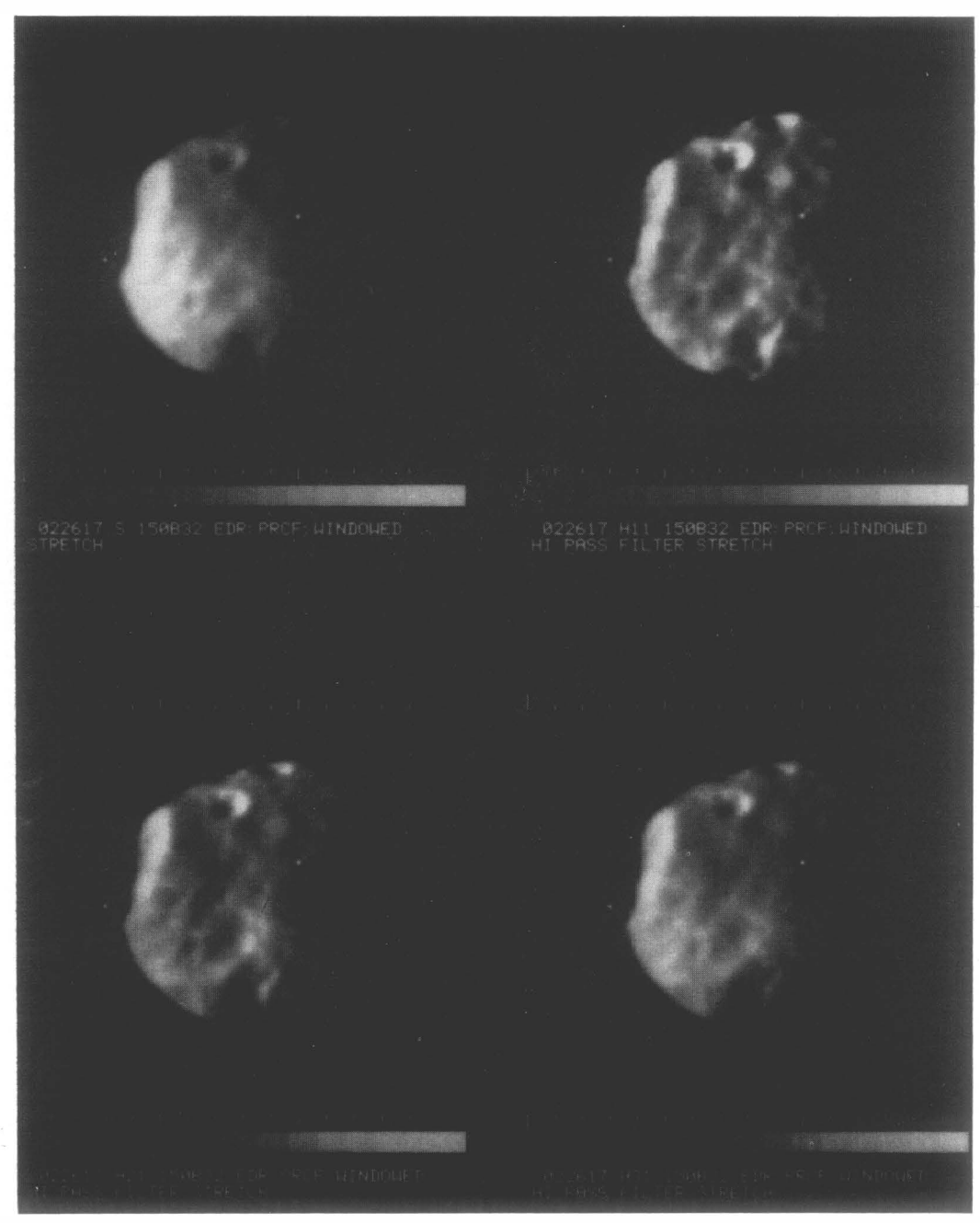


Fig. P19. Phobos. Revolution 150. DAS 06968713. Exposure = 48 ms. I. Left: IPL 499/101741. Stretch. Mag $4 \times$. Right: IPL 499/102234. High-pass filter and stretch. Mag $4 \times$.



II. Phase = 64°. Range = 14510km. S/C = (24°.2N, 344°.2W). SUN = (9°.5S, 39°.7W). Δ LAT = 40°; Δ LONG = 45°.



III. Stanford AI product GS01-022617.

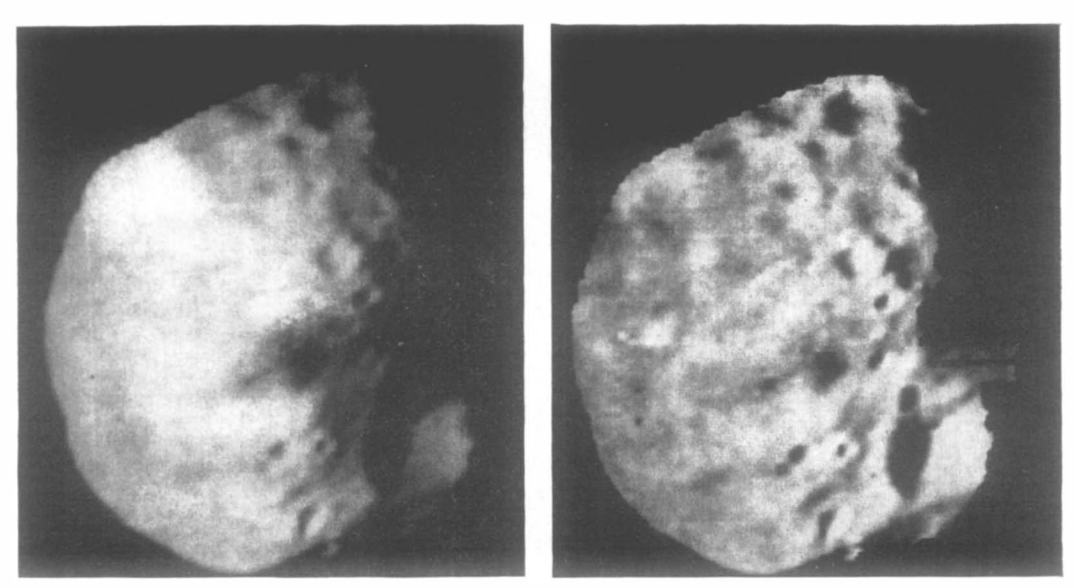
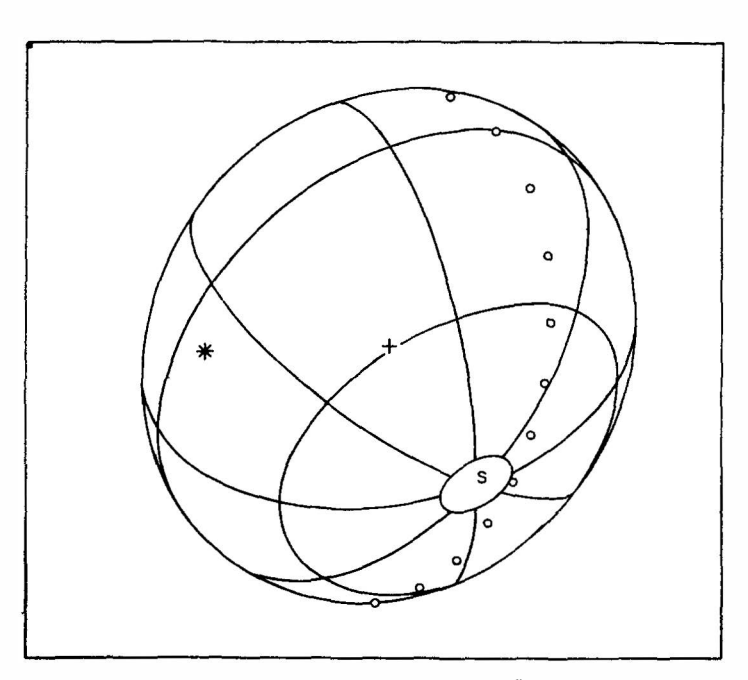
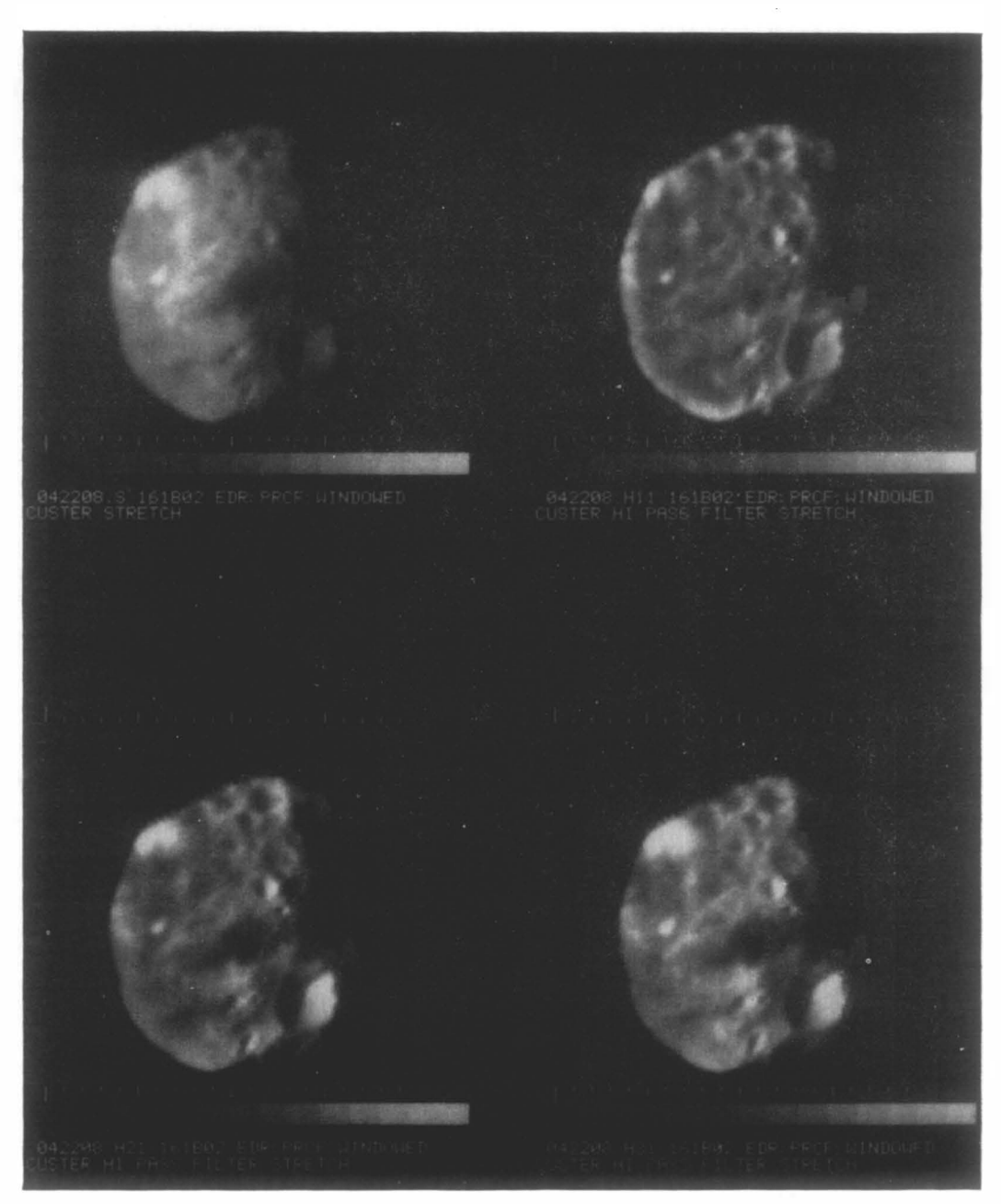


Fig. P20. Phobos. Revolution 161. DAS 07360363. Exposure = 48ms. I. Left: IPL 1182/084902. Stretch. Mag $4\times$. Right: IPL 1182/085421. High-pass filter and stretch. Mag $4\times$.



II. Phase = 45°. Range = $10000 \rm{km}$. S/C = $(39^{\circ}.1\,\rm{S}, 20^{\circ}.4\,\rm{W})$. SUN = $(8^{\circ}.7\,\rm{S}, 56^{\circ}.9\,\rm{W})$. $\Delta \rm{LAT} = 40^{\circ}$; $\Delta \rm{LONG} = 45^{\circ}$.

a Note: Hall is on the terminator at lower left.



III. Stanford AI product GS01-042208.



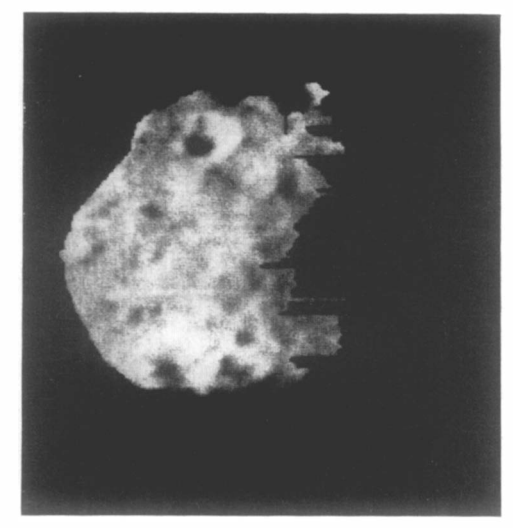
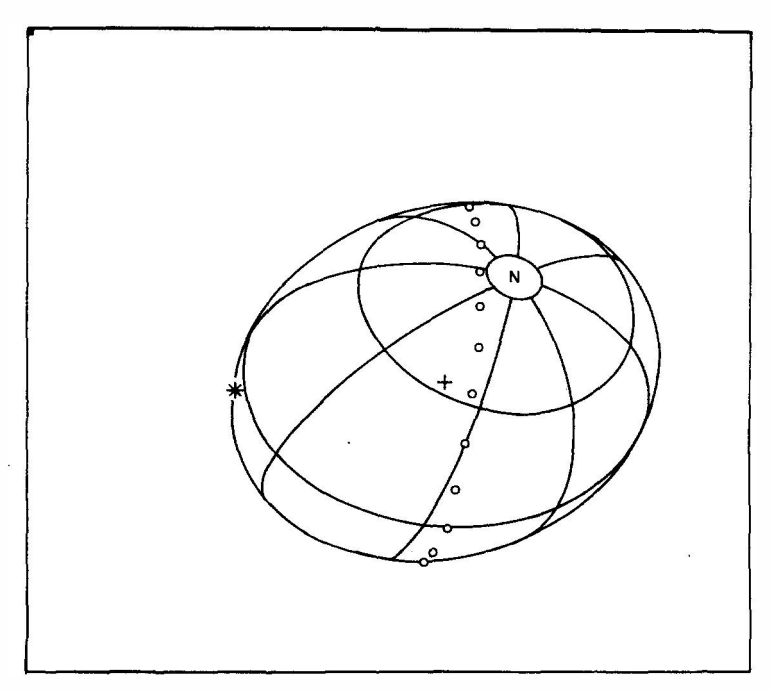
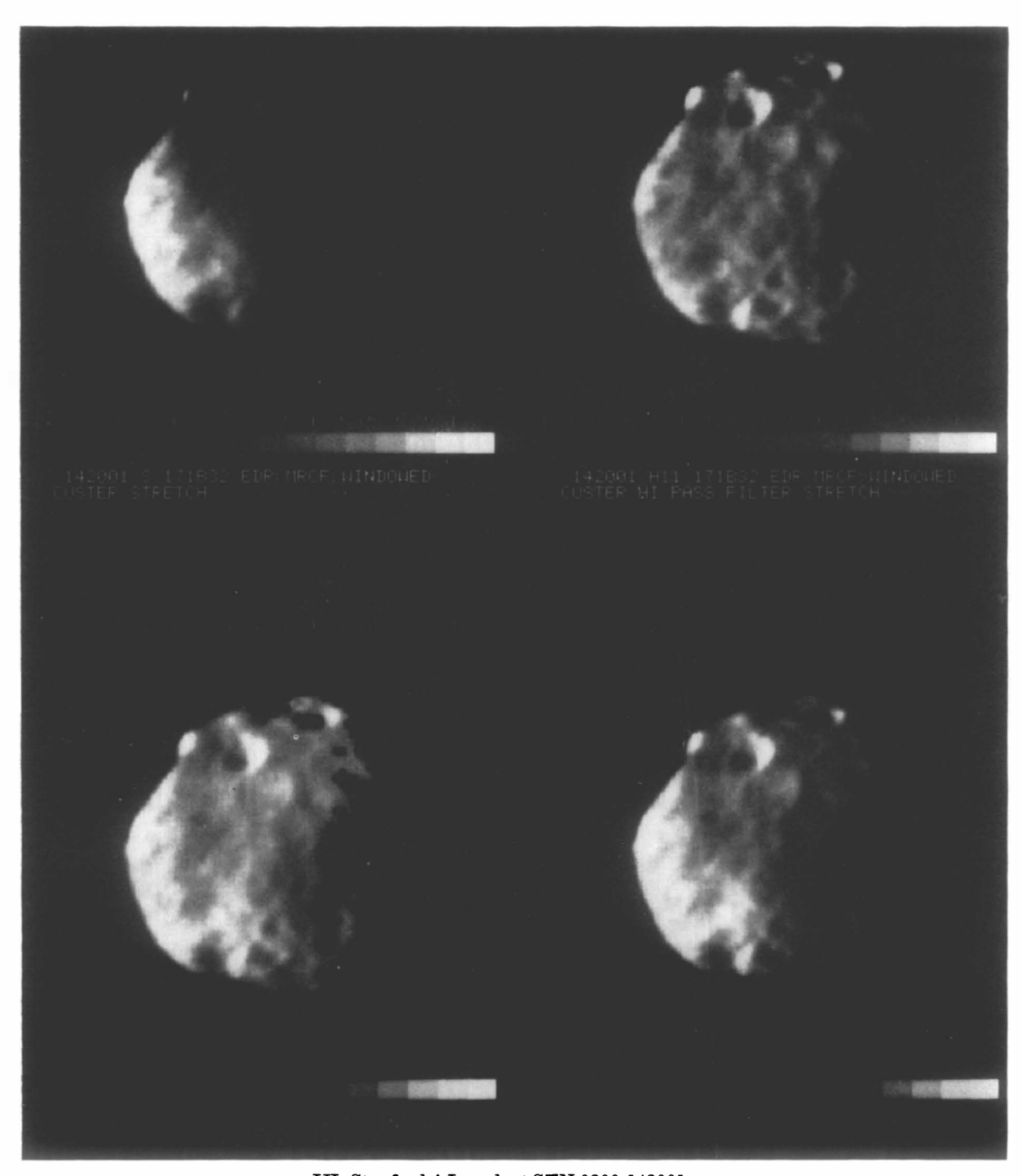


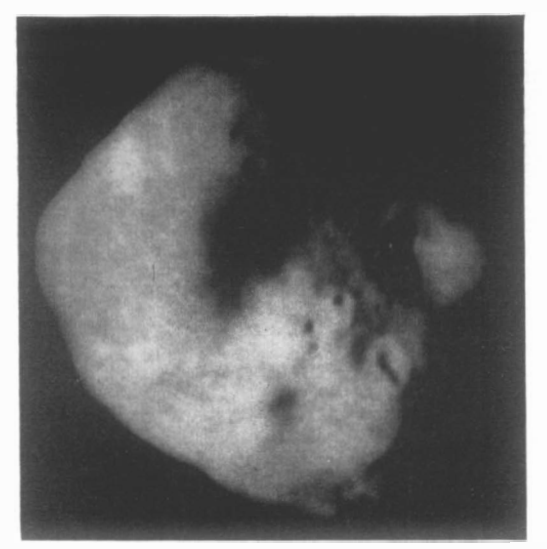
Fig. P21. Phobos. Revolution 171. DAS 07725973. Exposure = $48 \, \text{ms.}$ I. Left: IPL 1185/104821 Stretch. Mag $4 \times$. Right: IPL 1133/062033. High-pass filter and stretch. Mag $4 \times$.



II. Phase = 71°. Range = 13590km. S/C = (43°.4N, 332°.8W). SUN = (7°.1S, 27°.4W). Δ LAT = 40°; Δ LONG = 45°.



III. Stanford A I product STN 0200-142001.



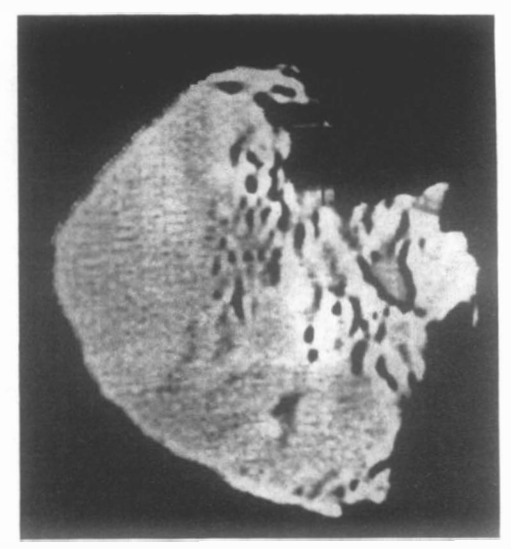
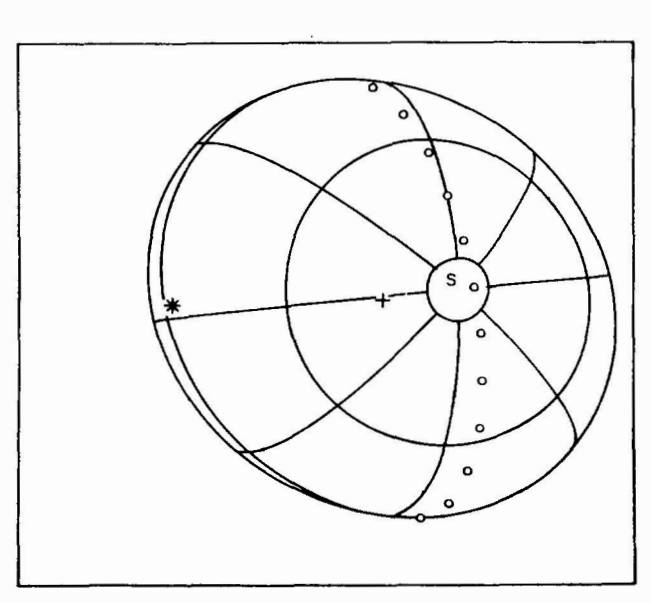
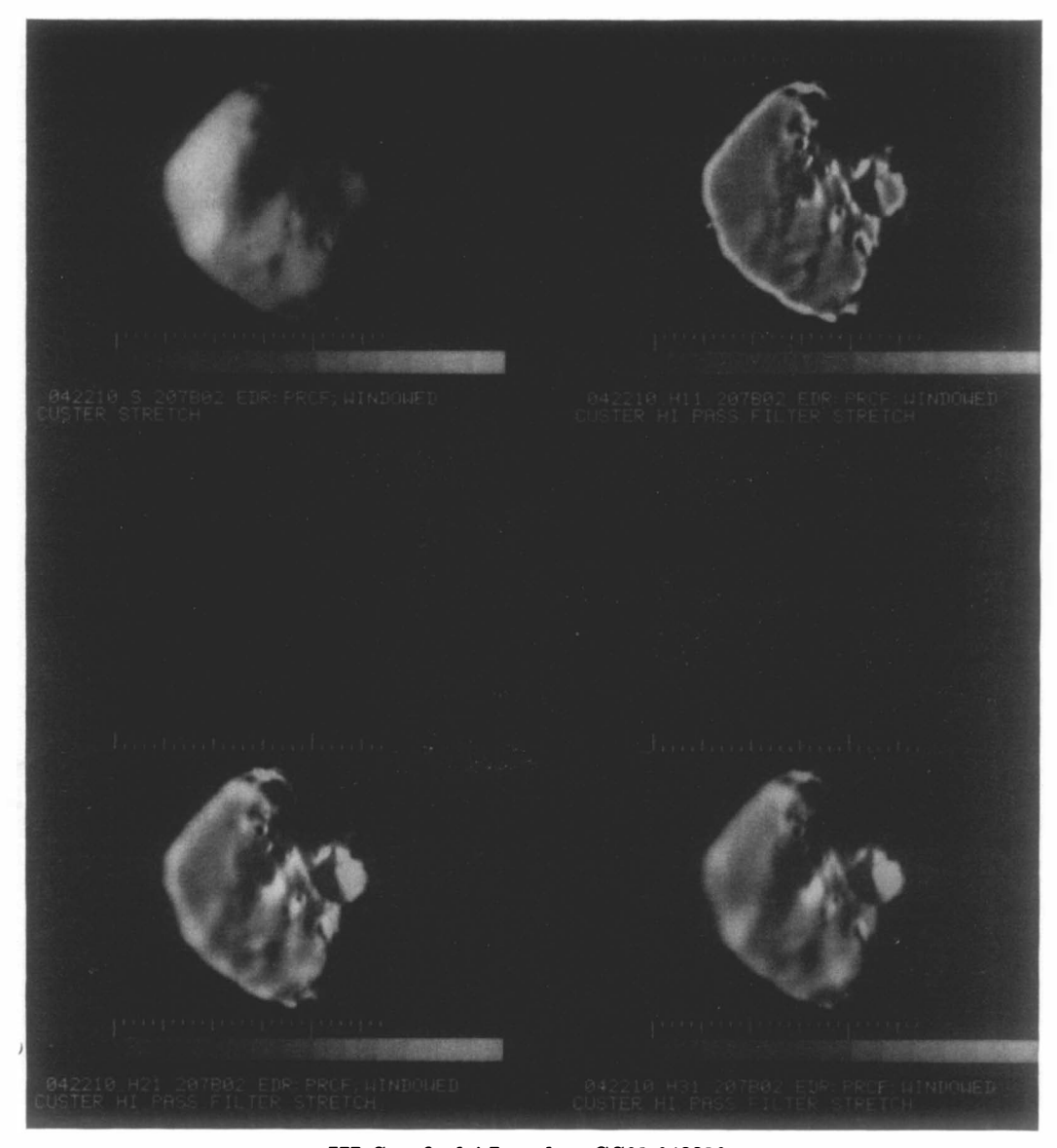


Fig. P22. Phobos. Revolution 207. DAS 09013279. Exposure = 192ms. I. Left: IPL 1294/110335. Stretch. Mag $4\times$. Right: IPL 1294/145905. High-pass filter and stretch. Mag $4\times$.

^a Note: Intentionally overexposed. Hall is on the terminator near center right.



II. Phase = 63°. Range = 6950 km. S/C = (66°.4 S, 45°.5 W). SUN = (3°.7 S, 41°.3 W). $\Delta LAT = 40°$; $\Delta LONG = 45°$.



III. Stanford AI product GS01-042210.



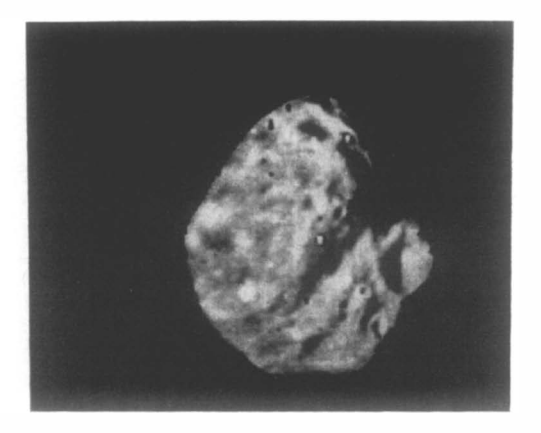
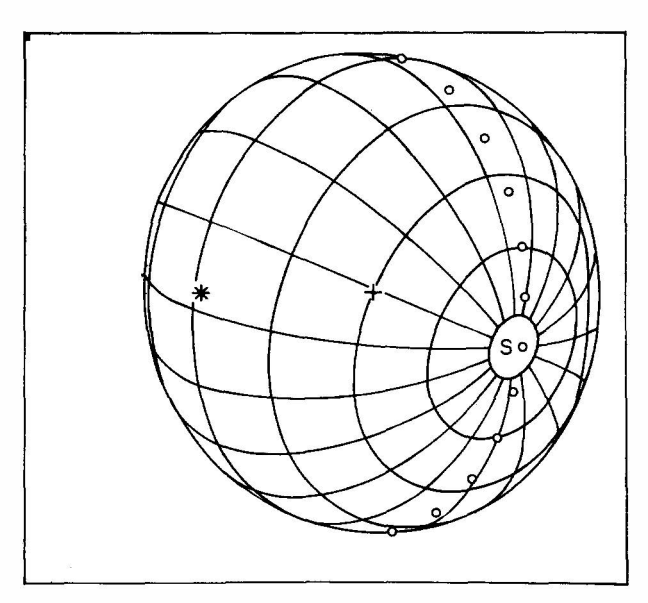
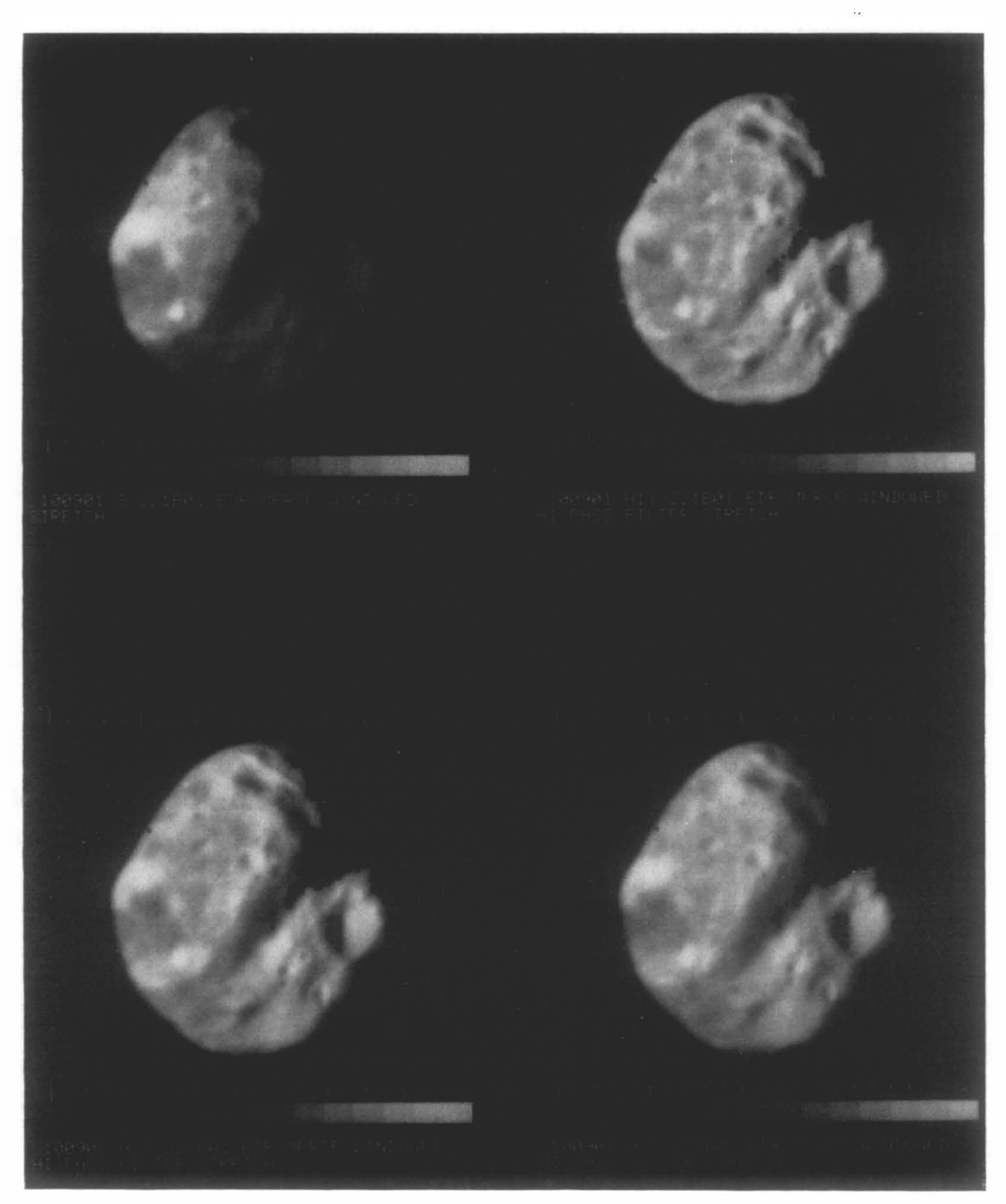


Fig. P23. Phobos. Revolution 221. DAS 09518243. Exposure = 48ms. I. Left: IPL 1295/133001 Stretch. Mag $4\times$. Right: IPL 1295/133729. High-pass filter and stretch. Mag $4\times$.

a Note: Hall is on the terminator near center right.



II. Phase = 41°. Range = 9800km. $S/C = (40^{\circ}.1 \, S, 21^{\circ}.6 \, W)$. $SUN = (2^{\circ}.1 \, S, 35^{\circ}.5 \, W)$. $\Delta LAT = 20^{\circ}$; $\Delta LONG = 20^{\circ}$.



III. Stanford AI product GS01-100901.

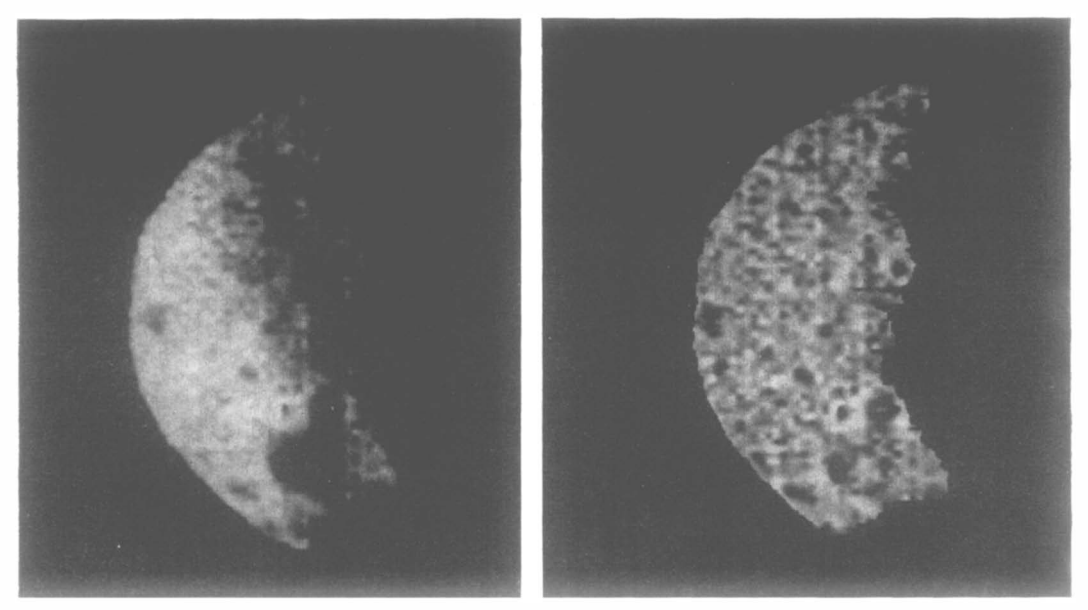
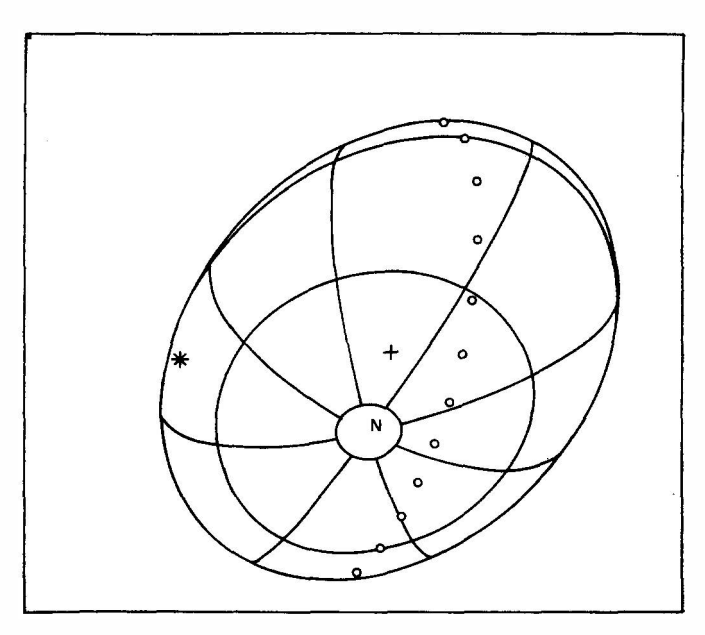
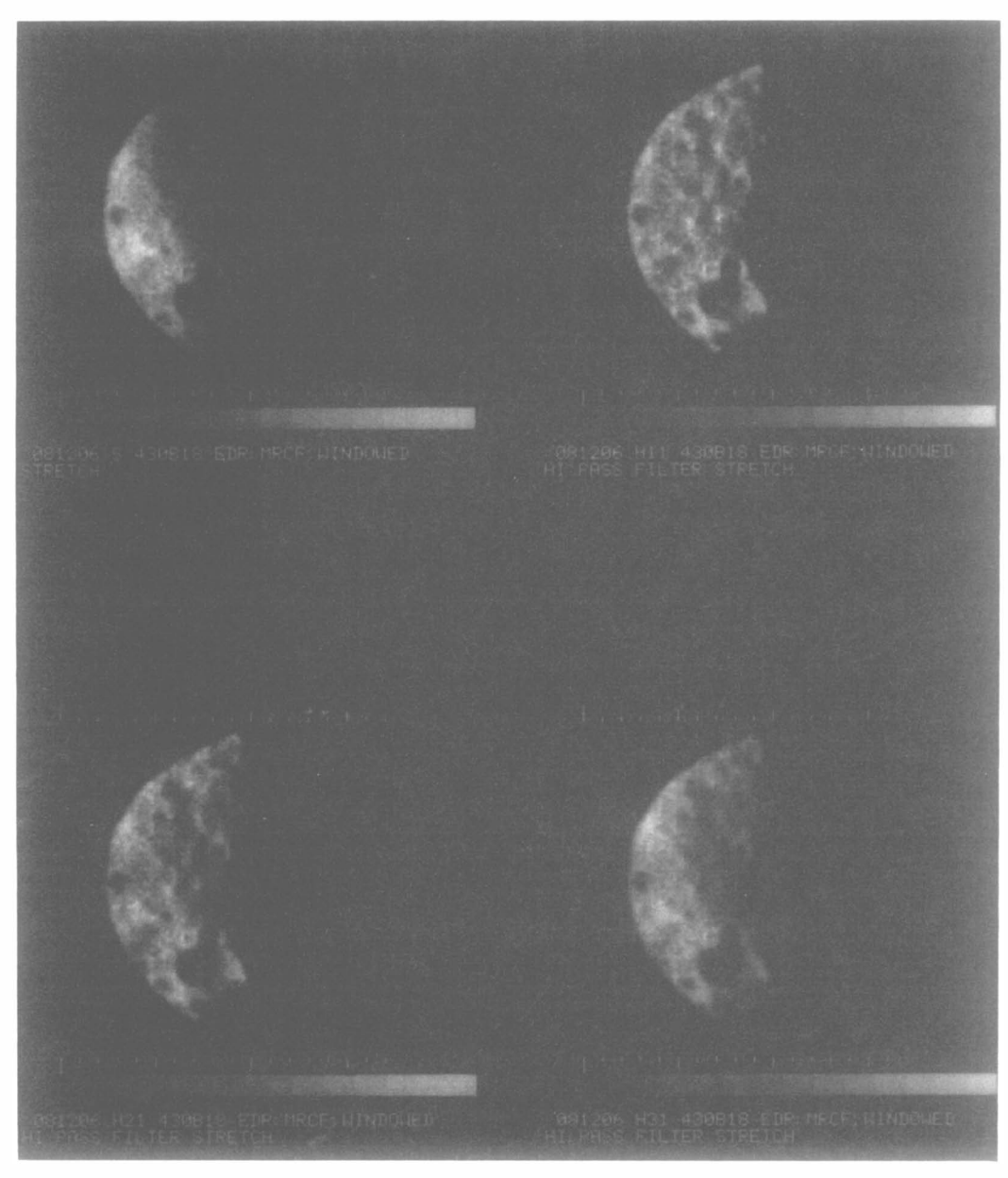


Fig. P24. Phobos. Revolution 430. DAS 11801376. Exposure = 24ms. I. Left: IPL 561/023536. Stretch. Mag $4\times$. Right: IPL 561/023906. High-pass filter and stretch. Mag $4\times$.



II. Phase = 77°. Range = 10710 km. S/C = (62°.3N, 340°.7 W). SUN = (16°.7N, 246°.8 W). Δ LAT = 40°; Δ LONG = 45°.

^a Note: Underexposed.



III. Stanford AI product GS01-081206.

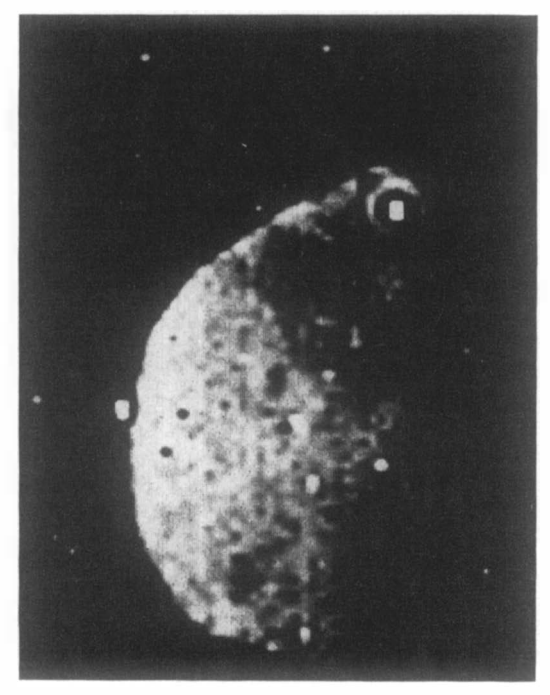
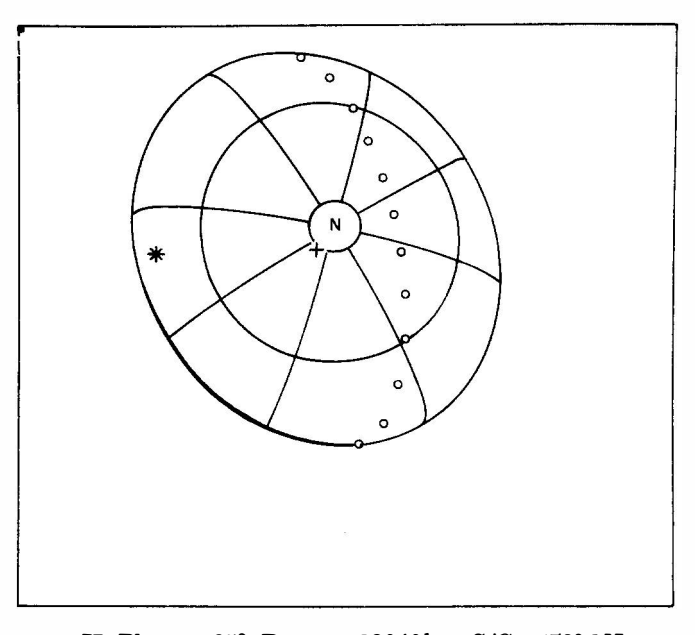
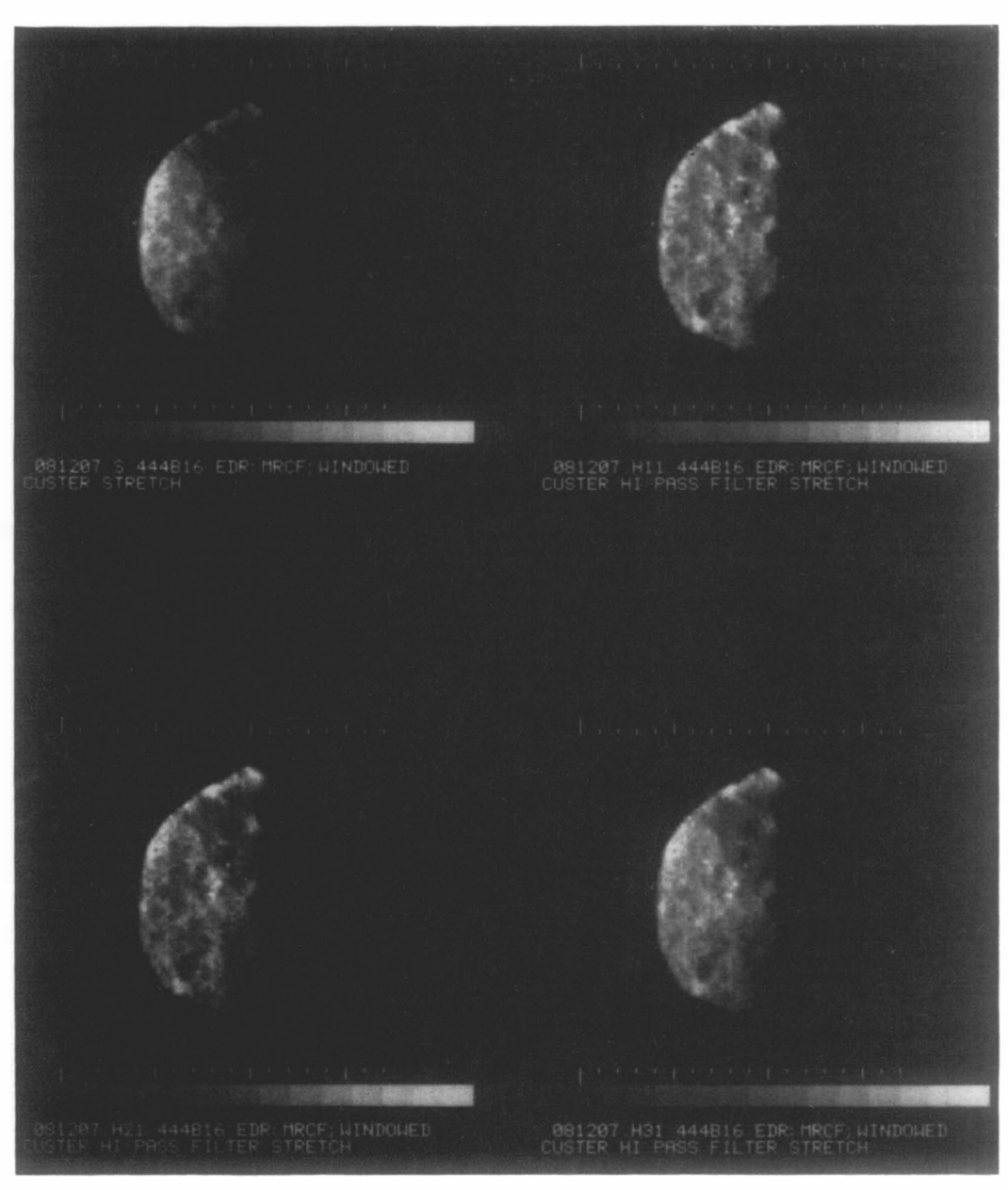


Fig. P25. Phobos. Revolution 444. DAS 12159222. Exposure = 24ms. I. IPL 653/211729. Stretch. Mag $4\times.^a$

a Note: Underexposed.



II. Phase = 65°. Range = 13040km. S/C = (79°.1 N, 248°.7 W). SUN = (18°.3 N, 298°.4 W). Δ LAT = 40°; Δ LONG = 45°.



III. Stanford AI product GS01-081207.

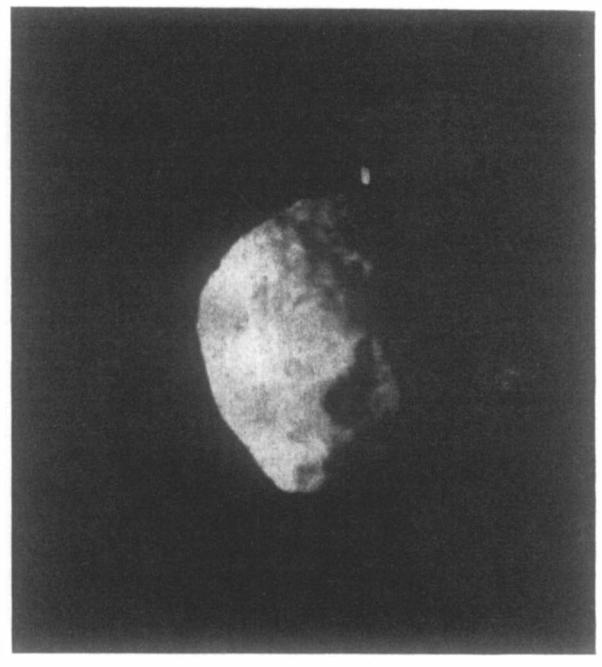
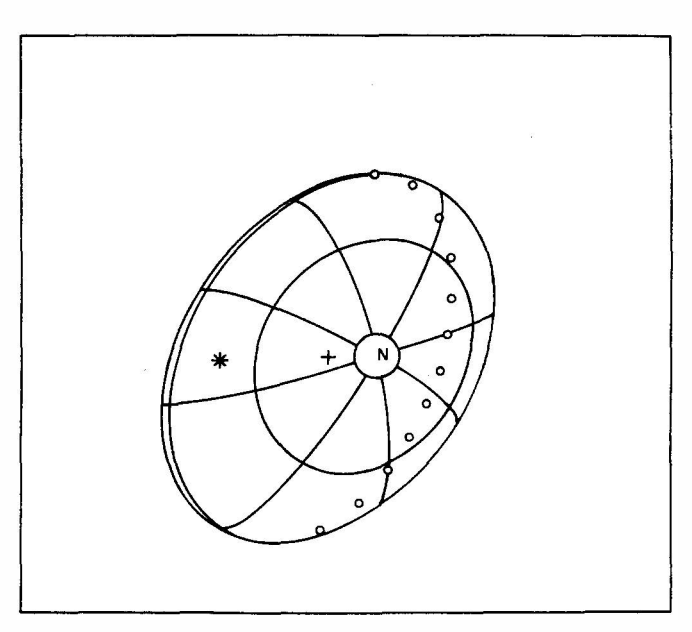
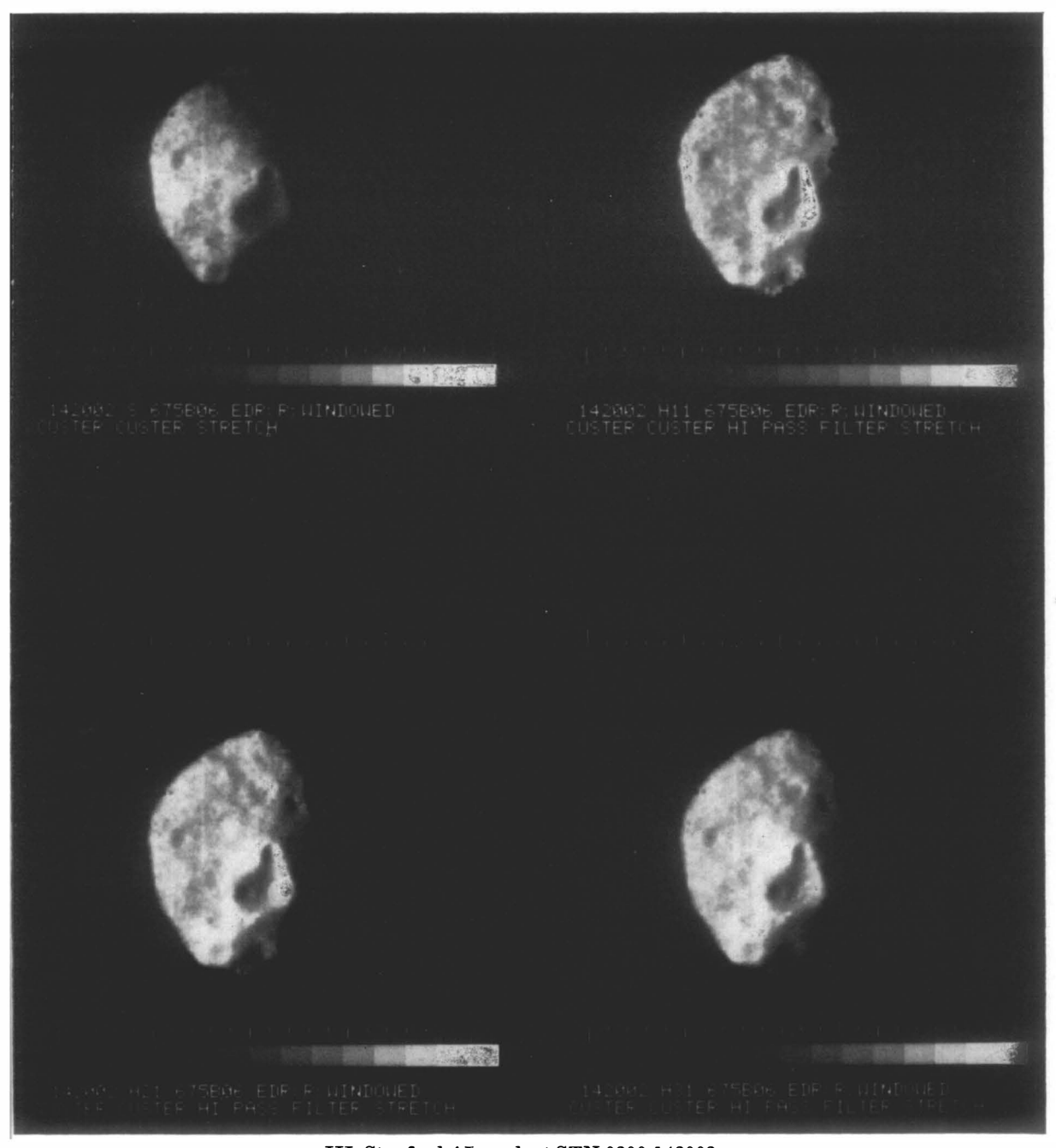


Fig. P26. Phobos. Revolution 675. DAS 13469628. Exposure = 24ms. I. IPL 571/233153. Stretch.

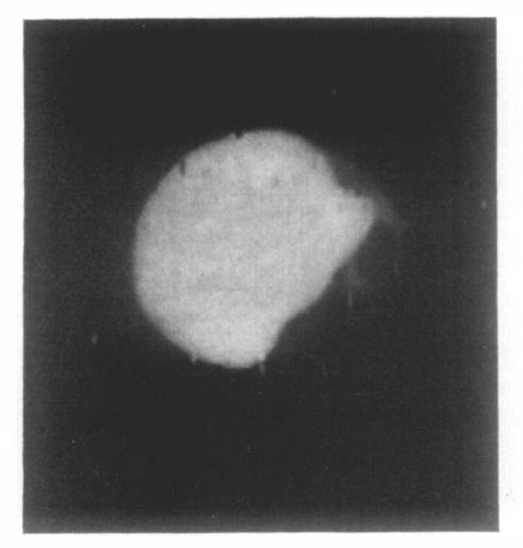
a Note: Underexposed.

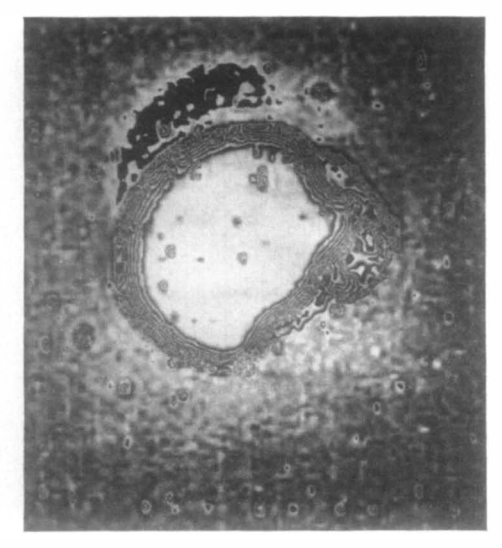


II. Phase = 43°. Range = 13950km. S/C = (68°.8 N, 240°.7 W). SUN = (25°.2 N, 240°.3 W). Δ LAT = 40°; Δ LONG = 45°.



III. Stanford AI product STN 0200-142002.

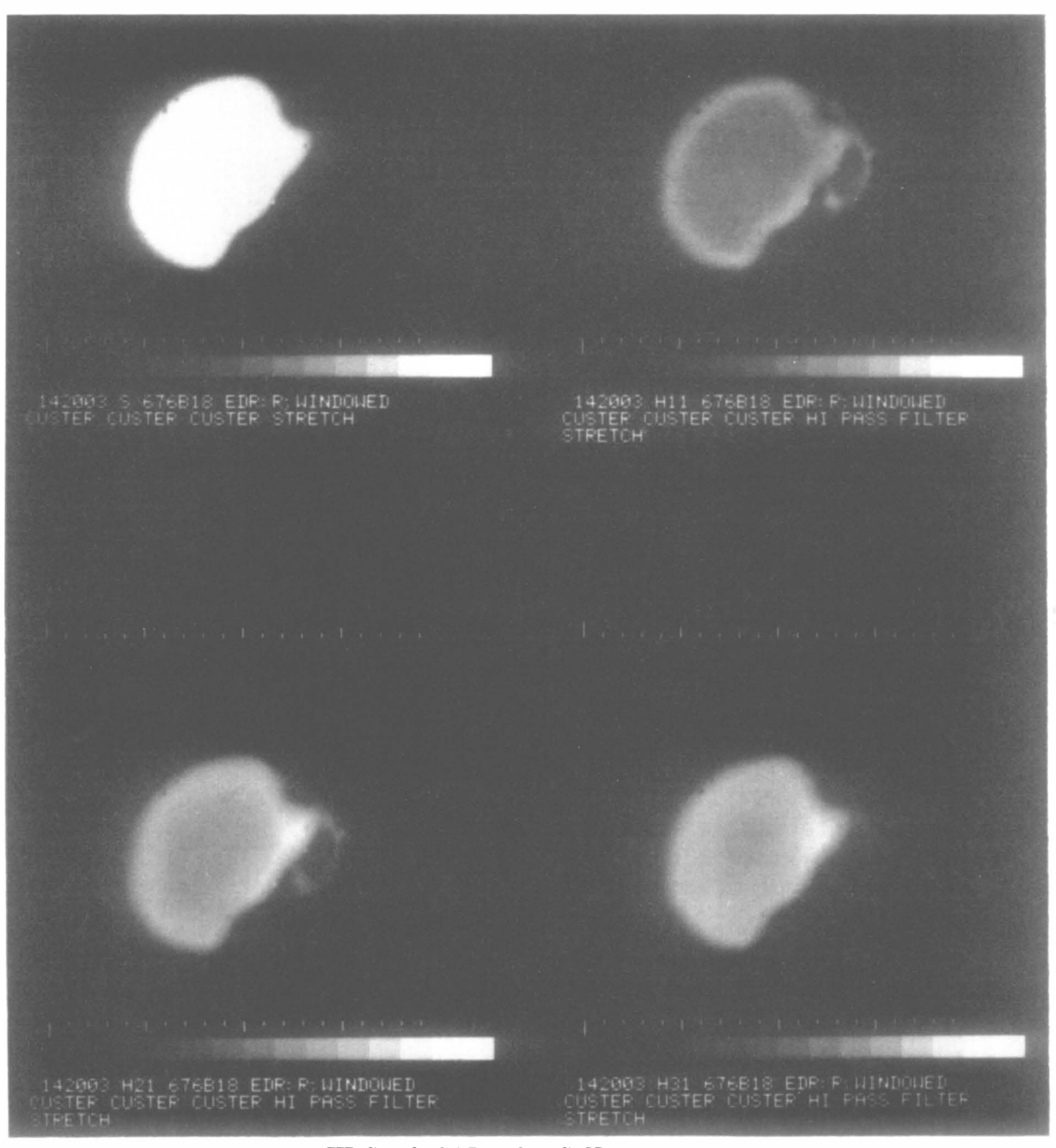




 $\label{eq:Fig.P27} Fig.\,P27.\ \ Phobos.\ Revolution\ 676.\ DAS\ 13511838.\ Exposure = 6144\,ms.\ I.\ Left: IPL\ 571/232449.$ Stretch. Right: IPL 571/232855. 9-bit data truncated to 8-bits. Stretch. \$^a\$

^a Note: Intentionally overexposed.

II. No grid.



III. Stanford A I product STN 0200-142003.